Structural analysis of octopine dehydrogenase from *Pecten maximus*

Inaugural-Dissertation

zur

Erlangung des Doktorgrades der

Mathematisch-Naturwissenschaftlichen Fakultät

der Heinrich-Heine-Universität Düsseldorf

vorgelegt von

Sander Smits

aus Papendrecht

Aus dem Institut für Biochemie
der Heinrich-Heine Universität Düsseldorf

Gedruckt mit der Genehmigung der
Mathematisch-Naturwissenschaftlichen Fakultät der
Heinrich-Heine-Universität Düsseldorf

Referent: Prof. Dr. L. Schmitt
Koreferent: Prof. Dr. G. Groth
Tag der mündlichen Prüfung: 09.09.2008

Zusammenfassung

Die Oktopine Dehydrogenase (OcDH) aus dem Adduktorenmuskel der Pilgermuschel *Pecten maximus* katalysiert die reduktive Kondensation von L-Arginin und Pyruvat zu D-Oktopin. Dieses Enzym, ein Modelprotein für Opin Dehydrogenasen oxidiert dabei das aus der Glykolyse entstandene NADH zu NAD^+ und hält so die ATP-Versorgung während extremer Belastungen aufrecht. Im Vergleich zu anderen Opin Dehydrogenasen zeichnet sich die OcDH durch eine extreme Substratspezifizität aus und reagiert nur mit L-Arginin als Aminosäure. In dieser Dissertation wurden strukturbiologische Experimente durchgeführt, deren Ziel es war, die dreidimensionale Struktur der OcDH zu bestimmen und auf diesem Wege den Reaktionsmechanismus und die hohe Substratspezifität molekular zu erklären. In den letzten Jahrzehnten wurde die Enzymaufreinigung etabliert und durch die Einführung von Affinitäts-Anhängsel am N- oder C-Terminus der Enzyme wurde eine effiziente Aufreinigung der Proteine ermöglicht. Die Wahl des Anhängsels und dessen Position kann die Kristallisation von Proteinen beeinflussen. Daher wurden Kristallisationsversuche der OcDH ohne und mit Histidine-Anhängsel untersucht. Nur OcDH mit fünf Histidinen am C-terminalen Ende des Proteins konnten erfolgreich kristallisiert werden. Zur Optimierung dieser Kristalle wurde in Anwesenheit des Kofaktors NADH kristallisiert. Die so erhaltenen Kristalle waren von einer Qulaität, die es ermöglichte, die dreidimensionale Struktur zu bestimmen, in der der Histidin-Anhängsel in der Öffnung der NADH- und Arginin-bindenden Domäne positioniert und durch ein komplexes Wassernetzwerk koordiniert wird. Dadurch wird die OcDH nicht nur in ihrer Konformation stabilisiert, auch entsteht die Möglichkeit für andere essentielle Kristallkontakte. Durch die Strukturbestimmung der OcDH im Komplex mit NADH sowie NADH/L-Arginin, NADH/Agmatine und NADH-Pyruvat konnten Informationen über Substratbindung, Selektion und den Reaktionsmechanismus gewonnen werden, die eine molekulare Beschreibung dieses Enzyms ermöglichen. So bindet und selektiert OcDH zum Beispiel seine Substrate mittels elektrostatischer Kräfte und Größenselektion, welche die Entstehung von Oktopin, ein stereoselektives Produkt mit zwei chiralen Zentren, mittels eines „molekularen Lineals“ garantiert.

Summary

Octopine dehydrogenase (OcDH) from the adductor muscle of the great scallop, *Pecten maximus*, catalyzes the reductive condensation of L-arginine and pyruvate to octopine during escape swimming. This enzyme, which is a prototype of an opine dehydrogenase (OpDHs), oxidizes glycolytically born NADH to NAD^+ thus sustaining anaerobic ATP provision during short periods of strenuous muscular activity. In contrast to some other opine dehydrogenases, OcDH uses only L-arginine as amino acid substrate. In this thesis experiments were performed to elucidate the structural organization of OcDH as well to clarify the reaction mechanism of octopine formation.

Over the last decade enzyme purification became more efficient and standardized through the introduction of affinity tags for rapid protein purification. Choice and position of the tag, however, might directly influence the process of protein crystallisation. OcDH-tagless and histidine tagged protein constructs such as OcDH-His_5 and OcDH-LEHis_6 have been investigated for their crystallisability. Only OcDH-His_5 yielded crystals, which however, were multiple. To improve crystal quality, the cofactor NADH was added resulting in single crystals suitable for structure determination. As shown by the structure, the His_5-tag protrudes into the cleft between the NADH and L-arginine binding domains of OcDH. Protein His-tag interactions are mediated mainly by water molecules. The protein is thereby stabilised to such an extent, which does not only allow its crystallisation, but also promotes the formation of additional crystal contacts. Together with NADH the His_5-tag obviously locks the enzyme into a specific conformation, which induces crystal growth. The prolongation of the His_5-tag by three amino acids (L-E-H) will not render similar contacts and no crystals were obtained with the construct OcDH-LE-His_6. The crystal structures of OcDH in complex with NADH, and the binary complexes NADH/L-arginine, NADH/Agmatine and NADH/pyruvate provide detailed information about the principles of substrate recognition, ligand binding and reaction mechanism. For example, OcDH binds its substrates through a combination of electrostatic forces and size selection, which guarantees that OcDH catalysis proceeds with substrate and stereo-selectivity giving rise to a second chiral center, via a “molecular ruler” mechanism.

Index

1 Introduction 1

1.1 Functional dependent anaerobiose 1

1.2 Terminal Pyruvate oxidoreductases 4

1.3 The great scallop: *Pecten Maximus* 5

1.4 Distribution of opine dehydrogenases 6

1.5 Biochemical analysis of OpDHs 6

1.6 The proposed reaction mechanism of OcDH 8

2 Aims and objectives 12

3 Material and Methods 13

3.1 Abbreviations 13

3.2 Chemicals used for crystallization 15

3.3 **Crystallographic methods** 16

3.3.1 Fundamentals of crystal growth 16

3.3.2 Means of reaching supersaturation 18

3.3.3 Crystallization by vapor diffusion 18

3.3.4 Batch/microbatch crystallization and Dialysis 19

3.3.5 Choice of crystallization conditions 21

3.4 Crystallization of OcDH 21

3.5 Basic principles of X-ray crystallography 22

3.5.1 Crystal systems and space groups 22

3.6 Proteins and X-rays 23

3.7 Principles of diffraction - Laue equations, Bragg´s law and the Ewald construction 24

3.7.1 Structure factors and electron density 27

3.8 The phase problem, a crystallographer's nightmare 28

3.8.1 The Patterson function 28

3.9 Solving the phase problem 29

3.9.1 Isomorphous replacement 29

3.9.2 Anomalous Diffraction 32

3.10 Molecular replacement 34

3.11 Dataset collection from crystals of OcDH 37

3.12 Computer programs 38

3.13 Analysis of the obtained models and graphical visualization 39

3.14 Structure deposition 39

4 Results *40*

4.1 Crystallisation of OcDH 40

4.2 Dataset collection of OcDH crystals 43

4.3 Structure determination 44

4.4 Final structure of OcDH-NADH 47

4.5 NADH binding site 49

4.6 His_5-tag and crystal contacts 50

4.7 The binary OcDH-NADH/L-arginine complex 52

4.8 The binary OcDH-NADH/pyruvate complex 55

4.9 Domain closure 56

4.10 Agmatine bound OcDH 58

4.11 Octopine and mercury bound crystals 61

5 Discussion *63*

5.1 Crystallisation of OcDH 63

5.2 His_5-tag induced crystallisation 64

5.3 Structure of OcDH 66

5.4 The L-arginine, Agmatine and Pyruvate binding sites 66

5.5 Comparison of OcDH with related crystal structures of dehydrogenases 70

5.6 A catalytic dyad combined with an "L-arginine sensor" 71

5.7 Substrate specificity and stereoselectivity of OcDH 72

5.8 Order of substrate binding 74

6 Outlook *76*

7 References *77*

8 Appendix *88*

9 Acknowledgement *94*

1 Introduction

Oxygen plays a crucial role in the energy supply for most known organism on earth, living under aerobe conditions. Substrate for an aerobic energy supply is glucose or its polymeric form glycogen. Where as glucose first has to be phosphorylated by the hexokinase via the hydrolysis of ATP, glycogen can be used in the Embden-Meyerhof-Parnas-pathway (glycolysis) directly. During glycolysis two or three ATP molecules can be generated, together with dead end products, pyruvate, NADH and water. Under aerobic conditions pyruvate can be further oxidized in the mitochondrial Krebs cycle. The electrons obtained here are further transferred to NADH and $FADH_2$ and finally to oxygen and as an end product water. Oxygen encounters for a continuous electron movement between the complexes of the respiratory chain, which ends in the synthesize of ATP by the ATP synthase. By complete oxidation of glucose in total almost 30 ATP molecules can be generated from one glucose molecule.

1.1 Functional dependent anaerobiose

Although oxygen represents almost 21% of the atmosphere, organisms can have short or long oxygen concentration deficiencies and need to maintain their regular energy supplying pathways. Two physiological situations are discriminated with low presence of oxygen, the functional anearobiose and the environmental anaerobiose, respectively (*1*). The functional anearobiose describes the case where the need of energy is bigger than the energy that can be generated, for example during intensive contraction for the muscle during “fight and flight” reactions (*1, 2*). In the case of environmental anaerobiose, the organism in general lives in environments with rather low or no oxygen levels. In both cases, ATP can not be synthesized in sufficient amount (*3*).

In contrast to the low environmental oxygen concentrations were the usage of energy is minimized, the need of energy during the functional anaerobiose is extremely high. The aerobic metabolism cannot cope with this, meaning that inside the mitochondria the low concentration of oxygen inhibits the production of enough

ATP (*4, 5*) needed at that moment. Furthermore the carrier and transport mechanism cannot supply enough reduction equivalents into the mitochondria (*6*). To prevent this lack of energy, at least to a certain amount, animals came up with three different metabolic pathways to generate ATP: the phosphagen kinase reaction, substrate chain phosporylation and the adenylate kinase reaction (*1*).

During functional anaerobiose, the energy is provided by the phosphagen kinase reaction. Here the high-energy phosphate group, of a phosphorylated guanidinium compound (phosphagen) is transferred to ADP resulting in the generation of one ATP.

In vertebrates the phosphagen used is creatine-phosphate, whereas in invertebrates the main component is L-arginine-phosphate (*7*). The phosphagen kinases transfer the phosphorylgroup to ADP, with high turn over numbers, a so-called fast supplier of newly synthesized ATP (*3, 8, 9*).

The trans-phosporylation can only supply energy for a short period (*10*). Is there even more need for ATP, the second reaction, the substrate phosporylation reaction is taking over ATP synthesis. Species with a high tolerance against hypoxia or anoxy have a high glycogen concentration in there tissue. For example in some scallops like *Mytilus edulis* or *Pecten maximus*, glycogen can be present in concentration up to 5 to 40% of their dry body weights (*11*).

During anaerobe glycolysis only 10% of the total energy can be gained compared to the oxidation of glucose. To maintain the energy levels from the glycolytic metabolism the flux-rate is increased, the so-called Pasteur effect (*12-15*). Allosteric control of key enzymes, protein modification for example the glycogen phosphorylase (*16*) or the phospho-fructokinase (*17*) play an important role in the regulation of anaerobic glycolysis (*18*). Due to the higher glycolysis rate, higher amounts of reduction products are formed, which cannot be used completely by the respiratory chain as they cannot be transported efficiently to the mitochondria (*3, 6, 19*).

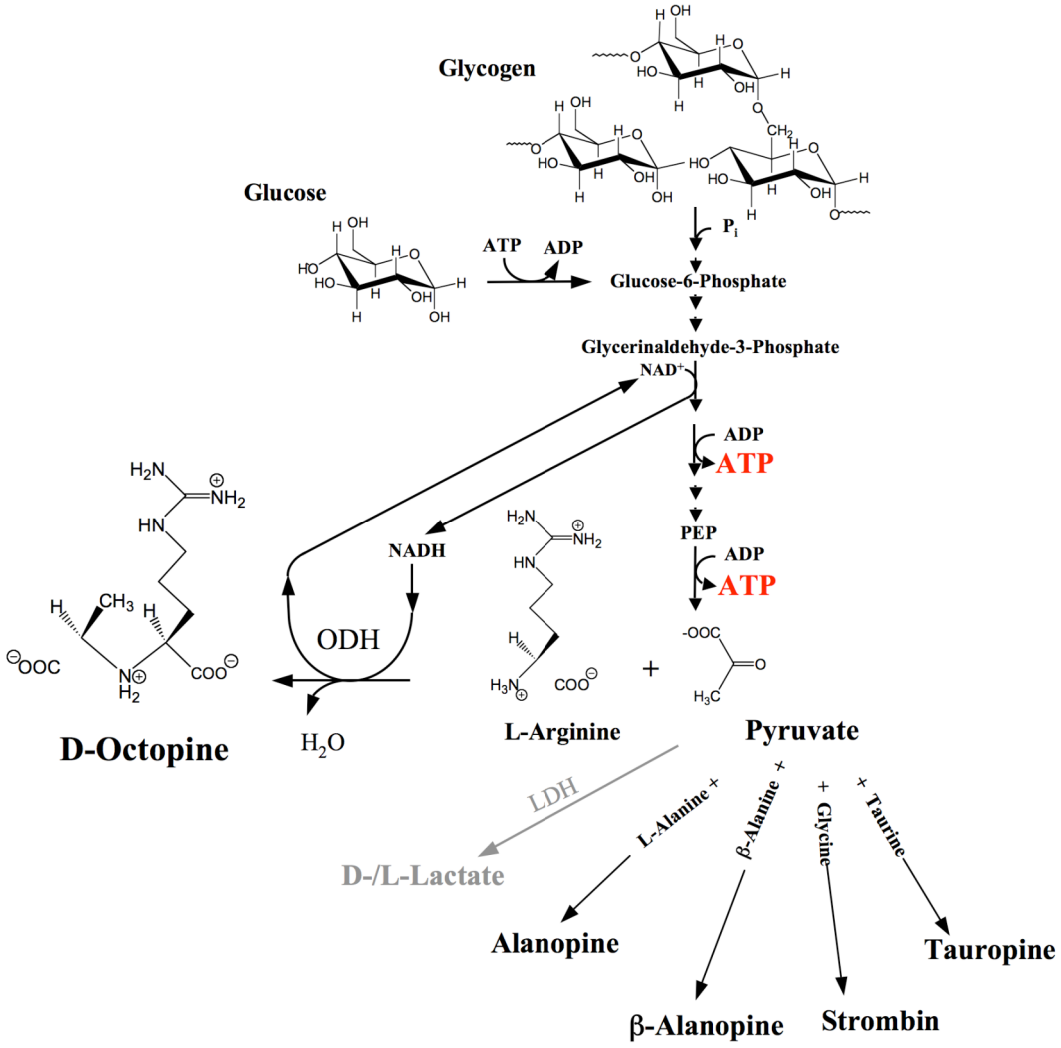

Figure 1: Overview of the different anaerobic metabolism in marine invertebrates. Different proteins playing a role in anaerobic respiration are highlighted as well as the dead end products of the pathway. Adapted from (*3*).

Although the muscles mainly use energy obtained from the anaerobic glycolysis during enhanced contractions (for example fight and flight reactions) the mitochondria are not suffering by low oxygen levels. The oxygen concentrations in mitochondria are sufficient to produce ATP, although resulting in lower amounts then needed by the contracting muscle (*4, 5, 20*). To maintain the anaerobic glycolysis the reducted products of glycerinaldehyd-3-phosphate, like pyruvate, have to be re-oxidized (Figure 1) as high concentrations are lethal to the organism.

1.2 Terminal Pyruvate oxidoreductases

Several terminal pyruvate oxidoreductases catalyze the oxidation of NADH. A well known member of this enzyme family is lactate dehydrogenase (Figure 1), L-Lactate: NAD^+ Oxidoreductase, EC 1.1.1.27; LDH). This enzyme catalyses the transfer of a hydride ion from NADH to pyruvate, with the end products NAD^+ and lactate (*6, 21*). LDH thereby maintains the redox state in vertebrates as well as spiders and insects during functional anaerobiose (*22*). The formed lactate can be easily detected in the tissue of these organisms (*21, 23, 24*).

In the muscles of Coelenteraten, Nemertinen, Cnidariern however, no lactate could be detected (*25*) as well as the presence or activity of the LDH. It remained the question how these organism supply energy during functional anaerobiose or how the anaerobic glycolysis functions. Nowadays it is well known that so called opine dehydrogenases terminated anaerobe glycolysis in these organisms (Figure 1) (*10, 14, 19, 22, 26*).

Opine dehydrogenases catalyse the reductive condensation of pyruvate with an amino acid in the presence of NADH (Figure 2). The endproducts are N-(carboxyalkyl)-amino acids, or opines, NAD^+ and water. Already in the twenties of last century Morizawa isolated an unusual amino acid, which later has been called octopine from the Cephalopoden *Octopus octopodia* (*27, 28*), a product formed after the condensation of pyruvate and L-arginine.

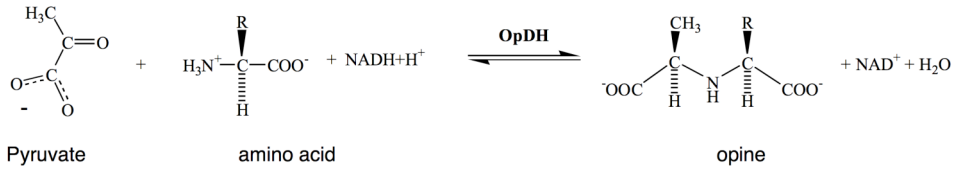

Figure 2: General reaction mechanism of opines dehydrogenases. Opine dehydrogenases catalyse the reductive condensation of pyruvate with an amino acid by the reduction of NADH with as end product opines and water.

In vitro synthesis allowed the formation of octopine from pyruvate and L-arginine in 1959(*29*). The enzymatic condensation of pyruvate and L-arginine is mediated by an enzyme called octopine dehydrogenase (Figure 1; OcDH, EC 1.5.1.11, N2-(1-carboxyethyl)-L-arginine: NAD^+ Oxidoreductase) (*29*), which was first isolated from

the adductor muscle from *Pecten Maximus* in 1969 (*30*). Members of this enzyme family have been identified in several different marine invertebrates. For example in Anneliden *Sipunculus nudus* (*31*), *Anodonta cygnea* (*32*), *Pecten jacobaeus* (*7*), *Loligo vulgaris* (*33*) and *Cerebratulus lacteus* (*34*).

1.3 The great scallop: Pecten Maximus

During flight reaction the level of L-arginine, in the adductor muscle of *Pecten Maximus*, is increasing due to the trans-phosporylation of arginine phosphate (Figure 1) dramatically. The released L-arginine is condensated with pyruvate to D-octopine in the resting phase (*2, 32*). During this reaction the products of the reduction reaction of glycerolaldehyd-3-phosphate-dehydrogenase are re-oxidised. OcDH thereby maintains the redox state of the muscle tissue at low oxygen levels (*35, 36*).

In different marine invertebrates different opine dehydrogenase mediate this reaction. For example the strombine-/ alanopine dehydrogenase use glycine or alanine as amino acids (EC 1.5.1.22, EC 1.5.1.17) (Figure 3).

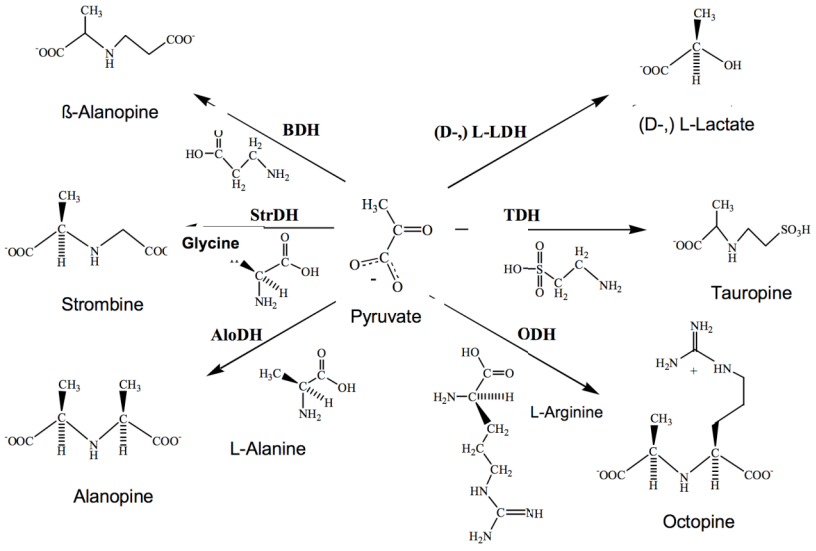

Figure 3: Terminal Pyruvate-oxidoreductases of anaerobic glycolysis.
Several pyruvate oxidoreductases were identified in invertebrates. The specificity lies in the different amino acids that are used in the opine formation (Adapted from (*38*))

Although OcDH is specific for L-arginine, other opine dehydrogenases are shown to have a rather broad substrate spectrum (*10, 17, 39*), like the amino acids

alanine, serine and methionine. Furthermore several isoforms of one enzyme can be found in one organism, like the examples in *Pecten Maximus* were seven isoforms of OcDH have been identified (*40-44*).

1.4 Distribution of opine dehydrogenases

Like LDH, OpDHs are found in almost all invertebrates. Up to date OpDHs or LDHs have been found in over 160 species of at least 18 animal families (*22, 45*). The OpDHs are in contrast to LDH not exclusively present in invertebrates. Already in 1993, a tauropine dehydrogenase was identified and purified from the algae *Rhodoglossum japonicum* (*46*). Furthermore several opine dehydrogenases have been identified in plant tumors (*47*).

Plant tumors are induced after the infections of plants with pathogenic bacteria like *Agrobacterium tumefaciens*. These bacteria contain a Ti (tumor inducing) plasmid which next to oncogens also harbor genes encoding for proteins for the synthesis of opines (*48-50*). The insertion of part of these plasmid in plants results in an oncogenic tissue and those infected plants start producing opines. The bacteria infecting the plants use these opines as carbon and nitrogen source. For transport and production of these opines, the gene encoding for opine permeases and opine oxidases are encoded on the Ti-plasmids as well. The opine oxidases are catalytically different from opine-synthasen (*38*). Opine dehydrogenases are further found in *Pseudomonaden, Rhizobiaceen* and some *Corynespecies* like *Arthrobacter sp* (*38, 51*), as well as some fungi species like *Cylindrocarpon* and *Fusarium* (*52*).

1.5 Biochemical analysis of OpDHs

Physiologically and biochemically, opine dehydrogenases are well characterised. In solution, OpDHs have a monomeric structure between 37 to 45 kDa; maximal reaction rate in the direction of opine formation is found at pH 6.5 – 7.5 and 8.0 – 9.5 in the reverse direction (*53*); a putative reaction mechanism derived from kinetic studies supposedly comprises an ordered ter-bi system suggesting NADH binding occurring first, followed by random binding of pyruvate and the respective L-amino acid (*54*).

The reductive condensation reaction of L-arginine with pyruvate is interesting, because a second chiral center is formed and as a corollary OpDHs display either (D, L) or (L, L) specificity. Amino acid sequence homology analysis has established that enzymes catalyzing product formation with (D,L) and product formation with (L,L) stereochemistry belong to two distinct protein subfamilies (*55*). Furthermore, among one subfamily sequence homology is around 20- 30%, while no significant homology exists between the two subfamilies.

Especially the OcDH from *Pecten Maximus* was used frequently for biochemical analysis studies in the past, due to its natural high abundance in the adductor muscle.

OcDH from *Pecten Maximus* is a monomeric protein of 43.3 kDa, the smallest functional unit among the NADH dependent dehydrogenase family (*10, 56, 57*). Two different studies were published on the kinetics of substrate binding (*58, 59*). Monneuse-Doublet and Olomucki postulate an ordered ligand binding were first NADH and pyruvate are binding, followed subsequently by the amino acid L-arginine. Pyruvate reacts with L-arginine under dehydration to a Schiff base. After formation of the transitions state, the hydride ion is transferred from NADH and D-octopine is formed. Also Schrimsherr and Taylor describe the initial binding of NADH. However the binding of the two other substrates, pyruvate and L-arginine is not ordered and occurs randomly (*59*). Already in 1972 it has been spectrophotometrically shown that upon binding of NADH the protein undergoes a small but significant conformational change. Besides this OcDH was used frequently in the past to investigate protein folding of monomeric proteins (*60, 61*).

Only recently the primary sequence of OcDH from *Pecten Maximus*, *Loligo vulgaris, Loligo opalescens* and *Sepia officinalis* were described (*57*), which were complemented by the sequences of other members of the enzyme family (*62, 63*) (see Appendix 1). They all consist of two clearly defined domains. The first domain binds the cofactor NADH and is on a protein sequence level highly conserved. They consist of a conserved ß-α-ß-α-ß motif, the so-called Rossmann-fold (*64, 65*). This ß-α-ß-α-ß motif was identified in all opine dehydrogenases from invertebrates. Inside the Rossmann-fold the consensus sequence GXGXXG (where X can be any amino acid) is present, which represents the high affinity-binding site for di-nucleotides like

NADH (*66-68*).

The binding site for pyruvate and L-arginine and the exact reaction mechanism of opine formation is still not clarified. For the LDH it is known that the active site contains an aspartate-arginine motif with the consensus sequence DXXR (where X can be any amino acid). Together with an additional histidine, a so called histidine-aspartate-arginine triad is formed, catalyzing the hydride ion transfer from NADH to pyruvate (*69-71*). A similar triad is shown to contain crucial residues inside the active site of the malate dehydrogenases (*72*).

By sequence homology studies a similar DXXR motif could not be identified in the different opine dehydrogenases, suggesting an at least slightly different reaction mechanism. In the nineteen seventies however, Thomé-Beau und Olomucki showed that a histidyl and a carboxyl group are crucial for the activity of OcDH (*73*). Inside the primary sequences of several OpDHs a conserved histidine, arginine as well as aspartate were found and a similar triad was postulated (*57, 74*). Furthermore in OcDH one cystidyl group appeared crucial for the catalytic reaction which was shown by thio specific reagent experiments which inhibited activity (*56, 75*).

It was not before 2000 that OcDH was cloned and overexpressed using commercial vectors (*57*). Finally a more detailed biochemical analysis using mutagenesis studies could be conducted. In contrast to earlier studies it was now possible to purify large quantities for biochemical studies. From 2.8 kg adductor muscle from *Pecten Maximus* only 50 mg OcDH could be purified by Van Thoai et al. (1969). With the recombinant system however similar amounts could be obtained with only a couple of liters of *E. coli* culture. Here OcDH can be easily purified using the genetically engineered His-tag.

1.6 The proposed reaction mechanism of OcDH

The only known structure of a member of the Opine dehydrogenases is the bacterial N-(1-D-carboxyethyl)-L-Norvaline Dehydrogenase (CENDH) (*76*). Similar to OcDH, CENDH catalyses the NADH dependent condensation of pyruvate with an amino acid. In contrast to OcDH, CENDH has a broader substrate specificity of small hydrophobic L-amino acids like methionine, isoleucine, valine and

phenylalanine. CENDH belongs to the (D,L)-opine dehydrogenase enzyme family. CENDH is a homo-dimeric protein of 359 amino acid (36 kDa) (*77*). In 1998 the structure of CENDH was solved in the apo form (*76*). The structure revealed the predicted two domain enzyme, domain I and domain II, connected via a small three amino acid long loop. Domain I contains the described Rossmann fold. Although the protein was crystallized in the presence of NAD^+, the density for NAD^+ could not be conclusively be assigned and therefore NAD^+ was not included in the structure. The conserved cluster of residues of CENDH included a His-Asp pair (His 202 and Asp 297) that is located adjacent to a conserved arginine (Arg 292) (Figure 4). Therefore the authors concluded that, if these residues play a role in the catalytic center of CENDH, then there is clearly a strong parallel to the other keto acid dehydrogenases whose chemistry is dependent on a His-Asp-Arg triad. OcDH has about 20% sequence identity with CENDH but it is expected to have a similar reaction mechanism (*57, 74*).

Based on sequence alignment several mutational study of OcDH were made to clarify the reaction mechanism of OcDH and a catalytic triad consisting of His212, Asp329 and Arg324 was proposed recently (*78*). This lead to the proposal of a reaction mechanism model, containing the commonly believed His-Asp-Arg triad (Figure 5). The proposed mechanism of octopine formation by the OcDH form *Pecten maximus* has been described as follows.

The putative catalytic mechanism starts with the attack of the α-amino group of L-arginine to the carbonyl C-atom of pyruvate forming an intermediate. The carboxyl-group of the pyruvate moiety of this intermediate is stabilized at the active site by interaction with arginine 324 as deduced from LDH.

Histidine 212 acting as an acid-base catalyst donates a proton to the carbonyl group of the pyruvate moiety of the intermediate. This proton-transfer is further used to stabilize the intermediate at the active site. Aspartate 329 increases the acidity of histidine 212 and thus enables the proton transfer to the transition state.

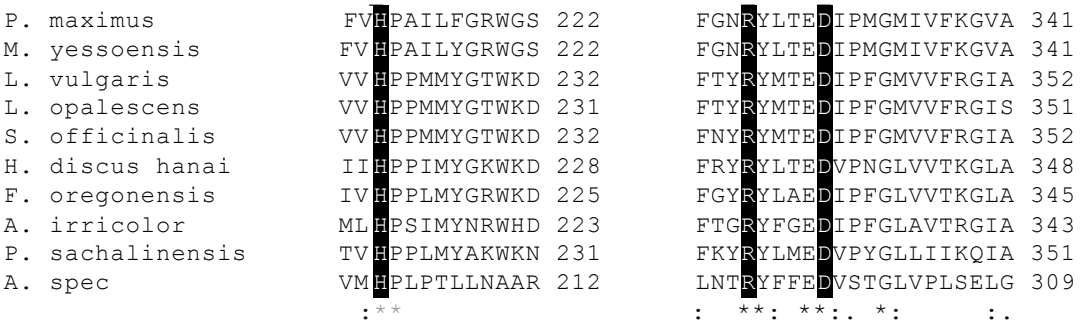

Figure 4: Part of a sequence alignment using several different opine dehydrogenases. Used are octopine dehydrogenases from *Pecten maximus*, *Mizuhopecten yessoensis*, *Loligo vulgaris, Loligo opalescens, Sepia officinalis* and *Pseudocardium sachalinensis*, the tauropine dehydrogenase from *Arabella irricolor* and *Haliotis discus hannai*, the N-(1-D-carboxyethyl)-L-Norvaline dehydrogenase (CENDH) from *Arthrobacter spec*, as well as a predicted Alanopine dehydrogenase from *Fusitriton oregonensis*. The chosen amino acids for mutagenesis are marked in black**.**

After elimination of a water molecule, the resulting Schiff-base is stabilized mesomerically. The hydride transfer from NADH to the transition state is the final step. As already proposed by Doublet and Olomucki (*56*) the hydride ion is not transferred to the α-keto acid as in LDH, but to the Schiff-base, which is formed by the condensation of the α-keto acid pyruvate and an amino acid. After hydride transfer D-octopine, the product of the reductive condensation of pyruvate and L-arginine, is released from the enzyme followed by NAD^+.

As already known from Olomucki (56) the cofactor NADH must bind to OcDH first. A conformational change caused by cofactor binding first will allow subsequent binding of the other substrates. Additionally, Britton et al mentioned in 1998 (76) that the amino acid substrate should bind to the enzyme-cofactor complex in CENDH before pyruvate causing another conformational change.

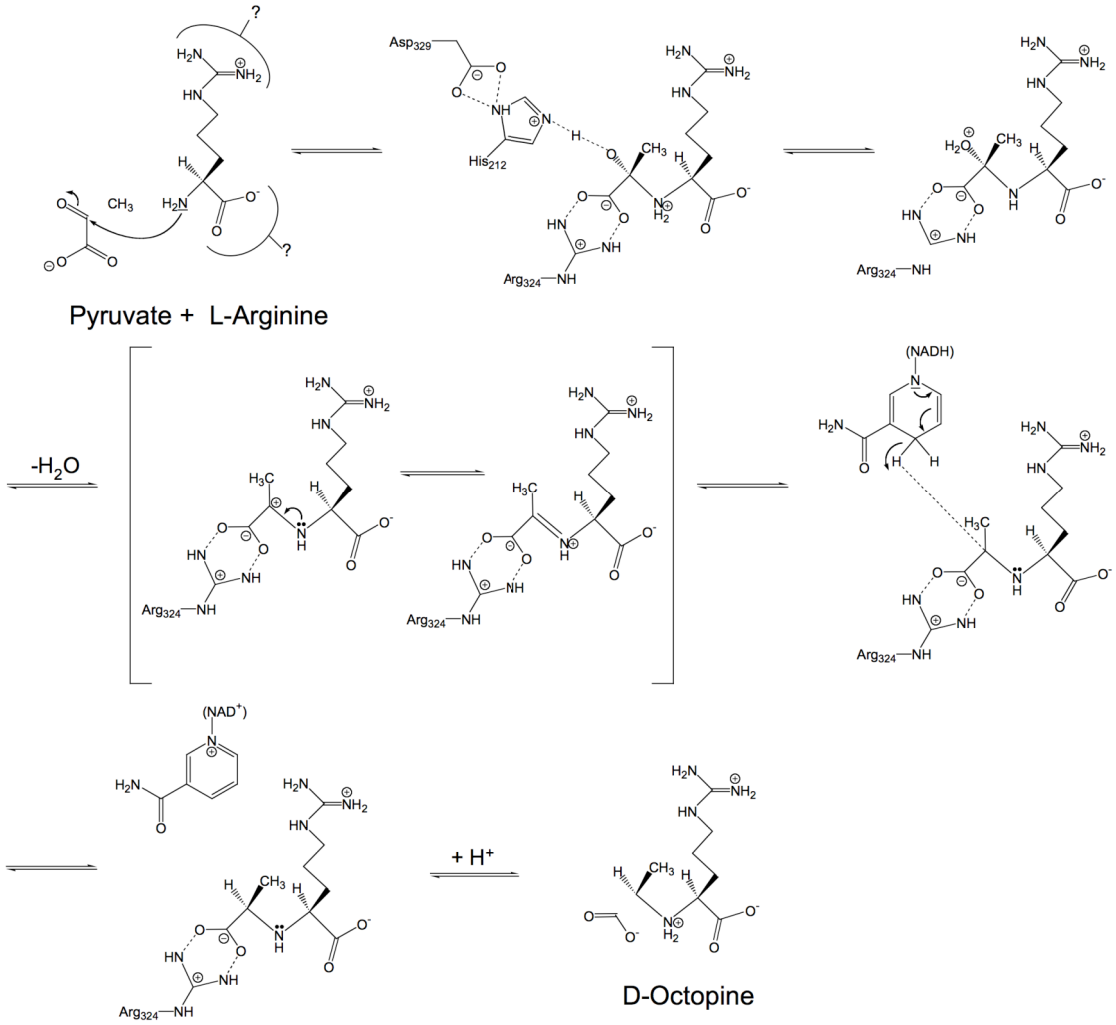

Figure 5: Possible reaction mechanism of the OcDH from *Pecten maximus*. Shown are the side chains of the amino acid building up the active site, Arginine 324, Aspartate 329 and Histidine 212. The exact fixation and binding site of the amino acid substrate are still not clarified.

This second conformational change brings the NADH-binding site in closer contact with the transition state and enables the hydride transfer. In case of ODH, thereby the abortive reduction of pyruvate to lactate is prevented.

2 Aims and objectives

The family of opine dehydrogenases have been known for several decades and several reaction mechanisms have been proposed. Besides the octopine dehydrogenase from *Pecten Maximus* several other enzymes have been investigated. A reaction mechanism composed of a catalytic triad has been proposed recently (*78*), consisting of His212, Asp329 and Arg324. To validate this reaction mechanism and to obtain a climp of the NADH, pyruvate and amino acid binding site structural studies leading to an X-ray structure will provide a detailed view and answer on substrate binding and the reaction mechanism of opine formation. Therefore the goal of this thesis was to obtain a structure of the OcDH by using X-ray crystallography, which subsequently will lead to new insight into the reaction mechanism of octopine formation. By using X-ray crystallography it would be possible to conclusively locate the substrate binding sites and detect the nature and the order of substrate binding.

3 Material and Methods

3.1 Abbreviations

3D	Three dimensional
σ	Sigma (electron density contour level)
Å	Ångström
ADP	Adenosindiphosphate
ASU	Asymmetric Unit
ATP	Adenosintriphosphate
BLAST	basic local alignment search tool
CENDH	N-(1-D-carboxyethyl)-L-Norvaline Dehydrogenase
DNA	desoxyribonucleic acid
DTT	Dithiothreitol
E.coli	Escherichia Coli
EDTA	Ethylenediaminetetra-acetic acid
GAPDH	Glycerinaldehyde-3-phosphate Dehydrogenase
Hepes	2-[4-(2-Hydroxyethyl)-1-piperazinyl]-ethansulfoacid
IR	isomorphous replacement
Kcat	Turnover rate
K_D	Dissociation constant
kDa	Kilo dalton
L	liter
LDH	Lactate dehydrogenase
MAD	multi-wavelength anomalous dispersion
MDH	Malate dehydrogenase
MES	2-(N-Morpholino)-ethansulfonacid
mg	milligram
MIR	multiple isomorphous replacement
mM	milli-Molar

NADH/ NAD^+	Nicotinamide-Adenine-Dinucleotide (oxidized/ reduced)
Ni-NTA	Nickelnitrilotracetateacid
OcDH	Octopine dehydrogenase
OpDH	Opine dehydrogenase
rmsd	root mean square deviation
SAD	single wavelength anomalous diffraction
SDS	sodium dodecyl sulfate
SDS-PAGE	sodium dodecyl sulfate-polyacrylamide gel electrophoresis
SeMet	selenomethionine
Ti	Tumor inducing
U	Unit, µmol min^{-1}
Wt	Wild type protein

3.1.1.1 One and three letter code of amino acids

Amino acid	One letter code	Three letter code	Amino acid	One letter code	Three letter code
Alanine	A	Ala	Asparagine	N	Asn
Cysteine	C	Cys	Proline	P	Pro
Aspartate	D	Asp	Arginine	R	Arg
Glutamate	E	Glu	Serine	S	Ser
Phenylalanine	F	Phe	Threonine	T	Thr
Histidine	H	His	Valine	V	Val
Isoleucine	I	Ile	Tryptophan	W	Trp
Lysine	K	Lys	Tyrosine	Y	Tyr
Leucine	L	Leu	Glycine	G	Gly
Methionine	M	Met			

3.2 Chemicals used for crystallization

1,2,3-Heptantriol	Fluka
2-Methylpentandiol	Fluka
2-tert-Butanol	Fluka
Ammonium acetate	Fluka
Ammonium sulfate	Fluka
Benzamidine	Fluka
BICINE	Fluka
Cacodylate	Fluka
Calcium chloride	Hampton Resaerch
Citratric acid anhydrous	Fluka
Ethylenglycol	Sigma
Glycerol	Carl Roth
HEPES	Fluka
Imidazol	Fluka
Lithium sulfate	Fluka
Magnesium acetate	Sigma
Magnesium chloride	Fluka
Magnesium sulfate	Fluka
MES	Fluka
MPD	Hampton Research
NaCl	Fluka
Ni-citrate	Hampton research
Nickel chloride	Sigma
Nickel chloride	Sigma
PEG 1000	Fluka
PEG 1500	Fluka
PEG 2000 MME	Fluka
PEG 3350	Hampton Research
PEG 400	Hampton Research
PEG 4000	Fluka
PEG 550 MME	Fluka

PEG 6000	Fluka
Sodium actetate	Fluka
Sodium chloride	Fluka
Sodium dihydrogen citrate anhydrous	Fluka
Tris	Fluka
Zinc sulfate	Riedel de Haen

Kits for protein crystallization	
Crystallization Basic Kit for Proteins	Sigma
Crystallization Extension Kit for Proteins	Sigma
The Mb Class	Qiagen
The Mb Class 2	Qiagen

Substrates used in protein crystallization	
L-arginine	Sigma
Pyruvate	Sigma
Agmatine	Sigma

3.3 Crystallographic methods

3.3.1 Fundamentals of crystal growth

Obtaining protein crystals still represents the major bottleneck in structure determination by X-ray crystallography. Growing protein crystals almost always involves excessive screening for suitable crystallization conditions as the search represents an almost empirical process. Crystal growth can be separated into two steps, nucleation and the enlargement of the nuclei (*79*), two processes occurring at certain regions in the phase diagram of the protein solution. Thus, obtaining information on the phase behavior of the protein solution likely minimizes the search for suitable crystallization conditions.

The solubility curve divides the phase diagram of a protein solution into two zones, the undersaturated and the supersaturated zone (Figure 6). At the solubility

curve the protein solution is in equilibrium between solid and dissolved state. The area under this curve represents the undersaturated zone, here neither nucleation nor crystals growth can occur. Above the solubility curve, in the supersaturated zone, nuclei form and subsequently crystals can grow. However, nucleation and crystal growth appear at different regions within the supersaturated area. Nuclei arise in the nucleation zone. In contrast, the metastable zone enables crystal growth but not nucleation. If very high supersaturation is reached, the nucleation process, which can be described as ordered precipitation, might be overruled by unordered precipitation. Thus, amorphous precipitate, a phenomenon often encountered in protein crystallization experiments, is formed. Therefore, the ideal crystallization experiment establishes conditions at which the protein reaches a level of supersaturation without forming amorphous precipitant but at which formation of a few nuclei is maintained. Once nuclei formed, the concentration of the protein in solution is lowered and ideally drops back into the metastable zone, where further growth of the nuclei is supported.

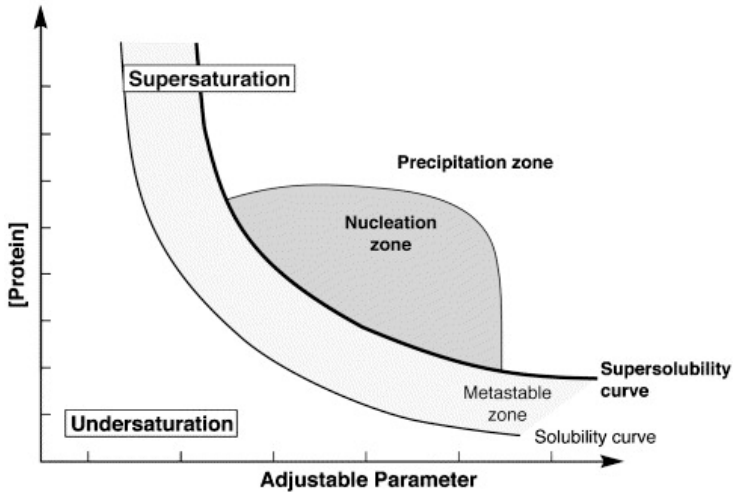

Figure 6: Example of a phase diagram of a protein solution. The solubility curve divides the phase diagram in an undersaturated and a supersaturated zone. The supersaturated zone can be further divided into the metastable, the nucleation and the precipitation zone. Taken from (*79*).

Even with the theoretical knowledge of nuclei formation and crystal growth, it is impossible to predict a priori at which conditions the protein crystallizes. In theory, the phase diagram of the protein in every crystallization experiment would need to be established and evaluated to find the most suitable condition for nucleation and

growth. However, knowing a few points in the phase diagram simplifies the empirical process of establishing crystallization conditions.

3.3.2 Means of reaching supersaturation

For a successful crystallization experiment the protein solution has to reach the supersaturated zone. This is achieved by manipulation of different variables, which influence the solubility of the protein solution. For example: temperature, salt concentration, pH-value, addition of polymers (for example poly ethylene glycol (PEG)).

For a crystallization experiment, one or more of these variables simultaneously effected in the crystallization setup. The precipitant itself may be a salt at high concentration, a polymer or an organic solvent.

Crystallization setup can be performed using different kind of techniques, micro batch, and dialysis or vapor diffusion.

3.3.3 Crystallization by vapor diffusion

In contrast to the batch method, the vapor diffusion experiment explores a wider area of the phase diagram (Figure 7) thereby increasing the probability of reaching the nucleation zone. For this experiment the protein is mixed with a precipitant solution (point 0 in the phase diagram). Then a drop of this mixture is placed over a reservoir, containing the precipitant solution. The experiment is sealed and the drop is left to equilibrate with the reservoir solution, which exceeds the volume of the drop at least 100-500 times. In ideal vapor diffusion setups the equilibration process initiate that the protein solution goes through the phase diagram, from the under saturated zone to the nucleation zone (endpoint E). During the equilibration nuclei can form, thus the protein concentration in solution is lowered and the crystals can grow. The time that the protein needs to pass all zones can be influenced by the variations in the volume of mother liquid, and or the ratio of the protein-mother liquid inside the crystallization drop.

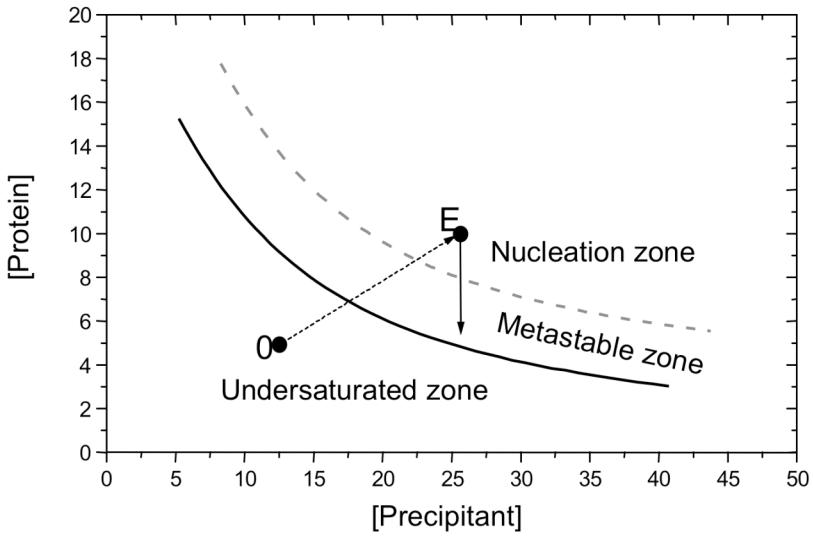

Figure 7: The process of a successful vapor diffusion experiment exemplified in the phase diagram.

The vapor diffusion method can be performed as sitting drop, hanging drop or sandwich drop as depicted in Figure 8 on the left, middle and right, respectively.

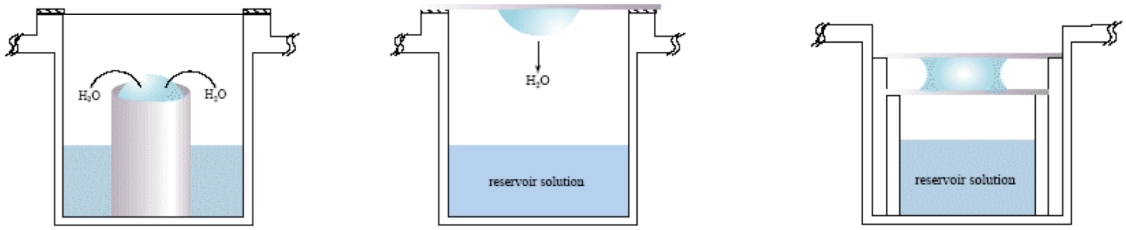

Figure 8: Different methods of setting up a vapor diffusion experiment. The sitting drop (left), the hanging drop (middle) and the sandwich drop (right) are exemplified. Adapted from Hampton Research (www.hamptonresearch.com).

The drop surface influences the kinetic of reaching the equilibrium between the drop and the reservoir, thereby often influencing the amount of crystals as well as their size.

3.3.4 Batch/microbatch crystallization and Dialysis

In earlier days the batch crystallization was applied to crystallize substances. Supersaturation is achieved by directly mixing the precipitant solution with the protein solution. One drawback of this method is that only one point, the endpoint of the

crystallization, which is reached directly after mixing the components, is investigated in the experiment. If this lies within the nucleation zone, the protein concentration in solution is lowered and possibly the metastable zone is reached. Since the invention of vapor diffusion methods the batch crystallization has lost its importance.

The dialysis experiment represents a rather tedious setup and necessitates high quantities of protein. This is probably the reason why in the last decade the application of the dialysis experiment became less important. However, if the protein shows an inverse phase diagram, the dialysis experiment represents a useful method for crystallization. In this technique the protein solution is placed in a micro dialysis bottom (Figure 9) and the setup is covered with a semi permeable dialysis membrane. By placing the micro dialysis button in water, the protein solution is slowly equilibrated against the surrounding solution, thus lowering the buffer and salt concentration of the setup ("salting in" effect). When the nucleation zone is reached crystals can start to form and, once reaching the metastable zone, grow to their final size. Furthermore, proteins with a "normal" phase diagram can also be crystallized with the dialysis method. In this case, a precipitant solution, containing precipitant, buffer and/or salt, is used as dialysis solution. However, this "salting out" application has been widely replaced by the vapor diffusion experiment.

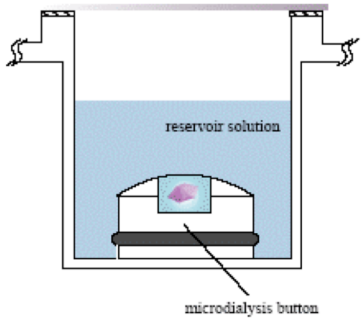

Figure 9: A dialysis setup. The protein solution is placed in the microdialysis button and dialyzed against a reservoir. Adapted from Hampton Research (www.hamptonresearch.com)**.**

3.3.5 Choice of crystallization conditions

Different proteins show different behavior in various solutions. In principle, it is impossible to predict a phase diagram for a protein solution *a prior*. Thus, to explore the best crystallization conditions for a protein, an empirical approach based on trial and error has to be done. The most common crystallization conditions are summarized in so called crystal screens, which are commercially available. Often these commercially available screens are used as starting point in crystallization experiments.

A grid screen is a systematic approach to evaluate crystallization conditions. In grid screens two parameters are varied, while the others are kept constant. Hereby, the steps can be varied in their size allowing for broader or narrow screening. However, a disadvantage of the grid screen is the necessity to explore many different conditions before a successful condition is found. With the emergence of sparse matrix screens (*80*) the application of grid screens was greatly reduced. Nowadays, mostly optimization of an initial successful condition is performed based on grid screening. In 1991 Jancarik and Kim published a first set of 50 independent, crystallization conditions (*80*). These conditions were empirically derived based on the knowledge of so-far successful crystallization conditions. These sparse matrix screens are composed of solutions which are very different in their composition. A broad variety of different buffers, salts and precipitants can be evaluated in one of these screen. Sparse matrix screens are therefore often used as starting point in crystallization experiments.

3.4 Crystallization of OcDH

Crystallization experiments with OcDH were performed as vapor diffusion experiments in either 96-well robot set ups or 24-well setup. Crystallization trials were carried out using the hanging-drop vapor diffusion method at 12 °C. Homogenous OcDH-His_5 was dialyzed against 10 mM Hepes pH 7.0, containing 1 mM EDTA and 1 mM DTT and concentrated to 20 mg mL^{-1} prior to crystallization. For crystallization of OcDH with co-substrate, 0.8 mM NADH was added to the protein solution. Crystals were grown by mixing protein solution with a reservoir solution containing 100 mM

MES pH 7.0 and Na-citrate ranging from 1.0 to 1.2 M, in a 1:1 ratio. Crystals normally grew in 3 to 5 days. Suitable crystals were cryo protected using 100 mM MES pH 7.0, 30 % (v/v) ethylene glycol, 1.15 mM Na-citrate and frozen in liquid nitrogen.
L-arginine bound crystals were obtained by soaking NADH bound OcDH crystals in 100 mM MES pH 7.0, 1.15 M Na-citrate, 0.8 mM NADH containing 10 mM L-arginine for at least 24 h and frozen as described before. Pyruvate bound crystals were obtained also by soaking the crystals in 100 mM MES pH 7.0, 1.15 M Na-citrate, 0.8 mM NADH and 10 mM pyruvate for at least 8 hours. The substrate bound crystals were frozen exactly same as unliganded OcDH as described above.

3.5 Basic principles of X-ray crystallography

3.5.1 Crystal systems and space groups

A crystal is build up by a periodic space-filling arrangement of the building block of a crystal called a unit cell. Hereby, the unit cells can be transferred into each other via x,y,z translations. The unit cell is defined by its lattice parameters, the cell lengths a, b and c as well as the cell angles α, β and γ. There are seven uniquely defined crystal systems. The molecules inside a unit cell can be symmetry related. Possible symmetry operations that a crystal can exhibit are mirror planes, inversion centers, rotation axis and screw axis. However, due to the chirality of biomolecules, mirror planes and inversion centers are not allowed in protein crystals leaving rotation axis or screw axis as the only possible symmetry applications. Combining the unit cell parameters with these possible symmetry operations establishes the space groups. In protein crystals 65 space groups are possible. The symmetry is defining asymmetric units (ASUs) are symmetric to each other by symmetry operators specific for the space groups.

Inside the ASUs the protein molecules are not symmetry related. Therfor the ASUs are the smallest building blocks inside protein crystals.
Table 1 lists the seven possible crystal systems and their minimum symmetry elements.

Crystal system	Conditions for cell geometry	Minimal symmetry element
Triclinic	None	None
Monoclinic	α = γ = 90°, β ≠ 90°	One 2-fold axis
Orthorhombic	α = β = γ = 90°	Three perpendicular 2-fold axes
Tetragonal	a = b; α = β = γ = 90°	One 4-fold axis
Trigonal	a = b; α = β = 90° γ = 120°	One 3-fold axis
Hexagonal	a = b; α = β = 90° γ = 120°	One 6-fold axis
Cubic	a = b = c; α = β = γ = 90°	Four 3-fold axes

Table 1: The seven crystal systems, their cell geometry and minimal symmetry elements. Taken from (*81*).

3.6 Proteins and X-rays

The scattering of X-rays by protein crystals can be described as an interaction of the electromagnetic incident X-ray beam with the electrons of the atoms. The incident beam forces the electrons to oscillate in the same frequency. Upon returning to the unexcited state radiation is emitted by the electrons, which has the same wavelength as the X-ray beam. However, the phase is shifted, initiating the biggest draw back in structure determination by X-ray crystallography.

For describing waves often the Argand diagram is used. Describing waves in complex numbers. Expressed as $|z|e^{i\Phi}$ where $|z|$ is the amplitude and Φ is the phase. By representing a complex number in an Argand diagram (Figure 10) with the real part written on the x-axis and the imaginary part displayed on the y-axis, the following equation can be derived.

$$z = x + iy = |z|(\cos\phi + i\sin\phi) = |z|e^{i\phi}$$

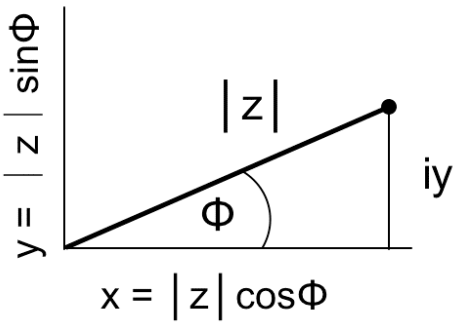

Figure 10 Representation of a complex number in an Argand diagram.

With a given wavelength a wave can be represented as a single complex number, determined by its amplitude and its phase.

$$W = Ae^{i(2\pi x/\lambda+\phi)} \qquad (2.4)$$

3.7 Principles of diffraction - Laue equations, Bragg´s law and the Ewald construction

To explain the diffraction of a beam on a three-dimensional lattice, different approaches can be used. Max von Laue discovered X-ray diffraction in 1912, and formulated the Laue equations. Rather straightforward and easy to understand is Bragg´s law, introduced 1913 by Lawrence Bragg.

To understand the Laue equations we can first consider the interference of rays on a one dimensional lattice being represented by equally spaced scatterers on a line Figure 11.

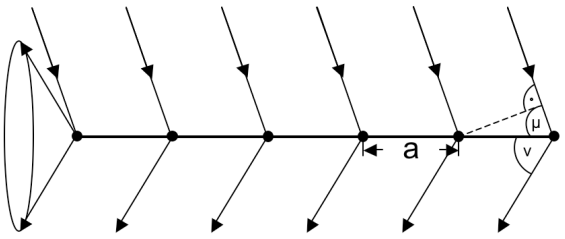

Figure 11: Interference of rays in an one dimensional lattice with the spacing a of the scatterers. The angle of the incident beam is μ. The outgoing rays are scattered at an angle v. Adapted from Massa (*82*).

Positive interference of the scattered waves is only occurring if all outgoing waves are in phase with each other. Therefore, the path-difference of the incoming wave and the outgoing wave has to be nλ, with n = 0, 1, 2, 3... . If the incident beam forms an angle μ with the line of scatterers, diffraction only occurs if the beam is diffracted with an angle v relative to the line of scatterers. As the diffracted wave is spreading in all directions, a cone, called Laue cone, can be formed with the opening of 2v that represents the directions of the possible diffracted beams.
The condition stated above can be formulated as follows:

$$a\cos\mu_a + a\cos\nu_a = n\lambda \qquad (2.5)$$

A crystal lattice is built up of lines of atoms, or scatterers, in all three dimensions. Therefore, two more Laue equations for the other two dimensions have to be formulated.

$$a\cos\mu_a + a\cos\nu_a = n\lambda$$

$$b\cos\mu_b + b\cos\nu_b = n\lambda$$

$$c\cos\mu_c + c\cos\nu_c = n\lambda \qquad (2.6)$$

Only if all three equations are satisfied simultaneously or all three Laue cones intersect at one point, diffraction is possible.Bragg showed that X-rays impinging on two parallel planes which exhibit an interplanar spacing of d_{hkl}, only show diffraction if the angle of the incoming beam is equal to the angle of the outgoing beam and their path-difference is nλ.

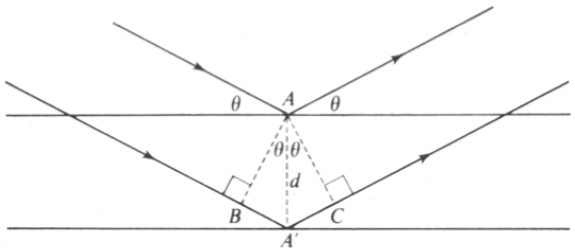

Figure 12: Reflection of parallel beams on parallel planes with interplanar spacing d. Adapted from Woolfson(*83*).

Bragg´s law is formulated in the following equation:

$$n\lambda = 2d_{hkl}\sin\theta \qquad (2.7)$$

If the path difference is one wavelength n = 1, if it is two wavelength n = 2 and so on. n determines the order of the reflection.
Braggs law can also be expressed as

$$\lambda = 2d_{hkl}\sin\theta \qquad (2.8)$$

where each reflection is generated by a set of planes with the spacing $d_{nk,nh,nl}$.

In a unit cell many different sets of parallel planes can be inscribed. A set of planes intersects the unit cell at the points h, k and l and is defined by these indices, also called Miller indices. Here, h describes the intersection of the plane with the cell edge a. If the edge a is intersected a/n, h exposes the value n. The same principle applies for k and l intersecting the cell edges b and c, respectively.
With this background it is easily understood that higher order reflections are generated by a set of planes exhibiting smaller spacing and thus carry higher resolution information.

To construct the direction of scattering, the reciprocal lattice and the Ewald construction was introduced. A set of parallel planes, on which diffraction of a beam can occur, can be also expressed by a vector S which has the length of the spacing between the planes and is oriented along their normal. For each set of hkl-planes such a vector can be constructed, thereby the origin of the reciprocal lattice is the starting point of each of these vectors. The end of the vector determines a point in the reciprocal lattice. Due to the reciprocal relation sets of planes with higher hkl-indices display a smaller vector.

By constructing Bragg´s law in reciprocal space and taking the reciprocal lattice in consideration the diffraction direction can be determined. This construction, represented in two dimensions (Figure 13), is also called Ewald sphere. The incident

beam s_0, exhibiting a length of $1/\lambda$, is directed to the origin O of the reciprocal lattice. Then a circle with radius $1/\lambda$ and its centre M being placed on the line s_0 is drawn. Diffraction occurs if the vector S, with its start at the origin O, has its endpoint P on the Ewald sphere. Under these conditions the resulting scattered beam is s.

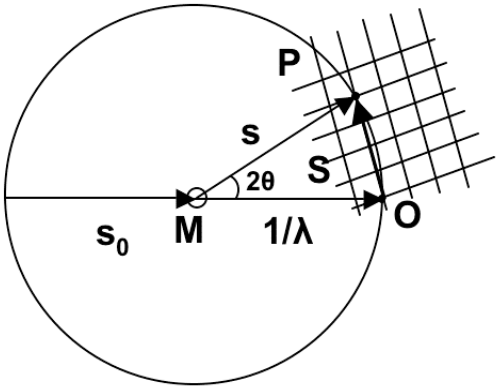

Figure 13: The Ewald construction. The Ewald construction relates the incident beam with the angle of reflection with the help of the reciprocal lattice. The construction of the Ewald circle is explained in the text.

3.7.1 Structure factors and electron density

The scattered ray, which produces a reflection, can be described as a Fourier series of scattered rays generated by the individual atoms in a unit cell. The Fourier series that describes this term is called a structure factor equation. Thus, a structure factor is a wave composed of contributions of all atoms in a unit cell.
Diffraction occurs by interaction of the impinging beam with the electrons of a molecule. Therefore, the diffracted beam contains information of the electron clouds of a molecule. The goal of crystallography is to calculate the electron density function $\rho(x,y,z)$ in dependence of the coordinates x, y and z, which is a periodic function as it repeats itself due to the regular array of a crystal.
Imagining that the electron density in the unit cell is composed of small volume elements, each structure factor can be written as a Fourier summation over these volume elements. Each term of this summation represents the diffraction of the electrons constituting to this volume element, i.e. the diffraction of the averaged electron density within this volume element.
Thus, the structure factor F_{hkl} can be expressed by a Fourier series with the

contribution of the averaged electron density of each of these volume elements or with infinitesimal small volume elements with the average values of ρ(x,y,z).

$$F_{hkl} = \int_V \rho(x,y,z) e^{2\pi i(hx+ky+lz)} dV \qquad (2.9)$$

As this equation is a Fourier series, its transform, also a Fourier series with the structure factor F_{hkl} as amplitude, can be written as

$$\rho(x,y,z) = \frac{1}{V} \sum_h \sum_k \sum_l F_{hkl} e^{-2\pi i(hx+ky+lz)} \qquad (2.10)$$

3.8 The phase problem, a crystallographer's nightmare

The aim of the crystallographic process is to obtain an interpretable electron density map covering the whole unit cell. The electron density distribution is given by a Fourier summation (see equation 2.10) with structure factors presenting the amplitudes of the waves that compose the Fourier series.
The structure factor describes a diffracted X-ray beam and thereby also expresses a wave function with a frequency equal to the frequency of the incident X-ray beam and an amplitude $|F(hkl)|$ which is proportional to the square root of the measured intensities I(hkl). However, the detectors used in a diffraction experiment can only detect the amplitude of the waves reflected in the spot intensity. The phase of a structure factor is lost during data collection. Thereby the calculation of the electron density map necessitates phase information of each structure factor, which has to be extracted indirectly. Different methods have been developed to gain phase information. The basic concept will be described below. All methods used to obtain phases rely on the calcultation of the Patterson function.

3.8.1 The Patterson function

The Patterson function P(uvw), developed in 1934 by Lyndo Patterson, is also called self convolution of a structure. In principle it is a Fourier summation like the

electron density function presented in equation 2.10 with the difference that in a Patterson function no structure factors are used as coefficients but the measured intensities of the reflections. Thus, no phase information is needed for the calculation of a Patterson function. The map can be calculated directly from the data obtained intensities by the diffraction experiment.

$$P(uvw) = \frac{1}{V} \sum_{h=-\infty}^{\infty} \sum_{k=-\infty}^{\infty} \sum_{l=-\infty}^{\infty} \left|F_{hkl}\right|^2 \cos\left(2\pi\left(hu + kv + lw\right)\right) \quad (2.11)$$

Here u, v and w represent vectors locating a point in the Patterson map.
Another way of expressing the Patterson function is given in equation 2.12 where u and r_1 represent vectors.

$$P(\vec{u}) = \int_{r_1} \rho\left(\vec{r_1}\right) \times \rho\left(\vec{r_1} + \vec{u}\right) d\vec{r_1} \quad (2.12)$$

A peak in the Patterson map at (uvw) means that two atoms are placed in the real cell which have the coordinates (x,y,z) and (x + u, y + v, z + w), with the Patterson function relating these atoms.

3.9 Solving the phase problem

3.9.1 Isomorphous replacement

Heavy atoms like mercury, platinum and bromide, expose many electrons concentrated in a small sphere. When implemented in a protein crystal they strongly contribute to its diffraction. By comparing the diffraction pattern of a protein crystal containing heavy atoms with the diffraction pattern of a “native” crystal, i.e. without heavy atoms, differences in the intensities of the reflections are revealed. This phenomen can only be seen when the to datasets are similar in quality and isomorph to each other, meaning that the normal protein intenstites are the same, as well as the unit cell and spacegroup. The observed differences can help to estimate the

phases of the structure factors.

A prerequisite of isomorphous replacement is the availability of at least two isomorphous crystals, a native and a heavy atom incorporated crystal. This is often achieved by co-crystallization with a heavy atom or soaking a heavy atom into native crystal in solution. The most important feature of the heavy atom of choice is that it is bound specifically to the protein, and to each protein in the unit cell. If the heavy atom is located differently in each protein in the crystals the obtained phases will not be strong enough for structure determination, which normally is described with the term occupancy which, is given as a number from 0 to 1 for 0 to 100% occupation of the heavy atom site.

The first step of isomorphous replacement is to locate the heavy atom. This is achieved by employing a difference Patterson function. In this Patterson function the difference in the structure factor amplitudes of the derivative and the native crystal, $|F_{PH}| - |F_P|$, is used as coefficient.

$$P(uvw) = \frac{1}{V} \sum_{h=-\infty}^{\infty} \sum_{k=-\infty}^{\infty} \sum_{l=-\infty}^{\infty} \left(|F_{PH}(hkl)| - |F_P(hkl)| \right)^2 \cos\left(2\pi\left(hu + kv + lw\right)\right) \quad (2.13)$$

In this step for each set of heavy atoms two possible positions are determined, (x + u, y + v, z + w) and (x - u, y - v, z - w). Structure factors produced solely by the heavy atoms are calculated and further employed in phase determination. As two possible positions for the heavy atoms are obtained, both have to be employed in the process and later it is evaluated which of these sets gives the right hand.

As all atoms in the unit cell contribute to each structure factor, the structure factors of the derivative crystal are composed of the contribution of the protein without heavy atoms and the contribution of the heavy atoms alone.

For any structure factor this can be formulated as:

$$F_{PH} = F_P + F_H \quad (2.14)$$

As we know the position of the heavy atoms we can solve this vector equation for F_P. Figure 14A shows the graphic representation of this procedure, also known as Harker

construction.

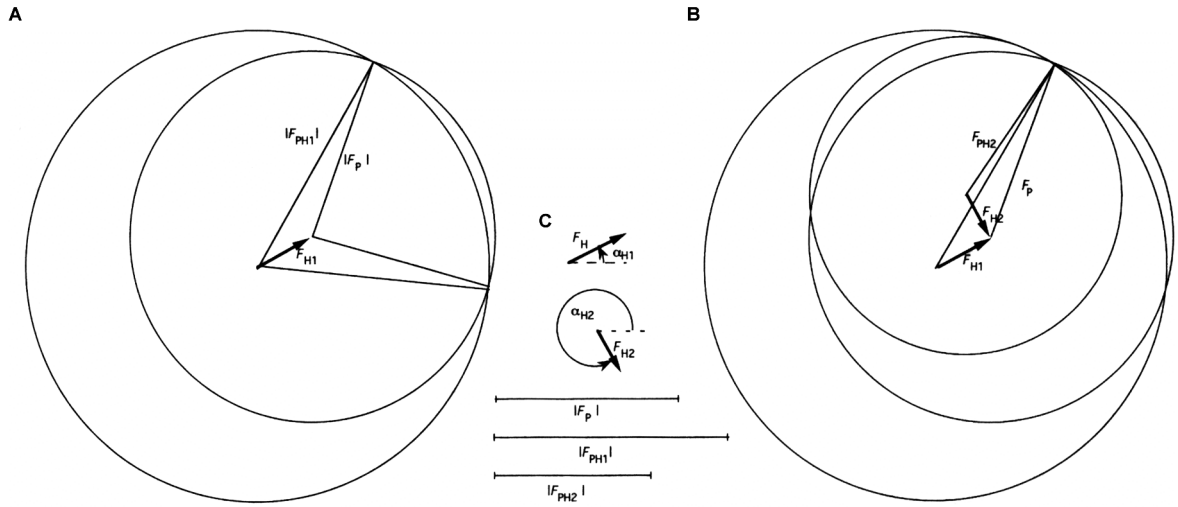

Figure 14: Harker construction for the graphical determination of phases. A The determination of phases with one heavy atom derivative is shown. **B** Determination with two heavy atom derivatives. C Known variables used for the Harker construction. Adapted from Blow (*84*).

The length of the vectors F_{PH} and F_P is defined by the measured intensities of the derivative and the native dataset. Besides, the vector F_H is known from the determination of the heavy atom positions by the difference Patterson function. First a circle with the radius of $|F_P|$ is sketched which represents all possible phase angles of F_P. The vector F_H is drawn such that the vector ends at the centre of the circle. The beginning of the vector is taken as the center for a second circle with a radius of $|F_{PH}|$. This circle represents all possible phase angles for F_{PH}. The vector equation given in 2.14 holds true at the intersection of the two circles. Thus, two possible phases for F_P are determined. The determination of two more possible phases is achieved by a second Harker construction using a second derivative. The intersection point of a construct using both heavy atom derivatives determines the phase for the structure factor F_P (Figure 14B).

In this way structure factors for all values of (h,k,l) can be determined and an initial electron density map can be calculated using equation 2.10. Dependent on the decision made for the set of heavy atoms either an electron density map for a protein with L-amino acids and right-handed α-helices or its mirror image is displayed. The correct choice of heavy atoms has to be evaluated by the crystallographer with the help of the resulting electron density map.

3.9.2 Anomalous Diffraction

A second method to determine phases exploits the characteristic of heavy atoms to change their scattering behavior at certain wavelengths (*85-87*). If the wavelength of the incident X-ray beam approaches the absorption edge of a specific heavy atom, the assumption that the scattering electron is a free electron holds no longer true. The electron also absorbs energy and thereby is promoted into a higher electronic state. Due to the absorption of photons the total coherent scattering is reduced and the phase of the coherently scattered rays is changed (Figure 15).

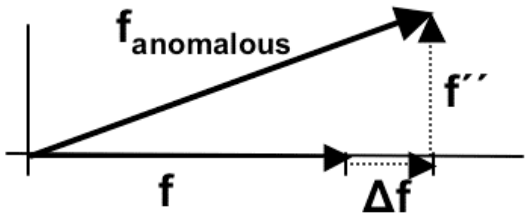

Figure 15: The anomalous scattering of a heavy atom at its absorption edge. The anomalous scattering is composed of a real (Δf) and an imaginary (f´´) component.

The scattering factor of an anomalous atom is composed of a real and an imaginary component and can be written as:

$$f_{anomalous} = f + \Delta f + if'' \qquad (2.15)$$

Due to anomalous scattering the structure factors of a Friedel pair, F_{hkl} and F_{-h-k-l}, normally showing same amplitudes and a relation of their phase by 180°, do not exhibit the same amplitudes and their phases become independent.
This effect is exploited in single or multiple wavelength anomalous diffraction (SAD or MAD). To obtain phases with either SAD or MAD, often the amino acid methionine in a protein molecule is replaced with Se-methionine. Se exhibits an absorption edge at a wavelength at 0.9795 Å. The imaginary component f´´ and the real component Δf of the anomalous scattering of Se is presented in Figure 16. Also three wavelengths

are shown at which an optimum MAD experiment can be conducted.

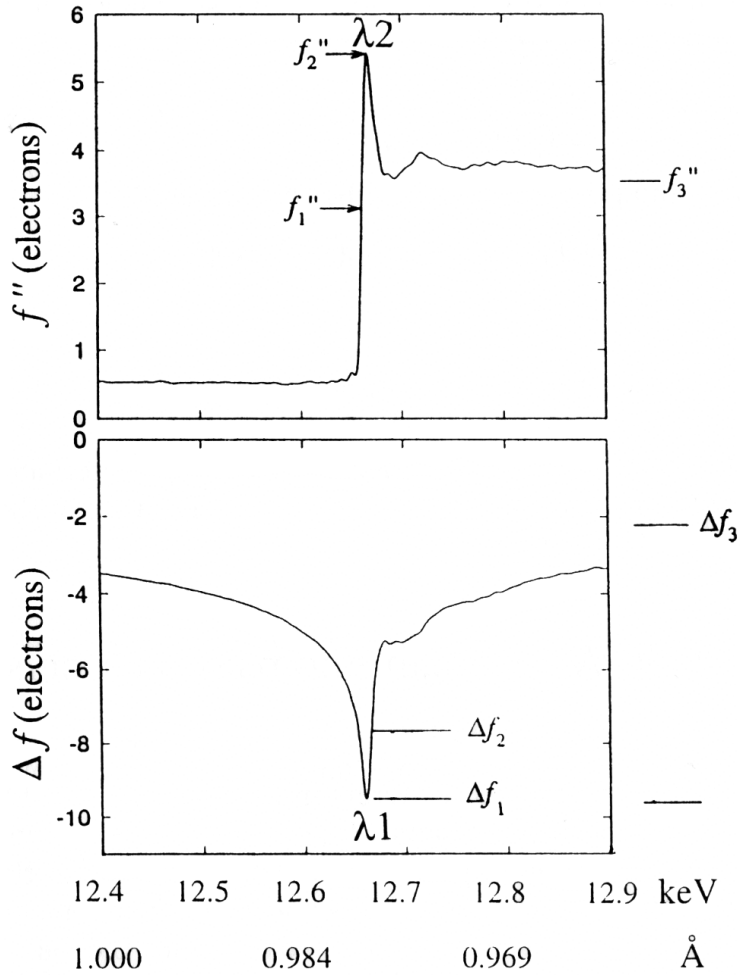

Figure 16: The composition of the anomalous scattering of a Se-atom, when the absorption edge is approached. Δf and f´´ represent the real and the imaginary component, respectively. In an MAD experiment data is collected at different wavelengths. The maximum of Δf is reached at wavelength λ_1. At λ_2 the imaginary component of the anomalous scattering shows its maximum. The third wavelength λ_3 is not shown in the pane. Adapted from Drenth (*81*).

For an MAD experiment, datasets at three different wavelengths are collected on for example a single seleno-methionine incorporated crystal. These are the wavelengths λ_1, λ_2 and λ_3, also called the inflection, peak and remote wavelength. λ_1 is chosen such that the real component Δf of the anomalous scattering is at its minimum. At λ_2 the imaginary component f´´ of the anomalous scattering is at its maximum. λ_3 represents a wavelength where the anomalous scattering is minimized. To obtain phases with a MAD experiment two different processes, the anomalous

MAD and the isomorphous MAD are distinguished. The latter process uses the large differences in the real component Δf of the anomalous scattering, whereas the relatively small contribution of the imaginary component f´´ is removed by averaging the Friedel mates of the inflection and the peak dataset. Again, the heavy atom positions can be determined with the help of a difference Patterson function for the remote and inflection datasets. The determination of two possible phases is analogous to the phase determination in a single isomorphous replacement by construction of intersecting Harker circles.

In a second step the difference between the Friedel mates, which reaches a maximum in the peak dataset, is utilized to calculate an anomalous difference Patterson function. Harker construction yields another set of phase angles. By a combined Harker construction with the isomorphous and the anomalous component one possible phase angle is obtained.

By collecting only one dataset at a single wavelength (SAD), the peakwavelength, can also already give enough information. Here the procedure is basically the same as in MAD experiments. The difference between the Friedel mates, which reaches a maximum in the peak dataset, is utilized to calculate an anomalous difference Patterson function. Harker construction yields another set of phase angles. When using this MAD or SAD successfully it is worth to mention that the data collection strategy should be shlightly change with respect to the resolution , redundancy, and R merge.

To solve a structure with MAD or SAD the most important paramter in data collections shifts to R—merge and redundancy. The resolution is not that critical as the error in the data set which gets smaller when the intensity can be averaged over an higher number of measured spots. Further more the wavelength of the X-ray source should be adjustable during data collection that, at the moment can only be achieved at specialized tunable beam lines present for example the synchrotrons DESY, SLS and ESRF.

3.10 Molecular replacement

When the structure of an homologues or the same protein is available (reference model) and the structure of a mutant of this protein or the protein in

complex with a ligand has to be determined, the available phase information of the known structure can be exploited to obtain initial phases for the new crystallized protein. This method is called molecular replacement and in principle can be applied to all proteins showing similar three-dimensional structure, which is often assessed by the homology of their primary sequences.

The existing model needs to be oriented in the new unit cell in such way that the resulting phases for the reference model apply to the new one. Structure factors can be calculated from the newly positioned reference model. The phases of these calculated structure factors are deduced for calculating an initial electron density utilizing the new diffraction data.

The process of orienting the model in the new unit cell is divided in two steps. First the orientation of the model, independent of its position in the unit cell, needs to be found by rotating the model. In a second step the correct position within the unit cell is assigned by transition of the model in three dimensions.
Both steps can be performed with the help of the Patterson function. Within the Patterson map the cross- and the self-vector peaks are revealed. Vectors originating from two atoms of the same molecule in the unit cell are called self-vectors. If the two atoms belong to different molecules within the unit cell, the vectors are called cross-vectors. As the distance between two atoms of different molecules mostly is larger than the distance between atoms within the same molecule the peaks in the Patterson map originating from self-vectors are concentrated around the origin. Peaks from cross-vectors are located further away. The correct orientation of the model can be ascertained with the help of self-vectors whereas the translation, used to position the model correctly in the unit cell, is achieved with the help of cross-vectors.

The Patterson function describes the vector between two atoms independent of the position of the atoms in the unit cell. A rotation of a molecule in real space would result in the rotation of its Patterson map around the origin of the map. Thus, if the Patterson map of the model is rotated, a position is revealed where the model Patterson map overlays best with the Patterson map derived of the new reflection data. Thus, information about the rotation function can be extracted (Figure 17).

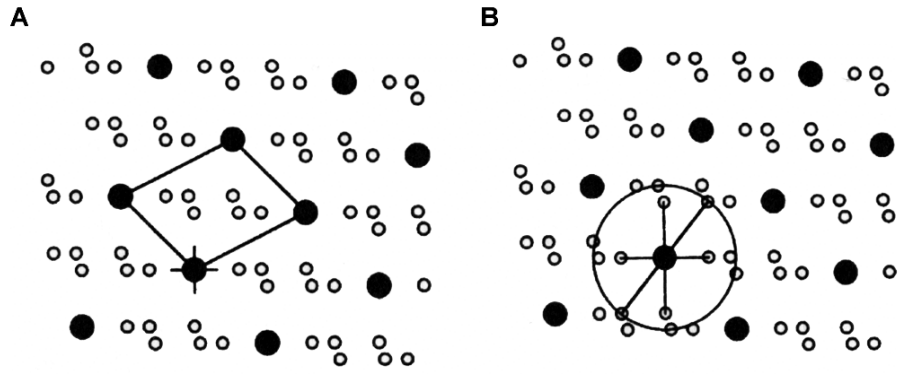

Figure 17: The rotation function search. A The Patterson map of the unknown crystal structure is outlined with its unit cell. **B** The Patterson function of the search model is rotated such that the peaks of the model function overlay with the Patterson map of the unknown crystal. The rotation function can be determined. Adapted from Blow(*84*).

After the determination of the correct orientation of the model the next step is to position the correctly oriented model in the unit cell. This step is only needed in cases where the crystal exhibits symmetry other than the lattice symmetry and the crystal origin needs to be defined relative to the rotation axes. Therefore, the position of the rotation axes in the crystal is determined relative to the orientation of the model. This can be achieved by calculating a Patterson function for the model with an arbitrary chosen rotation axis. The location of the axis influences the position of the Patterson peaks but not their constellation Figure 18. Comparing this Patterson function with the Patterson map of the reflections reveals the self-vectors on the same position and the cross-vectors being displaced. With the help of the translation function a vector can be determined which relates the cross-vector peaks, as shown in a two-dimensional example in Figure 18. By doubling this vector and applying it to the arbitrary chosen axis of the model the position of the real axis is revealed. Thus, the position of the model relative to the rotation axes can be determined.

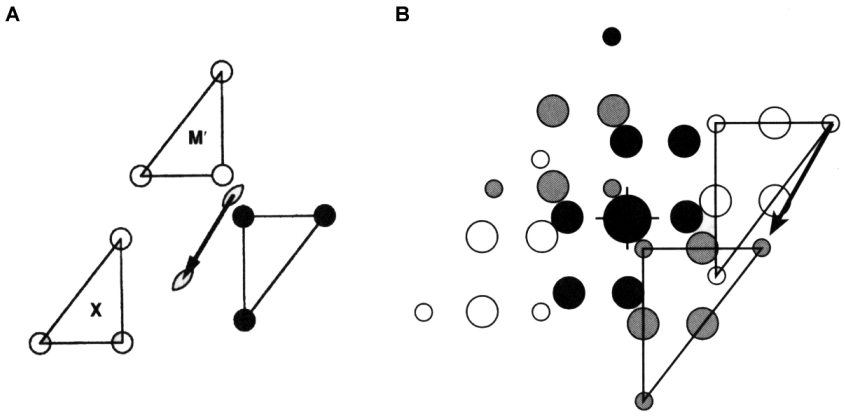

Figure 18: The translation function search to obtain a twofold axis of an unknown structure relative to the origin of the model structure. A The symmetry related model M´ generated by an arbitrary chosen twofold axis. By translation M´ can be superimposed with the unknown structure X. Therefore, the vector of this translation applied on the arbitrary chosen axis relates the model structure with the unknown structure X. **B** Using a common origin the Patterson functions of the search model and MM´ and the unknown structure are overlaid. The peaks resulting from self-vectors are indicated in black, those of cross-vectors are indicated in open circles (X) or as grey circles (MM´). The vector which relates the cross-vector peaks of the model MM´ with the cross-vector peaks of X is double the vector that relates the twofold axes shown in A. Adapted from Blow (*84*).

3.11 Dataset collection from crystals of OcDH

Datasets of OcDH with and without substrates were collected at the BW7A and X12 beamlines, EMBL, at the DESY synchrotron, Hamburg (Germany). Detailed information on data collection statistics are shown in Table 1. A single SAD dataset of OcDH-NADH protein crystals containing seleno methionine was collected at beamline X12 (EMBL, DESY, Hamburg) at resolution of 2.8 Å. For all datasets the optimal data collection strategy was calculated using the program BEST (*88*). All datasets were processed with DENZO (*89*) or the XDS program packages. The seleno- methionine postions and afterwards initial phases as well as automated model building was performed using the program AUTORICKSHAW (*90*). Eleven of the twelve possible seleno-methionine sites were initially found. The model was further refined using REFMAC5 (*91*) and COOT (*92*) resulting in a complete model of the OcDH-NADH complex. This model was used as the template to phase the high resolution dataset of OcDH at 2.1 Å using the molecular replacement program PHASER (*93*). The quality of the electron density allowed automatic water picking

using Arp/Warp (*94*), which where manually checked on their correct assignment. Two other datasets were collected, OcDH-NADH/L-arginine at 3.1 Å and OcDH-NADH/pyruvate at 2.6 Å. These datasets were phased using the molecular replacement program PHASER (*93*), and futher refined using REFMAC5 (*91*) and COOT (*92*). Dataset set and refinements statistics are listed in Table 3 and 4. In the OcDH-NADH/pyruvate structure however, the density of one loop (amino acids 281-290) was poor and excluded from the final model.

3.12 Computer programs

	Program	Reference
Data collection and processing		
	BEST	(*88*)
	XDS	(*95*)
	DENZO	(*89*)
Structure calculation and building		
	AUTORICKSHAW	(*90*)
	SOLVE /RESOLVE	(*96*)
	SHELXE	(*96, 97*)
Structure refinement		
	CCP4I	
	PHASER	(*93*)
	REFMAC5	(*91*)
Structure Validation		
	PROCHECK	(*98*)
	DYNDOME	(*99*)

Table 2: Programs used to process the datasets and programs used to calculate, refine and validate the structure of OcDH.

3.13 Analysis of the obtained models and graphical visualization

The quality of the obtained models was assessed with the program PROCHECK(*98*). Secondary structure elements were detected with Stride(*100*). To detect possible hinges and rigid bodies the HingeProt server was utilized(*101*). The rotational movement of the subdomain was analyzed DynDom. All representations of structures were generated with PyMOL(*102*).

3.14 Structure deposition

Coordinates have been deposited in the protein data bank (www.pdb.org) under accession codes 3C7A (ODH-NADH), 3C7C (ODH-NADH/L-arginine) and 3C7D (ODH-NADH/pyruvate).

4 Results

4.1 Crystallisation of OcDH

The cloning and heterologous overexpression increased the yield of OcDH (*78*), allowing biochemical and structural characterisation. For crystallisation purposes, three different constructs of OcDH, OcDH-tagless, OcDH-His_5 and OcDH-$LEHis_6$, respectively were previously cloned (*57, 103*). In OcDH-$LEHis_6$, due to a vector artefact two additional residues, a leucine and a glutamate, were encoded between OcDH and the His-tag. The His-tags were placed at the C-terminus as the important NADH binding site is encoded in the first N-terminal 20 amino acids. André Müller from the Zoophysiology group of the Heinrich-Heine University of Düsseldorf kindly provided the purified protein solutions.

OcDH-His_5 and OcDH-$LEHis_6$ were purified by Ni-NTA chromatography yielding a protein sample with purity larger 98%. The homogeneity of the sample was secured by an additional size exclusion chromatography step. Thus, homogenous OcDH-His_5 or OcDH-His_6 could be isolated as shown on silver stained SDS PAGE gel, yielding almost 20 mg homogenous enzyme per liter of cell culture for both species. The purification of OcDH-tagless required several chromatography steps, yielding 3-5 mg per liter of cell culture, with a purity >98%. In terms of activity, the three different constructs were undistinguishable (data not shown), and comparable to OcDH purified directly from *Pecten maximus* (*30*).

Although extensively tried, the constructs OcDH-tagless and OcDH-$LEHis_6$ never yielded any crystals. Probably OcDH adopts multiple conformations, which prevented crystal formation. The purified OcDH-His_5 however, yielded small crystals when using a commercial screen. Self-made grid screens subsequently optimized the initial conditions.

For initial crystallisation conditions of OcDH, the vapour diffusion method using sitting drops was used in a 96 well plate setup. Commercially available sparse matrix screens (Sigma) were used to examine a large number of crystallisation conditions. The protein concentration was empirically chosen and set at 10 mg/ml, however, at

this concentration OcDH appeared stable and no aggregation, precipitation or small crystals were observed. Therefore the protein concentration was increased to 20 mg/ml. This yielded initial crystals using the same screens, which were further optimized. Mixing protein solution with reservoir solution containing 100 mM MES pH 7.0 and Na-citrate ranging from 1.0 to 1.2 M in a 1:1 ratio grew crystals of ODH-5His, which continued growing to their final size in 3 to 5 days (Figure 19A). The crystallisation temperature appeared crucial for the formation of the crystals. Crystals only grew when the setup was incubated at a constant temperature of 12 °C. Small variations such as for example incubation at 8°C, 10°C or 16°C did not result in protein crystals. Furthermore OcDH appeared extremely stable as visible aggregation or precipitation was hardly ever observed.

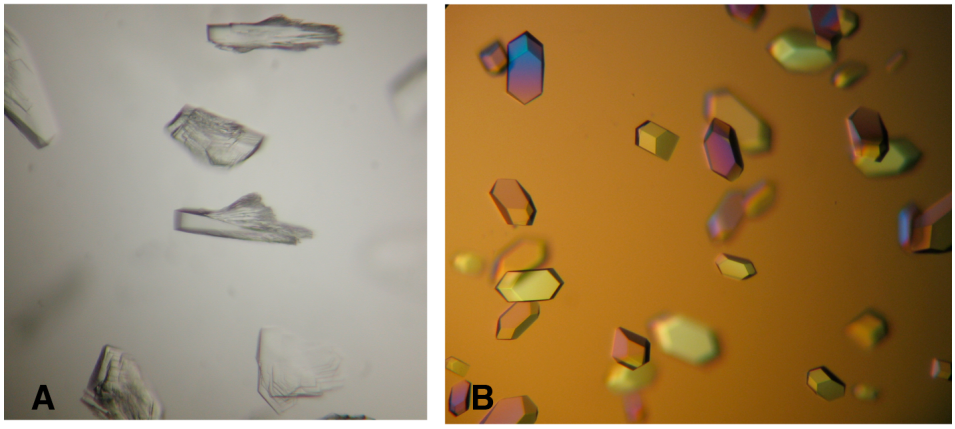

Figure 19: Crystals of ODH-His$_5$. Crystals of ODH-5His were grown by mixing protein solution with reservoir solution containing 100 mM MES pH 7.0 and Na-citrate ranging from 1.0 to 1.2 M in a 1:1 ratio. **A)** Crystals of apo ODH-His$_5$ **B)** Crystals of ODH-His$_5$ with bound cofactor NADH.

The OcDH-His$_5$ crystals were thin plates clumbed together (Figure 19A). Unfortunally, these could not be separated by mechanical manipulation without destroying them. The crystals were mounted in a cryo-loop and flash frozen in liquid nitrogen after soaking in cryo-protectant buffer (mother liquid supplemented with 30% glycerol). These apo OcDH crystals diffracted X-rays to a resolution of 2.6Å, however, the diffraction pattern revealed multiple lattices on one diffraction image (Figure 20A) and neither the XDS (*95*) nor the DENZO (*89*) program package were able to conclusively calculate the unit cell constant from these images. Several

attempts to change the crystals orientation within the beam in order to find a spot with a single or processable diffraction pattern did not succeed. Any effort to improve the crystal quality by for example seeding, temperature ramping experiments or even the search for new crystallisation conditions, only yielded crystals of similar diffraction quality and were still multiple.

In another approach, the cofactor NADH was added to OcDH at a final concentration of 0.8 mM prior to crystallisation. This yielded crystals under conditions comparable as the conditions without NADH, at 100 mM L^{-1} Hepes pH 7.5, 1,4 M L^{-1} Na-Citrate at 12 °C (Figure 19B). Similar to apo OcDH the incubation temperature appeared critical. They were single crystals and diffracted to 2.1Å (Figure 20B), the quality was good enough for dataset collection, processing and subsequent structure determination. The data obtained by these crystals were processed by the XDS or DENZO program packages.

The crystallisation was reproducible and yielded crystals with a final size of 50x50x100 μm after five days of incubation. As the addition of NADH improved the crystal quality, NADH was supplemented to the OcDH-His_5 protein solution prior to crystallisation in all further experiments.

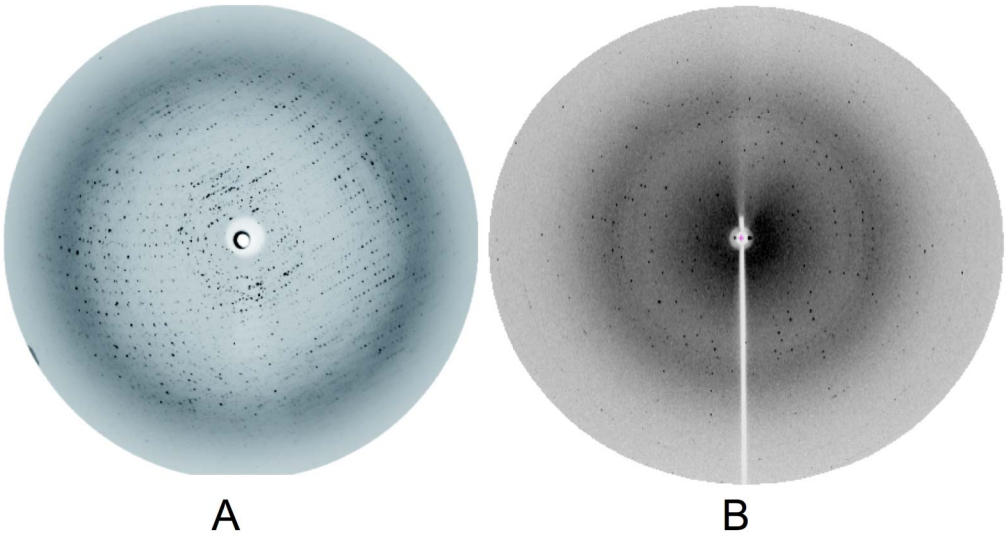

Figure 20: Diffraction of OcDH crystals. A) Diffraction pattern of apo-OcDH collected from a cluster of crystals. Rotation width was 0.5 degrees. The crystal also appeared multiple in the X-ray analysis and could not be used for subsequent structure determination. **B)** Crystals of OcDH-NADH. These crystals were grown as single crystals and also diffracted X-rays to a resolution limit of 2.1Å.

Several datasets were collected at the EMBL outstation DESY Hamburg. Efforts to crystallise OcDH in the presence of its natural substrates, arginine, pyruvate or octopine respectively, abolished crystal formation.

Therefore the substrates where individually soaked into preformed OcDH-NADH crystals. Here the selected substrates at a concentration of 0.8 mM (final volume 0.2μl) were added to the crystallisation drop containing OcDH-NADH crystals and the setup was monitored for 24 hours. The addition of pyruvate as well as octopine cracked the crystals after 2 hours and therefore, the maximum soaking duration was reduced to 1 hour. Arginine however did not damage the crystals even after 24 hours and this duration was used for soaking this substrate. All crystals were "back soaked" into a solution not containing the substrate and further washed in suitable freezing conditions (crystallisation conditions plus 30% glycerol) and flash frozen in liquid nitrogen.

4.2 Dataset collection of OcDH crystals

To allow data collection at 100 K, which reduces radiation damage, all crystals of OcDH were washed with a cryoprotective buffer prior to freezing in liquid nitrogen. Cryoprotectant solutions consisted of the corresponding reservoir solution supplemented with 30% (v/v) ethylene glycol. A 2.1Å dataset was collected at the X12 beam line at the EMBL outstation DESY Hamburg (statistics are listed in Table 3). All crystals were initially screened by two different diffraction images 90 degrees apart from each other. This allows initial unit cell and space group determination using DENZO (*89*). The optimal data collection strategy was obtained using the program BEST (*88*). The OcDH-NADH crystals exhibit $P4_12_12$ symmetry and the calculated Mathew coefficient predicted one monomer of OcDH in the asymmetric unit. The dataset had a resolution of 2.1Å as judged by the overall completeness of 93.0% (96.5% in the highest resolution shell), the overall R-merge of15.8 (38.0% in the highest resolution shell) and the overall signal to noise ratio of 6.8 (3.0 in the highest resolution shell). Six other datasets were collected with either anomalous scatters (Hg and SeMet) present to obtain either the crucial phase information or the substrate bound form of OcDH (pyruvate, L-arginine agmatine and octopine). The

final dataset statistics are given in Table 3.

Crystal parameters at 100 K	SeMet (NADH)	Mercury (NADH)	Native (NADH)	Pyruvate (NADH)	L-arginine (NADH)	Agmatine (NADH)	Octopine (NADH)
Space group	$P4_12_12$	$P4_12_12$	$P4_12_12$	$P4_12_12$	$P4_12_12$	$P4_12_12$	$P4_12_12$
Unit Cell parameters							
a, b, c (Å)	99.1 99.1 125.7	99.7 99.7 126.1	99.8 99.8 126.5	95.9 95.9 117.9	95.0 95.0 120.2	96.2 96.2 117.4	99.3 99.3 125.3
Data collection and processing							
Wavelength (Å)	0.97854	0.97854	0.97854	0.8148	0.8348	0.8148	0.8148
Resolution (Å)	20-2.7 (2.8-2.7)	20-2.7 (2.8-2.7)	20-2.1 (2.2-2.1)	20-2.6 (2.60-2.7)	20.-3.1 (3.2-3.1)	20-2.8 (3.0-2.8)	20-2.8 (3.0-2.8
Mean redundancy	8.4	2.4 (2.0)	5.1	6.1 (6.3)	6.9 (7.0)	4.4 (4.5)	4.8 (3.9)
Unique reflections	24818	25760	37905	17525	71952	11968	26170
Completeness (%)	93.0 (96.5)	86.7 (90.6)	93.0 (96.5)	99.9 (99.8)	99.5 (99.9)	89.2 (92.5)	95.9 (98.8)
I/σ	6.8 (3.0)	9.5 (2.1)	6.8 (3.0)	26.91 (5.1)	13.0 (5.9)	13.6 (4.5)	5.1 (2.8)
R_{merge}[a]	16.4 (28.8)	11.2 (34.8)	15.8 (38.0)	6.2 (36.0)	16.2 (36.4)	10.3 (36.3)	13.4 (32.1)

Table 3: Crystallographic parameters. Crystal parameters and data collection statistics are derived from XDS (*89*). Values for the highest resolution shells are given in brackets.

$$R_{sym} = \sum_{hkl}\sum_{i}\left|I_i(hkl) - \langle I(hkl)\rangle\right| \Big/ \sum_{hkl}\sum_{i} I_i(hkl)$$

$$R_{mrgd-F} = \sum \left|A_{I_{h,P}} - A_{I_{hQ}}\right| \Big/ 0.5 * \sum A_{I_{h,P}} + A_{I_{hQ}}$$

4.3 Structure determination

X-rays are scattered by the electrons of the protein inside the crystals during a radiation experiment. The diffracted beam is collected at the detector and contains the information of the amplitude, which correlates with the observed intensity. The exact phase of the scattered beam however is lost during data collection, most times referred to as the " phase problem" in X-ray crystallography. To regain this phase information several methods like MAD and SAD have been developed (see Material and Methods for more details).

To obtain the essential phase information of OcDH two strategies were pursued.

First the methionines inside the protein were replaced by seleno methionines by expression in minimal media were methionine was exchanged by seleno methionine. This resulted in a SeMet-OcDH protein solution.

SeMet-OcDH was crystallised under the same conditions as “native” OcDH, again NADH was added prior to crystallisation. In a second approach p-Chloromercuribenzoic acid (C_7H_5ClHgO), at a final concentration of 1mM, was soaked into preformed OcDH-NADH crystals overnight. These crystals were back soaked with cryoprotectant buffer to reduce the amount of unspecifically bound mercury. Both strategies yielded diffracting crystals and datasets were collected for both crystals at 2.7 Å and 2.8Å respectively (Table 3).

Initial phases were obtained by a single SAD dataset obtained from crystals grown from seleno methionine incorporated OcDH. To minimize radiation damage during data collection a lower X-ray dose was used, reflected in the lower resolution of 2.8Å. The wavelength was set at 0.978Å, slightly off the edge of seleno methionine. Initially the program AUTORICKSHAW (*90*) found 17 possible seleno-methionine sites inside the OcDH-SeMet dataset (Figure 21). OcDH contains twelve methionines, and the eleven sites, with the highest occupancy, were further refined using the program RESOLVE (*96*). The cut off in the number of sites used for refinement was chosen at site number twelve as the expected drop in occupancy to only 24% was observed here.

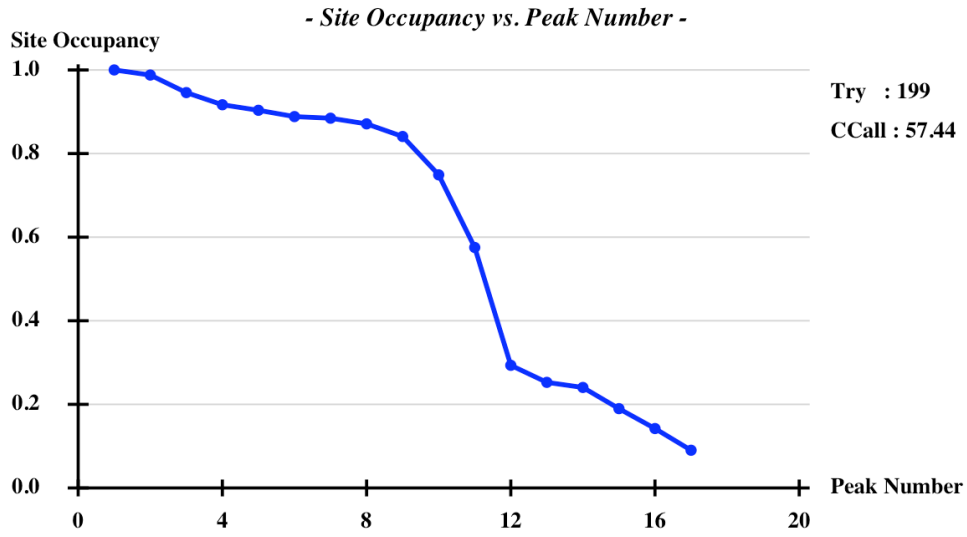

Figure 21: Selenomethionine site found by the program ShelXE. Shown are the possible Se-site found in the OcDH-SeMet data set with their corresponding occupancy.

The eleven sites and thereby the initial phase information were further refined and optimized using the program RESOLVE (*96*). This program automatically builds amino acids into the electron density, which further improves the obtained phases. As shown in Figure 22A, 209 out of a total of 404 amino acids were automatically build based on the OcDH sequence. Another eighty-two amino acids were modelled into the electron density as glycines as the corresponding density was not good enough to highlight and identify the nature of the side chain with proper certainty. Already at this stage the two different domains of OcDH were clearly visible in the structure. When highlighted as a cartoon representation, also the secondary structure elements become visible, identifying the Rossmann fold domain by its characteristic β-strand build up (Figure 22B, left domain).

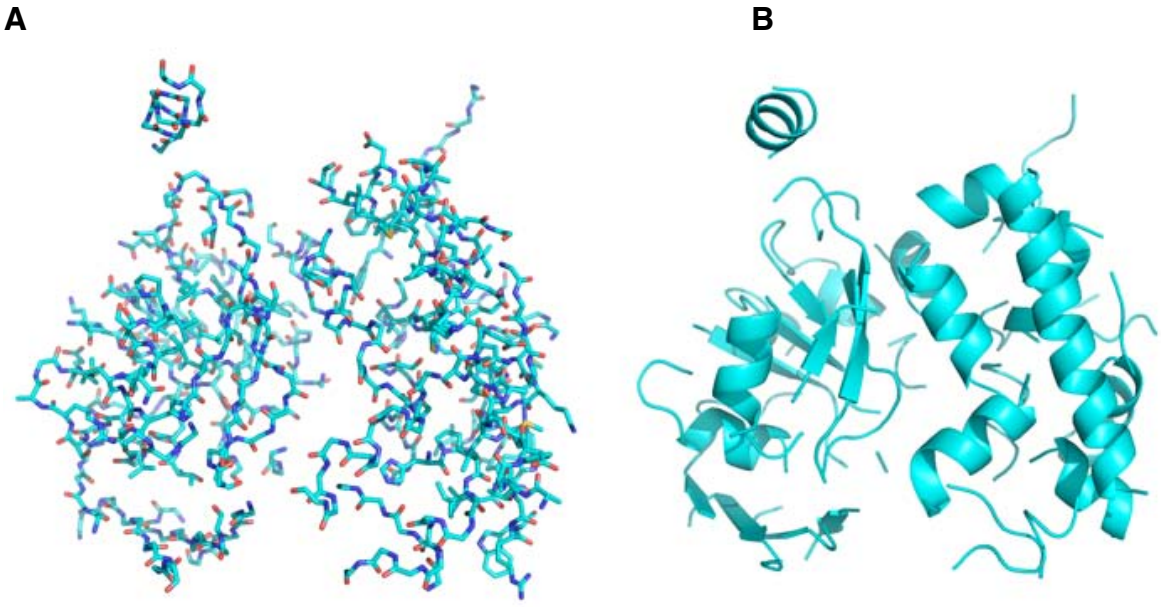

Figure 22: Initial model of OcDH as build by the program RESOLVE using initial phases. A) Stick model of the automatically build OcDH protein model. **B)** Highlighting the secondary structures in the model. Here two domains can be detected. The Rossmann fold domain (left) identified by its characteristic beta sheet structure as well as a second domain (right) containing mainly alpha helical features.

After several rounds of refinement and manually rebuilding using the program COOT (*92*) the initial structure of seleno methionine incorporated OcDH was solved. This model was used as template to phase the high resolution data set using the

molecular replacement technique with the program PHASER (*93*). For the Native, Pyruvate, L-arginine, Agmatine, Hg and Octopine datasets a monomer was found in the asymmetric unit with a high Z-score ranging from 13 to 23 indicating unique solutions. Refinement and manually rebuilding were done using REFMAC5 (*91*) and the program COOT (*92*), respectively. In the case of the high resolution OcDH-Native dataset, the quality of the electron density allowed automatic water picking using ArpWarp (*104*) at 2 σ and the waters were manually checked for their correct assignment. All refinement and model building statistics are found in Table 4.

	Native (NADH)	Pyruvate (NADH)	L-Arginine (NADH)	Agmatine (NADH)	Octopine (NADH)
B. *Refinement*					
R_F[b] (%)	20.5	25.2	19.5	24.5	23.5
R_{free}[c] (%)	25.0	29.0	24.0	27.2	26.2.0
rmsd from ideal					
Bond lengths (Å)	0.09	0.004	0.06	0.07	0.08
Bond angles (deg.)	1.079	0.808	0.978	0.995	0.921
Average B-factors (Å^2)					
Ramachandran plot					
Most favored (%)	100	94.2	96.4	95,3	96.4
Allowed (%)		5.4	3.6	4.5	3.6
Generously allowed (%)		0.4		.2	
Disallowed (%)					
D. *Model content*					
Monomers/ASU	1	1	1		1
Protein residues	2-404	2-280 ,291-404	2-404	2-404	2-404
Ligand	1 NADH	1 NADH 1 pyruvate	1 NADH 1 Arginine	1 NADH 1Agmatine	1 NADH 1 Arginine
Other	8 ethylen glycol 251 water				

Table 4: Refinement statistics of the different OcDH datasets. Refinement statistics were obtained from REFMAC5 (*91*) and Ramachandran analysis was performed using PROCHECK (*98*). [a] R_{sym} is defined as $R_{sym} = \sum_{hkl}\sum_{i}\left|I_i(hkl) - \langle I(hkl)\rangle\right| \Big/ \sum_{hkl}\sum_{i} I_i(hkl)$ and R_F as [b] $R_f = \sum_{hkl}\left\|F_{obs}\right| - \left|F_{calc}\right\| \Big/ \sum_{hkl}\left|F_{obs}\right|$. R_{free} is calculated as R_F but for 5% randomly chosen reflections that were omitted from all refinement steps.

4.4 Final structure of OcDH-NADH

The structure of OcDH consists of two domains separated by a deep cleft (Figure 23). Domain I comprises residues 1-199, which form a central eight-stranded

β-sheet of mixed parallel and anti-parallel character flanked by a number of α-helices and also by a smaller four stranded β-sheet that contains both parallel and anti-parallel strands. Part of the eight stranded β-sheet is organized as a six-stranded parallel sheet which resembles the classical Rossmann fold commonly found in dinucleotide binding enzymes (*65*).

This domain contains a classic alpha unit that includes a dinucleotide binding helix that separates the first two β-strands of the OcDH structure. The amino acid sequence in the loop joining the first β-strand to the first alpha helix includes a glycine rich region with a sequence GGGNGA fitting the consensus GXGXXG/A sequence which often delineates the di-nucleotide binding site in dehydrogenases (*65*). Domain I is connected to the N-terminus of the domain II via a so called type 1 connection (*105*). Domain II is entered by a short helix-kink-helix (alpha8-alpha9) followed by two antiparallel beta-sheets. The structure continues with a bundle of helices of which one is a very long helix (amino acid 232-264) which gives the second domain its rigid structure.

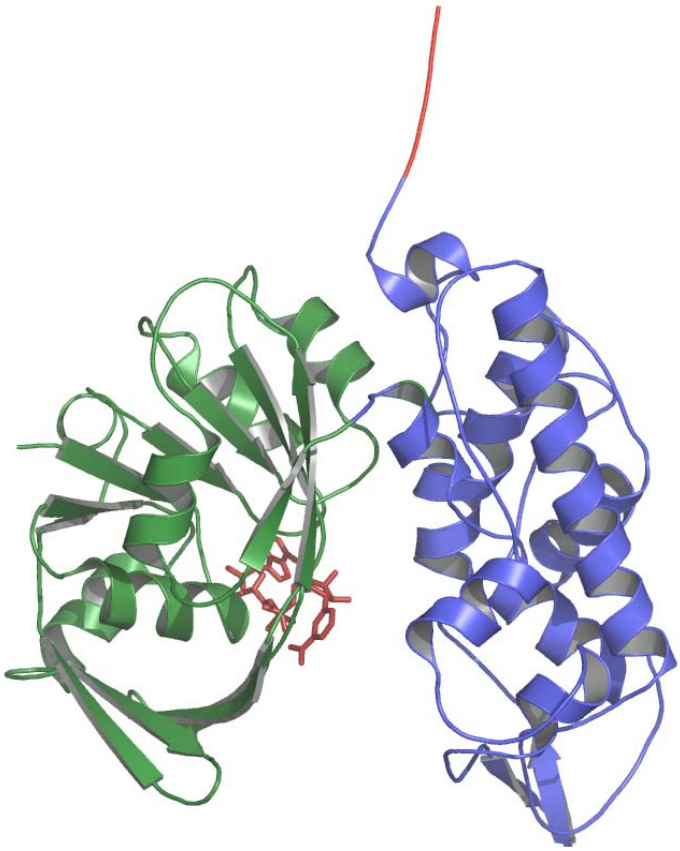

Figure 23: Overall structure of OcDH. In green domain I containing the NADH (in red) binding site. The second domain is visualised in blue. The His_5-tag is shown as red tail on top of the protein and the bound cofactor, NADH, is shown as sticks.

4.5 NADH binding site

Analyzing the initial electron density identified the binding site of the cofactor in the 2.8 Å SAD data set. NADH is bound to the Rossmann fold by interactions typically observed in dehydrogenases (Table 5). While the pyrophosphate moiety interacts with Asn12 and Gly13 of the consensus sequence (GGGNGA), Phe35, Glu38 and Gly10 establish further interactions with the cofactor. Here, Phe35 undergoes phi-phi stacking with the adenine ring and Glu38 forms a hydrogen bond with the hydroxyl groups of the ribose ring.

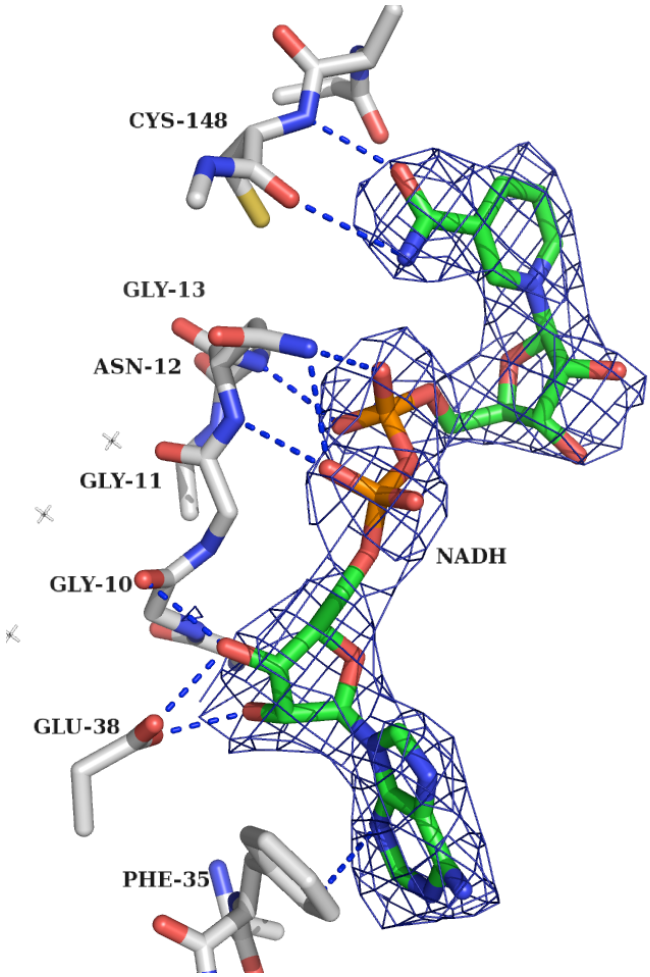

Figure 24: NADH is bound in the syn conformation. The electron density represents the final 1Fo-Fc map of the 2.1Å native OcDH dataset contoured at 1σ.

Gly10 being part of the consensus motif of dinucleotide binding proteins also interacts with the ribose moiety of NADH. Already during the first rounds of refinement, it became apparent that the nicotine amide moiety adopts the syn-

conformation. As shown in Figure 24, this syn-conformation of NADH is only stabilized by interactions of the amide group with the backbone oxygen and nitrogen of Cys148 (highlighted as sticks in Figure 24 and
Figure 27). Obviously, the syn-conformation suggests that the hydride transfer from NADH to the Schiff base adduct between L-arginine and pyruvate occurs from the pro-(S) site.

	Residue	Interaction	Distance [Å]
NADH-binding	NADH		
	C2	Phe35 (CD1)	3.5
	AO2*	Glu38 (OE1)	3.1
	AO3*	Glu38 (OE2)	3.1
	AO3*	Gly10 (O)	3.1
Pyro-phosphtate1 (AP)	AO2	Asn12 (N)	3.2
	AO2	Asn12 (ND2)	3.4
Pyro-phosphtate2 (NP)	NO1	Asn12 (ND2)	3.2
	NO2	Gly13 (N)	2.9
Nicotine amide ring	NO7	Cys148 (N)	3.2
	NN7	Cys148 (O)	3.6

Table 5: Summary of the interactions of NADH with OcDH.

4.6 His_5-tag and crystal contacts

The cloned C-terminal His_5-tag is located in the opening cleft of a symmetry related monomer, introducing a predominant crystal contact. The his_5-tag however, did not influence the binding of the substrate, which were obtained by extensive soaking with arginine and pyruvate (see below), although in these structures the three-dimensional position of single histidines is slightly changed. The His_5-tag protrudes in the cleft between domains I and II (Figure 25). From the histidines of the His-tag, His402 interacts with the side chain of Val307 directly, whereas His403 interacts with the NO2 moiety of NADH. Interestingly, position and orientation of the

other histidines inside the His-tag are stabilized via a complex water network (Figure 25). Here, His400 interacts via two water molecules with amino acids Val307 and His401, His401 via two water molecules with amino acid Tyr325, His402 via one water molecule with amino acid Tyr325, His403 via two water molecules with amino acids Thr143,Leu 116, Pro116 as well as Tyr235, His 404 interacts via one water molecule with Lys163, Tyr 235, Tyr282, Tyr283, and Tyr303 .

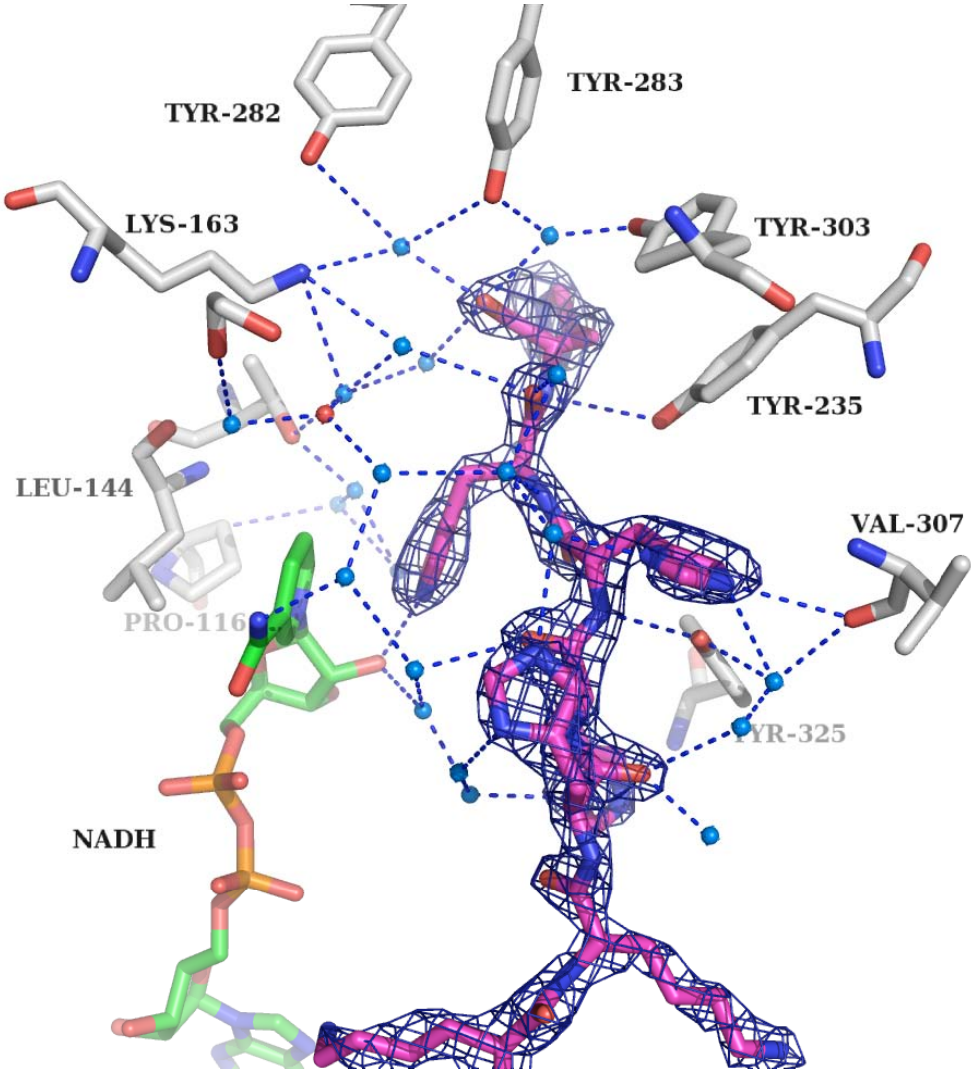

Figure 25: His-tag mediated crystal contacts. The his-tag (magenta) is shown together with the surrounding water molecules (indicated as blue spheres). Highlighted are the side chains (white) that interact in first or second line with the his-tag via a water network. The cofactor NADH is coloured in green. The density surrounding the his-tag, which was omitted from the structure for refinement, highlights the quality of the structure.

The complete His-tag thereby opens up both domains to a certain extent, and

the structure is fixed in this conformation, or phrasing it differently OcDH cannot adopt a more closed conformation. The electron density surrounding the His_5-tag is of high quality (Figure 25). The water molecules were build automatically using ArpWARP (*104*) and manually checked for proper density.

By the limited opening of the cleft between the two domains crystal contacts are created. They are located at the bottom of both domains as shown in Figure 26 (middle panel). Here, Phe35, Glu38, Asp37, Glu40, and Arg41 of domain I of monomer A interact with Gly173, Thr174, Ala175 and Lys176 of domain I of a crystallographically related monomer B, respectively. The crystal contacts in domain II are mediated by Val313, Asp314, and Ala315 interacting with Thr373, Gly374, and Lys 375, respectively.

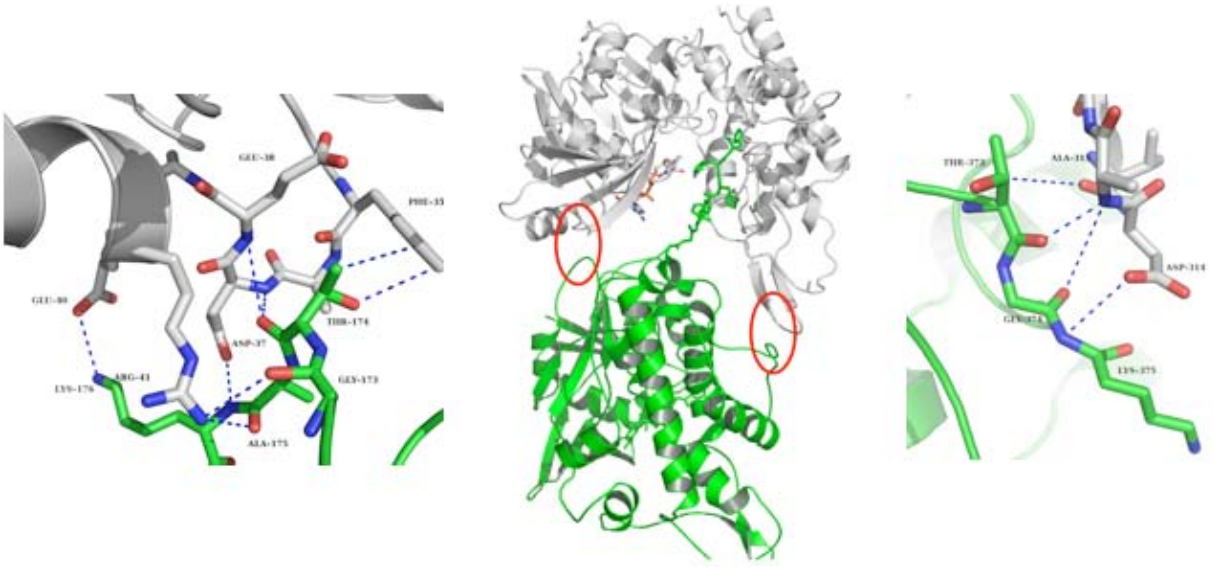

Figure 26: Crystal contacts mediated by the His_5-tag. The crystal contact mediated by the His_5-tag is shown. **Left and right panel)** A zoom in of the protein-protein mediated crystals contact in OcDH. The top of domain I is interacting with the bottom of domain I of a crystallographically related monomer. The same holds true for domain II. **Middle panel)** Overall structure of OcDH showing the His_5-tag (green) protruding into the cleft between the two domain of the neighbour molecule (white). The red circles indicate the protein-protein mediated crystal contacts.

4.7 The binary OcDH-NADH/L-arginine complex

Unfortunally, the co-crystallization of OcDH with L-arginine did not result in crystal formation. Therefore, soaking experiments with preformed OcDH-NADH crystals were performed. L-arginine was added at a concentration of 0.2mM to the

crystallization drop containing OcDH-NADH crystals. They were monitored for up to 24 hours. Optically the crystals showed no damage after soaking and were subsequently mounted into a cryo loop after back soaking them in a solution containing no arginine. This is important to remove any unspecific bound L-arginine (see Materials and Methods for details and Table 3).

The dataset was processed and refined to a resolution of 2.8 Å, and initial phases were obtained by molecular replacement using the program PHASER and the OcDH-NADH structure as template. The resulting Z-score was relatively low (Z score 7.4), likely due to the conformational change observed inside the structure (see below). The final refinement statistics are listed in Table 4.

Like OcDH-NADH the overall structure of OcDH-NADH/L-arginine is composed of two domains between which the only significant difference is the rotation of the domain II towards domain I.

In this binary complex (Figure 27), NADH is bound to OcDH in an identical fashion as in the OcDH-NADH complex and stabilized in the syn-conformation through equal interactions with the backbone of Cys148. The substrate, L-arginine, which is located above His212, is coordinated via a hydrogen bond between its α-carboxyl oxygen and N3 of His212 as well as hydrogen bonds of the α-amino group, with the backbone of Tyr208 contributing directly to substrate binding (Figure 27). The guanidinium group, on the other hand, is fixed inside the binding pocket via a salt bridge with Glu142 (highlighted in green in Figure 27), van-der-Waals interactions with Trp278 and hydrogen bonds with the backbone carbonyl of Met206. While His212, Trp278 and Met206 are located in domain II, Glu142 is part of domain I. The exact distances between L-arginine and OcDH are listed in Table 6.

This already suggests that L-arginine binding involves both domains of OcDH likely triggering a domain closure. Such a motion is further supported by the fact that Met206, Tyr208 and His212 are located in a rather flexible helix-kink-helix motif which forms the N-terminal part of domain II (for further details see Discussion). N3 of His212, which participates in ligand binding, is coordinated by Asp329 via a hydrogen bond forming the Asp-His proton relay system. In the OcDH-NADH/L-arginine structure, L-arginine is perfectly fitting in the described pocket (Figure 27). Binding of the guanidine group of arginine is coordinated by two amino acids located in both

domains, Q142 of domain I and W278 of domain II, respectively (Figure 27).

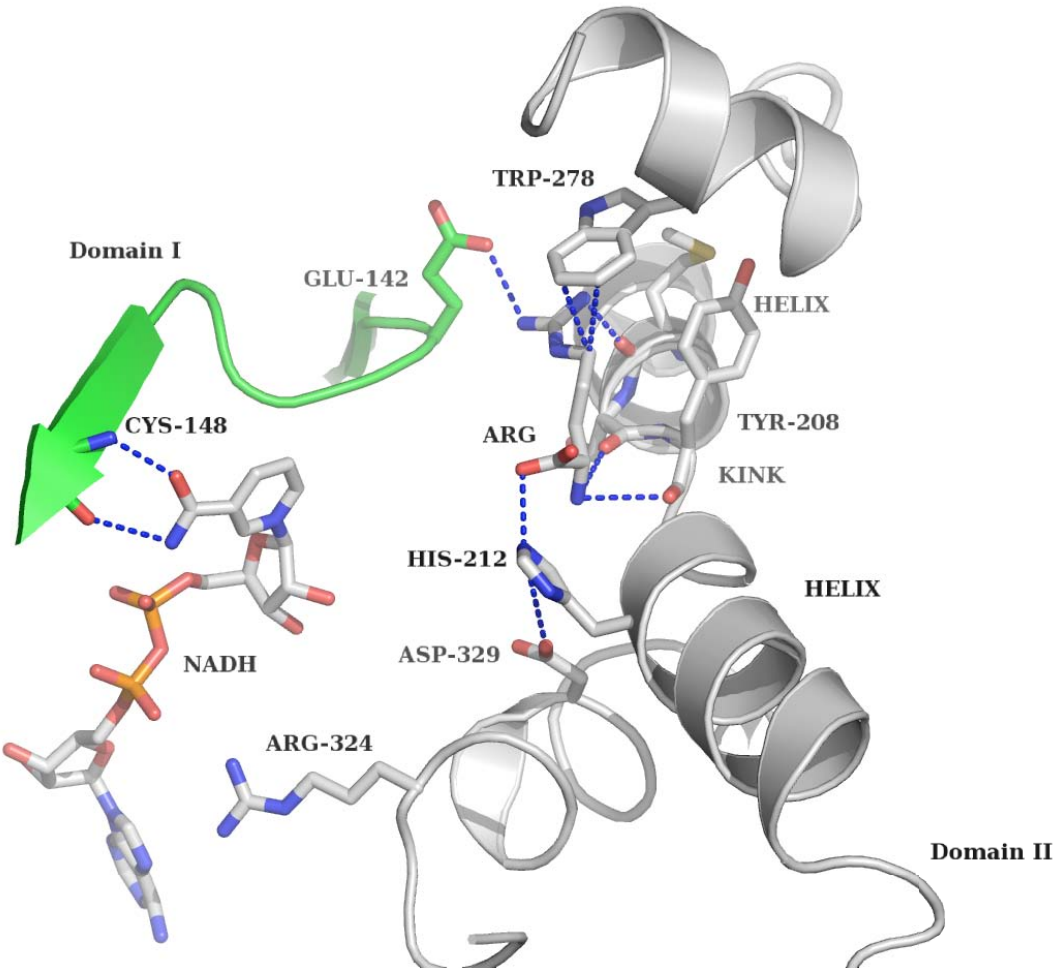

Figure 27: View of the arginine binding pocket in OcDH. The arginine-binding pocket is located in domain II, directly at the N-terminal helix-kink-helix motif of domain II. The side chain of L-arginine is coordinated by Trp278, backbone interactions with Tyr208 (domain II) and Glu142 (domain I). The Cα of L-arginine is bound by His212 of the Asp-His dyad. NADH is bound in a canonical fashion to the Rossman fold, while interactions of the amide side chain of the nicotine amide ring with the backbone atoms of Cys148 (domain I) ensure the syn-conformation of NADH.

Further more the aliphatic part interacts with the oxygen atoms of the backbone in the kink of the helix–kink-helix motif entering the second domain (amino acid 206-209). Domain movement analysis using the DYNDOME server (*106*) revealed a 42° rotation of the second domain towards the NADH binding domain (Figure 29).

Substrate	Residue	Interaction	Distance [Å]
L-arginine	OXT	His212 (N3)	2.9
	N1	Tyr208 (O)	3.4
		Ser207 (O)	3.6
	Cb	Ser207 (O)	3.2
	CD1	Trp278 (CH2)	3.6
	NH2-1	Trp278 (CE2)	3.2
	NH2-1	Trp278 (CE2)	3.5
	NH2-1	Met206 (O)	2.7
	NH1	Met206 (O)	3.4
	NH1	Glu142 (OE1)	3.1
Pyruvate	O3	His212 (N3)	3.0
	O2	Gln118 (NE2)	3.6

Table 6: Summary of the interactions of L-arginine and pyruvate with OcDH.

4.8 The binary OcDH-NADH/pyruvate complex

For the binary OcDH-NADH/pyruvate complex (Figure 28), which was obtained via soaking of pyruvate into preformed OcDH-NADH crystals as described for L-arginine (see above), a 3.1 Å dataset was collected. Initial phases were obtained by molecular replacement using the program PHASER (*93*) and the OcDH-NADH/L-arginine structure as template. Pyruvate is coordinated through Gln118 (domain I) and His212 (domain II). The side chain of Gln118 coordinates the carboxyl moiety of pyruvate, whereas His212 imposes orientation restraints and interacts with the carbonyl group via a hydrogen bond (Figure 28 and Table 6). The binding site is optimally suited for pyruvate as a substrate. Identical to OcDH-NADH and OcDH-NADH-L-arginine, NADH is bound to the pyruvate complex in a syn-conformation, which is coordinated by the backbone of Cys148. Like in the OcDH-NADH/L-arginine complex domain II is rotated towards domain I (Figure 29).

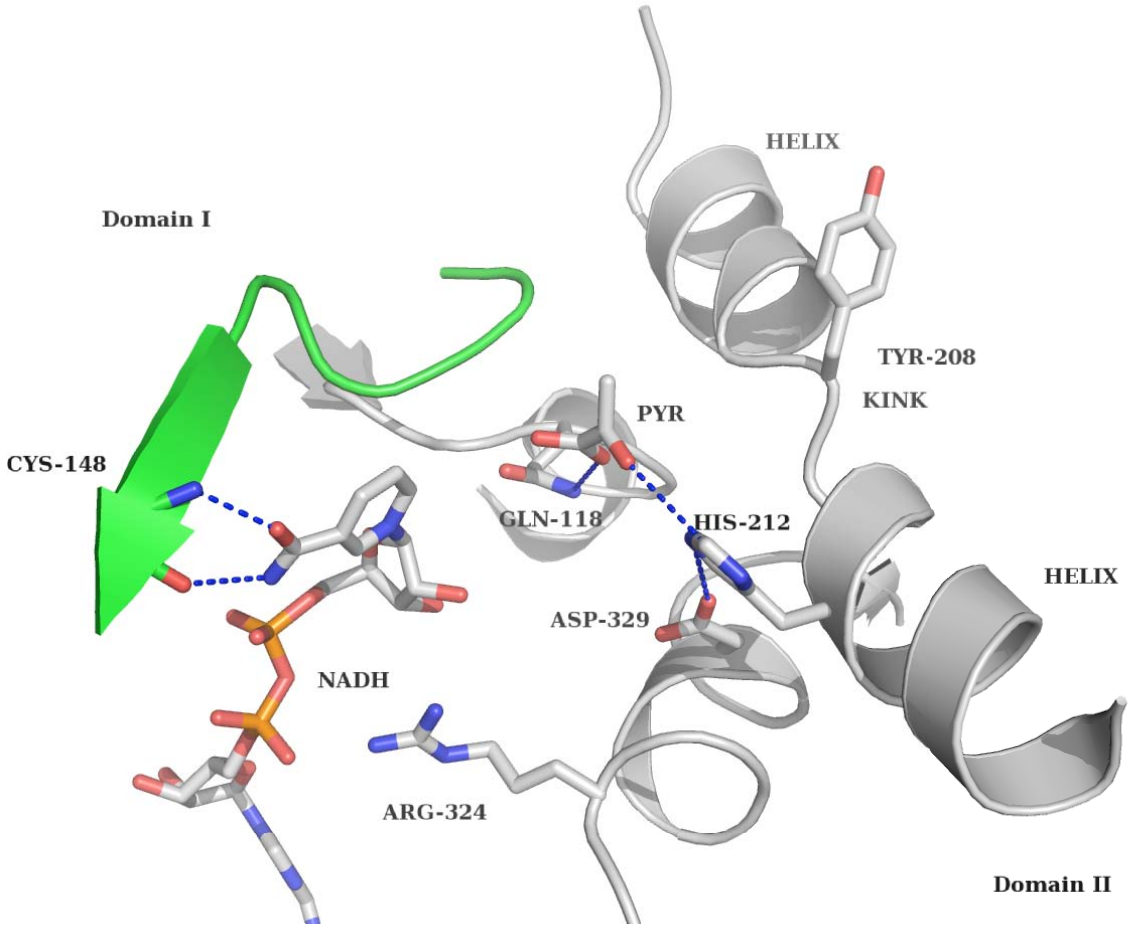

Figure 28: View of the pyruvate binding site of OcDH. His212 (domain II) and Gln118 (domain I) bind pyruvate with distances of 3.1 Å and 2.8 Å, respectively.

4.9 Domain closure

Structural analysis of the different OcDH complexes, OcDH-NADH, OcDH-NADH/L-arginine and OcDH-NADH/Pyruvate, respectively, revealed a domain movement in the tertiary complexes. To analyse the movement an overlay of the structures was made using the program LSQMAN and the DYNDOME server (*106*). As fixed anchor point, domain I was chosen as the NADH binding site is expected to be the same in all three structures. As shown in Figure 29 domain II rotates towards domain I. Domain movement analysis using the DYNDOME server revealed a 42° rotation of the second domain towards the NADH binding domain (Figure 29).

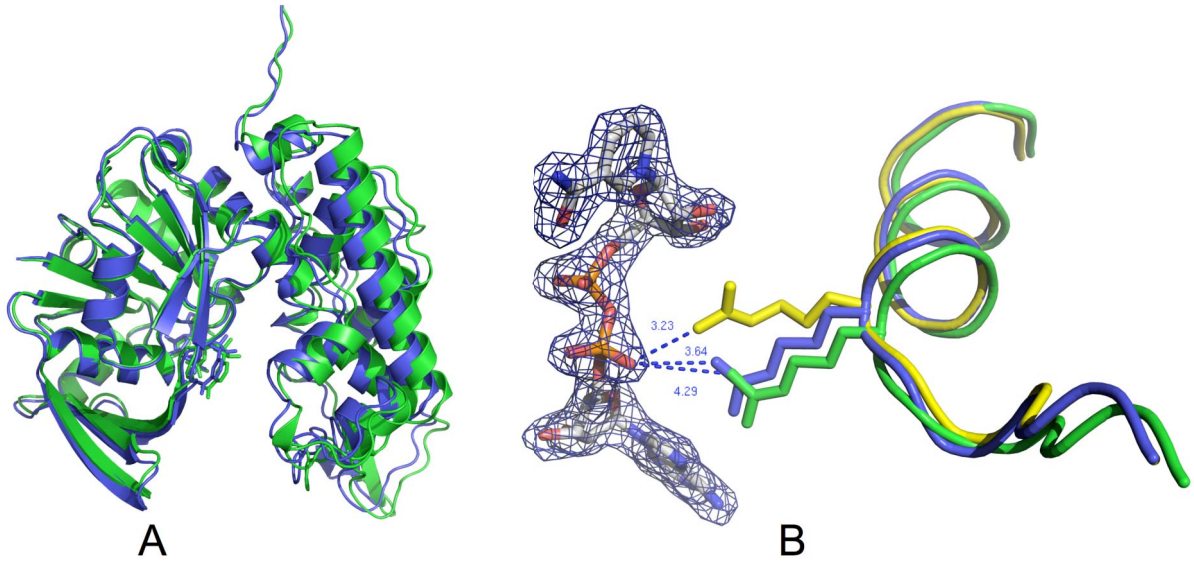

Figure 29: The role of arginine 324 in substrate-dependent domain closure of OcDH. A: Superposition of the ODH-NADH (green) and the ODH-NADH/L-arginine (blue) complexes highlight the inward rotation of domain II. The rmsd is 0.753 Å over 404 Cα atoms. **B:** Superposition of the ODH-NADH (green), ODH-NADH/L-arginine (blue) and ODH-NADH/pyruvate (yellow) complexes. The interactions between NADH and Arg324 are highlighted and the corresponding distances are shown in Å. The final 2Fo-Fc electron density contoured at 1σ for NADH from the ODH-NADH structure is shown**.**

The crystal structures reveal that Arg324 is not involved in L-arginine or pyruvate binding (see above). Rather, it plays a crucial role due to its close proximity to the pyrophosphate moiety of NADH in domain closure. A comparison of the OcDH-NADH (colored green in Figure 29A) and the OcDH-NADH/L-arginine complexes (colored blue in Figure 29A) revealed a 42° rotation of domain II towards the NADH binding domain (domain I) in the latter complex as calculated using the DYNDOME server (*106*). This domain closure is triggered by the interaction of Arg324 (domain II) with the pyrophosphate moiety of NADH bound to the Rossman fold in domain I. In the OcDH/NADH complex the distance between Arg324 and the pyrophosphate moiety of NADH is 4.2 Å (Figure 29B). In the binary OcDH-NADH/L-arginine and the binary OcDH-NADH/pyruvate complexes, this distance shortens to 3.4 and 3.2 Å, respectively, increasing the strength of the salt bridge interaction (Figure 29B) and points to a “sensor role” for Arg324.

4.10 Agmatine bound OcDH

Agmatine ((4-aminobutyl)guanidine, NH_2-CH_2-CH_2-CH_2-CH_2-NH-C(-NH_2)(=NH)) is the decarboxylation product of the amino acid L-arginine an intermediate in polyamine biosynthesis and is discussed as a putative neurotransmitter (*107*). It is synthesized in the brain, stored in synaptic vesicles, accumulated by uptake, released by membrane depolarization, and inactivated by agmatinase. Agmatine binds to α2-adrenergic receptor and imidazoline binding sites, and blocks NMDA receptors and other cation ligand-gated channels. Furthermore it inhibits nitric oxide synthase (NOS), and induces the release of some peptide hormones (*108*).

In direct comparison to arginine, agmatine is lacking the carboxyl group. In the OcDH-NADH/L-arginine structure the functional important His212 coordinates this carboxyl group. To investigate whether the COOH group is an important part in domain closure the crystal structure of OcDH-NADH/agmatine was determined.

As for the other substrates, agmatine was soaked into preformed OcDH-NADH crystals. After washing with mother liquid supplemented with 30% v/v ethylene glycol flash frozen in liquid nitrogen. An 2.8 Å dataset was collected and initial phases were obtained from molecular replacement using the program PHASER (*93*) and the OcDH-NADH/Pyruvate structure as template. The high Z score of 22.8 indicated one unique solution. The structure was further build using COOT (*92*) and several rounds of refinement using REFMAC5 (*91*). Dataset statistics can be found in Table 3, refinement statistics and unit cell contents are summarized in Table 4.

Already during the initial round of refinement and manually rebuilding it became obvious that agmatine is bound inside the structure in a similar fashion as L-arginine (Figure 30).The guanidinium headgoup of agmatine is coordinated via interactions with the sidechains of Glu142 (domain I) and Trp278 (domain II) as well as backbone interactions with Met206 (domain II).

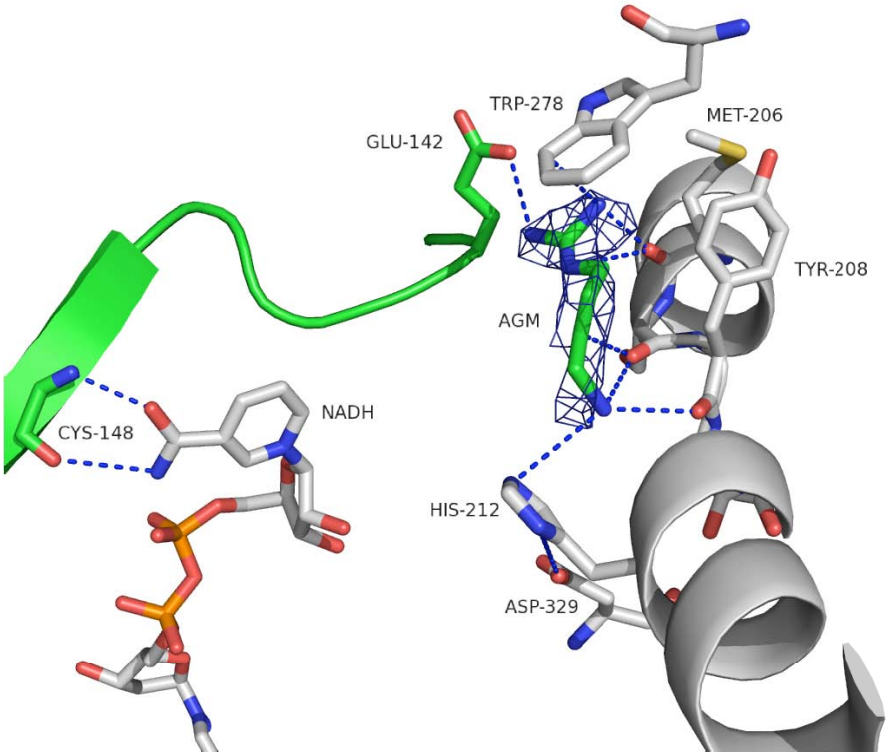

Figure 30: View of the agmatine-binding pocket of OcDH. The agmatine-binding pocket is located in domain II, directly at the N-terminal helix-kink-helix motif of domain II. Agmatine is coordinated by the side chain Trp278, backbone interactions with Tyr208 (domain II) and Glu142 (domain I). NADH is bound in a canonical fashion to the Rossman fold, while interactions of the amide side chain of the nicotine amide ring with the backbone atoms of Cys148 (domain I) ensure the syn-conformation. The final 2Fo-Fc electron density contoured at 1 σ for agmatine is shown as blue mesh.

The C_{β} is bound via backbone interactions of Ser207. The exact distance are listed in Table 7. The density of agmatine however is of reasonable quality (Figure 30), indicating that agmatine is bound inside the monomers in the crystal slightly different. The density of agmatine represents the average of these. Interestingly His212 does not interact with Agmatine. The distance between His212 and the agmatine O3 atom is 4.1 Å, a weak interaction.

Substrate	Residue	Interaction	Distance [Å]
Agmatine	N1	Tyr208 (O)	3.2
		Ser207 (O)	3.7
	Cb	Ser207 (O)	3.6
	CD1	Trp278 (CH2)	3.6
	NH2-1	Trp278 (CE2)	3.8
	NH2-1	Met206 (O)	2.8
	NH1	Met206 (O)	3.8
	NH1	Glu142 (OE1)	3.2
	O3	His212 (N3)	4.1

Table 7: Summary of the interactions of agmatine with OcDH.

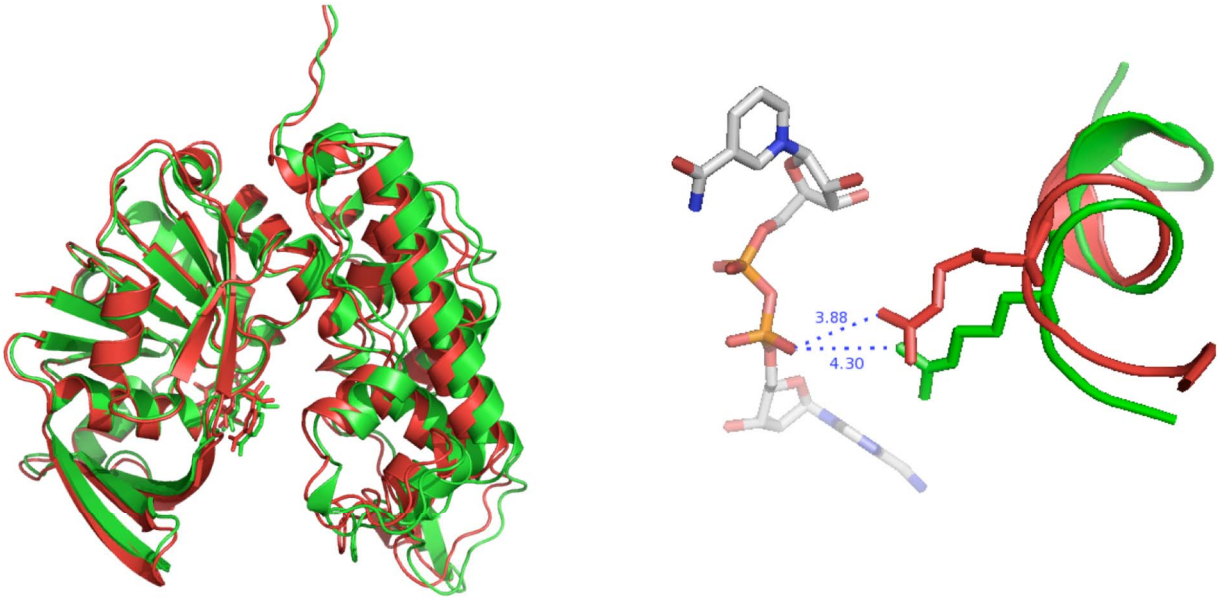

Figure 31: Substrate-dependent domain closure of Agmatine bound OcDH A): Superposition of the ODH-NADH (green) and the ODH-NADH/agmatine (red) complexes highlight the inward rotation of domain II. The rmsd is 0.748 Å over 404 Cα atoms. **B):** Superposition of the ODH-NADH (green) and ODH-NADH/agmatine (red) complexes. The interactions between NADH and Arg324 are highlighted and the corresponding distances are shown.

The binding of agmatine induces a similar rotational movement of domain II towards domain I (Figure 31). The movement is almost identical to the domain closure

observed in the OcDH-NADH/L-arginine and OcDH-NADH/Pyruvate structures. The salt bridge interaction of Arg324 towards the pyrophosphate moiety of NADH strengthens a indicated by the distance which shortens from 4.3 to 3.8Å (Figure 31). The DYNDOME server revealed a 39° rotation of domain II towards the NADH binding domain (domain I) in the Agmatine complex when compared to the OcDH-NADH complex. The interactions of agmatine towards OcDH (Table 7) are weaker when compared to the interactions of L-arginine, as indicated by larger distances between agmatine and OcDH (Table 6). Likely the strength of these interactions directly influences the degree of domain closure within the crystal.

4.11 Octopine and mercury bound crystals

As for the other substrates octopine was soaked into preformed OcDH-NADH crystals. After washing with mother liquid supplemented with 30% v/v ethylene glycol the soaked crystals were flash frozen in liquid nitrogen. An 2.8 Å dataset was collected and initial phases were obtained from molecular replacement using the program PHASER (*93*) and the OcDH-NADH structure as template. The overall structure of the structure resembles the OcDH-NADH structure. Inside the structure no density was present which would allow placing octopine into the structure with good certainty. Likely, octopine did not bind to OcDH. This is also reflected in the length of the unit cell axis, which was more similar to OcDH-NADH than to OcDH-NADH/L-arginine or OcDH-NADH/Pyruvate. This indicates no domain movement as seen upon binding of L-arginine as well as pyruvate.

As for the other substrates, a 1mM p-chlormercurybenzoate was soaked into preformed OcDH-NADH crystals, however for a different purpose. If specifically bound to OcDH, the mercury atoms can be detected in a fourier difference map and used to phase the OcDH structure. In parallel to the SeMet data a 2.7 Å dataset from the mercury soaked crystals was collected. P-chlor-mercurybenzoate was chosen as mercury compound as it was shown to bind to OcDH (*103*). Four mercury positions were identified using the program SHELXE and initial phases were obtained. The program RESOLVE however could not automatically build amino acids into the

density, likely due to a rather low initial phasing power. Due to this as well as the success with the SeMet dataset the mercury dataset was initially not further refined. The structure of the mercury bound OcDH was later solved by molecular replacement using the OcDH-NADH structure as template. The obtained structure indeed contained four bound mercury atoms. The overall structure and the orientation of the NADH binding site was identical to the OcDH-NADH structure.

Therefore, these two structures will not be further discussed. For completness, dataset statistics for the octopine as well as the mercury dataset can be found in Table 3, refinement statistics and unit cell contents for both structures are summarized in Table 4.

5 Discussion

5.1 Crystallisation of OcDH

Until now no crystal structure is known for Opine dehydrogenases from invertebrates, although various members of this enzyme family have extensively studied by physiological and biochemical means (*38*). The major bottleneck of protein crystallisation is the amount of protein needed in a homogenous solution. The cloning and purification of OcDH was only recently published (*78*) allowing mutational, biochemical and finally structural studies.

In recent years, His-tagged enzymes have been extensively used in protein biochemistry for rapid and efficient protein purification. The role of the His-tag in protein crystallisation, however is under considerable debate ever since (*109*). On the one hand a His-tag can inhibit crystallisation, which can be overcome by cleaving off the His-tag via a genetically engineered, specific protease cleavage site. Conversely, in most cases the His-tag does not interfere with crystal formation, although and due to its flexibility the polyhistidines can rarely be detected in the electron density map.

Three different constructs were used to crystallise OcDH, OcDH-tagless, OcDH-His_5 and OcDH-LEHis_6, respectively. The His-tags were placed at the C-terminus, since the important NADH binding site is encoded in the first N-terminal 20 amino acids. In OcDH-LEHis_6, two additional amino acids, leucine and glutamate are located between OcDH and the His-tag as encoded on the plasmid.

Although extensively tried, the constructs OcDH-tagless and OcDH-LEHis_6 never yielded any crystals. Probably OcDH can adopt multiple conformations, which prevented crystal formation. The purified OcDH-His_5 however, yielded small crystals when using a commercial screen that could be optimized with the help of tailored grid screens. By optical examination and X-ray diffraction experiments, the crystals appeared multiple (Figure 19A and Figure 20A). Several attempts to improve these crystals did not succeed. The observation of multiple crystals suggested that the protein can adopt several conformations during crystal growth, a generally accepted disadvantage in crystal growth (*110*).

It was known for other NADH binding enzymes, like the LDH or several alcohol

dehydrogenases that the addition of the cofactor causes structural changes inside the protein (*111*). Also for OcDH from *Pecten maximus* a structural change upon binding of NADH has been reported (*56*). Therefore cofactor NADH was added to OcDH-His_5 at a final concentration of 0.8 mM prior to crystallisation. This produced crystals under conditions comparable with the conditions in the absence of NADH (Figure 19b). The incubation temperature appeared to be critical. These crystals were single and diffracted to 2.1Å, which were suitable to collect a dataset from. The addition of this cofactor further stabilized the orientation of the two domains towards each other via the interaction of the domain I bound NADH with Arg324 located in domain II. This amino acid plays a crucial role as an Arg-sensor due to its close proximity to the pyrophosphate moiety of NADH and in domain closure. In the OcDH/NADH complex the distance between Arg324 and NADH is 4.2Å, which is quite a close distance, a so called relaxing state. In the absence of NADH, this relaxing state is disrupted and OcDH can probably adopt several open conformations reflected by the multiple crystals obtained.

During data collection the phase information of the X-ray wave which reach the detector is lost resulting in the so called “phase problem”. To regain the phase information crystals of seleno methionine incorporated OcDH were grown at similar conditions. By using the technique of single anomalous dispersion, the location of eleven of the twelve methionines inside the asymmetric unit could be identified. As seen later in the refined structure the starting methionine is missing, which is a common observation in protein structures solved by X-ray crystallography.

5.2 His_5-tag induced crystallisation

The structure of OcDH revealed that the His_5-tag protudes into the opening cleft of a symmetry related monomer inside the crystal (Figure 3). From the histidines of the His_5-tag, His402 interacts with the side chain of Val307 directly, whereas His403 interacts with the NO2 moiety of NADH. Interestingly, position and orientation of the other histidines inside the His_5-tag are stabilized via a complex water network (Figure 25 and Figure 26). The complete His_5-tag thereby opens up both domains to a certain extend, and together with the addition of NADH, OcDH is fixed in a stable

conformation, or phrasing it differently OcDH cannot adopt a more closed conformation.

By the limited opening of the cleft between the two domains crystal contacts were created. A disruption of any one of these interactions by a further opening of the cleft between the two domains would loosen or even diminish crystal formation. This is in line colloquial with the observation that crystals without the cofactor were multiple and of less quality.

Any prolongation of the His_5-tag would probably result in a similar orientation of the tag inside the cleft, stabilized via a complex water network, but would destroy the domain-domain crystals contact. This could explain why OcDH-LEHis_6, which possess not only one extra histidine, but is also prolonged by one leucine and glutamate residue, did not yield any crystals. The two proteins would be too far apart to form similar protein-protein crystals contacts as in the presence of OcDH-His_5. In addition the specific role of the His_5-tag further also explains why OcDH-tagless did not crystallise; the two domains are too flexible and a stable conformations can only be induced by the protruding His_5-tag.

Fusion (or chimeric) proteins are utilized in the forefront of protein science for almost all applications in biochemical research. Especially His-tags (*112*) have gained great popularity over the last decade as a purification tool for recombinant proteins. The often tacit assumption is that these tags have no effect on the structure and function of the protein (*113*). For crystallising the protein of interest sometimes it is useful to remove the affinity tag prior to crystallisation. OcDH is one example were not only the presence but also the size of the His-tag is crucial for crystallisation as it induces additional and important crystal contacts. A similar observation is seen in the structure of a 116-residue protein, (PDB code 1v30), were a long C-terminal helix which includes the His-tag (LEHHHHHH), protrudes outside the molecule and packs with another molecule about the crystallographic twofold axis (*114*). Similar to us, the authors noted that they were unable to obtain crystals of the wild-type sequence, i. e. without His-tag, under the same crystallisation conditions.

5.3 Structure of OcDH

Already in the primary protein sequence two distinct domains can be found in OcDH, a NADH-dependent glycerol-3-phosphate dehydrogenase like domain (domain I) and an octopine dehydrogenase specific domain (domain II; interpro database). Each domain comprises approximately half of the protein. Domain I contains the classic Rossman fold of dinucleotide binding proteins (*65, 111*). The octopine dehydrogenase specific domain starts with a short helix-kink-helix motif (helix a8-helix a9) followed by two antiparallel β-sheets and several helices. Both domains together build up the L-arginine and pyruvate binding sites.

5.4 The L-arginine, Agmatine and Pyruvate binding sites

In contrast to the OcDH-NADH complex, which was co-crystallised, the binary complex of OcDH-NADH/L-arginine was obtained through soaking of L-arginine into preformed OcDH-NADH crystals (see Materials and Methods and Results for details). This obviously raised the question whether this complex reflects a physiological situation. In the OcDH-NADH/L-arginine binary complex (Figure 27).

NADH is bound to OcDH in an identical fashion as in the OcDH-NADH complex and stabilized in the syn-conformation through equal interactions with the backbone of Cys148. The substrate L-arginine, which is located above His212, is coordinated via a hydrogen bond between its α-carboxyl oxygen and the N3 of His212 as well as via hydrogen bonds of the α-amino group with the backbone of Tyr208 contributing directly to substrate binding (Figure 27; further details are given in Table 6). The guanidinium group, on the other hand is fixed inside the binding pocket via a salt bridge with Glu142 (highlighted in green in Figure 27, van-der-Waals interactions with Trp278 and hydrogen bonds with the backbone carbonyl of Met206. While His212, Trp278 and Met206 are located in domain II, Glu142 is part of domain I, suggesting that L-arginine binding involves both domains of OcDH and likely triggers a domain closure. Such a motion is further supported by the fact that Met206, Tyr208 and His212 are located in a rather flexible helix-kink-helix motif, which forms the N-terminal part of domain II (for further details see below). N3 of His212, which participates in ligand binding, is coordinated by Asp329 via a hydrogen bond forming the Asp-His proton relay system (*69*). These interactions are supported by

mutagenesis studies and demonstrate that the binary complex obtained by soaking reflects the natural state [16]. More important however is Arg324, which has been proposed to be part of a catalytic triad similar to LDH or MDH (*69, 72*), is too remote to participate in L-arginine binding. In all OpDHs identified so far in invertebrates, residues His212 and Asp329 are conserved supporting the idea of a general catalytic mechanism (Table 8). Although Glu142 and Trp278 are conserved as well, the L-amino acid substrate differs in the various members of the OpDH family, which may require a particular mechanism for substrate recognition and selection. The only other available three-dimensional structure of an enzyme of the OpDH superfamily is that of the apo form of N-(1-D-carboxylethyl)-L-norvaline dehydrogenase (CENDH) from *Arthrobacter sp.* strain 1C (*76*). CENDH catalyses the NADH-dependent reductive condensation of hydrophobic L-amino acids such as L-methionine, L-isoleucine, L-valine, L-phenylalanine or L-leucine with α-keto acids such as pyruvate, glyoxylate, α-ketobutyrate or oxaloacetate with (D,L) specificity (*51*). Crystals of CENDH were obtained in the presence of NAD^+. Although no cofactor could be assigned in the final electron density, this structure allowed an analysis of the reaction mechanism and the principles of governing substrate selection.

	△		△		△ ◊		△		◊ ◊	
Pecten maximus ODH	IVGLPSQAGFE	122	MSFETLPWACR	149	IMSYS-FVHPA	214	DIYQWYLEY	282	DFGNRYLTEDIPMGM	334
Mizuhopecten yessoensis ODH	IVGLPSQAGFE	122	MSFETLPWACR	149	IMSYS-FVHPA	214	DIYQWYLEY	282	DFGNRYLTEDIPMGM	334
Loligo vulgaris ODH	IVGLPSQPGFQ	131	VSFESLPWACR	158	LLADA-VVHPP	224	HLFDWYKLN	292	DFTYRYMTEDIPFGM	345
Loligo opalescens ODH	IVGLPSQPGFQ	130	VSFESLPWACR	157	LLADA-VVHPP	223	HLFDWYKLN	291	DFTYRYMTEDIPFGM	344
Sepia officinalis ODH	IVGLPSQPGFQ	131	VSFESLPWACR	158	LLADS-VVHPP	224	HLFDWYKLN	292	DFNYRYMTEDIPFGM	345
Pseudocardium sachalinensis ODH	IVGLPGQPGFE	128	MSIETLPWACR	155	FLYRP-TVHPP	223	SMQDCFIGE	291	DFKYRYLMEDVPYGL	344
Haliotis discus hannai TDH	IVGMPGQPGFE	127	MSFESLPWACR	154	LATKS-IIHPP	220	HLYDWYLRD	288	DFRYRYLTEDVPNGL	341
Arabella irriciolor TDH	VVGFPGQPGFD	121	MNFVSLPWACR	148	IMAVNGMLHPS	215	HMHPYYIGA	283	DFTGRYFGEDIPFGL	336
Fusitriton oregonensis AloDH	IIGLPGQPGFE	124	LSYESLPWACR	151	LMTKS-IVHPP	217	HLLEWYRQD	285	DFGYRYLAEDIPFGL	338
Marphysa sanguinea AloDH	LVGLPGQPGFE	123	MAFESLPWACR	148	LMSVNSYIHSS	215	HVLQWYLRV	283	NFKHRYLSEDIPYGL	336
Marphysa sanguinea StrDH	LVGLPGQSGFE	123	MSFESLPWACR	148	LMATNGYIHPS	215	HIWQWYLRV	283	DFKHRYLMEDIPFGL	336
Arthrobacter spec. CENDH	IILNPGATGGA	115	GETSSMLFTCR	143	LTNVNAVMHPL	204	SVCEWYKES	262	NLNTRYFFEDVSTGL	302

Table 8: Sections of a protein sequence alignment for different opine. dehydrogenases. Protein sequences used are octopine dehydrogenases from *Pecten maximus, Mizuhopecten yessoensis, Loligo vulgaris, Loligo opalescens*, *Sepia officinalis* and *Pseudocardium sachalinensis ,* tauropine dehydrogenase from *Arabella irricolor* and *Haliotis discus hannai*, the annotated alanopine dehydrogenase from *Fusitriton oregonensis*, the alanopine dehydrogenase and strombine dehydrogenase from *Marphysa sanguinea* and the carboxyethylnorvalin dehydrogenase (CENDH) *from Arthrobacter spec 1C*. Highlighted in red are the amino acids involved in the binding of L-arginine (in OcDH: Glu142 and Trp278) and pyruvate (Gln118) as well as in green the His-Asp dyad (in OcDH: His212 and Asp329) and a functionally important L-arginine (in OcDH: Arg324). For sequence aligment clustalW was used (www.ebi.ac.uk/CLUSTALW)

CENDH forms a homodimer already suggesting profound structural differences with regard to substrate selection in OcDH. CENDH possesses a similar binding site as OcDH composed of His202, Asp297 and Trp258 (Figure 32). In the former enzyme however the side chain of Val197 points into the putative substrate-binding site. Therefore, only substrates such as norvaline or small hydrophobic amino acids are accommodated in the assumed binding site of CENDH (*77*). In clear contrast, the corresponding amino acid in OcDH (Tyr 208 located in the kink of the helix-kink-helix motif) is flipped out of the binding site, allowing the large side chain of L-arginine to bind efficiently.

Val197 is part of a helix, while Tyr208 is located in a kink. However, both catalytic important histidine residues His212 in OcDH and His202 in CENDH) superimpose perfectly, which is achieved by the presence of a single amino acid gap in the sequence of OcDH as shown by the corresponding alignment (Table 8). Thus, the positioning of the respective side chains of Val197 and Tyr208 in CENDH and OcDH generates a “molecular ruler” which distinguishes substrates based on size, a simple but effective mechanism.

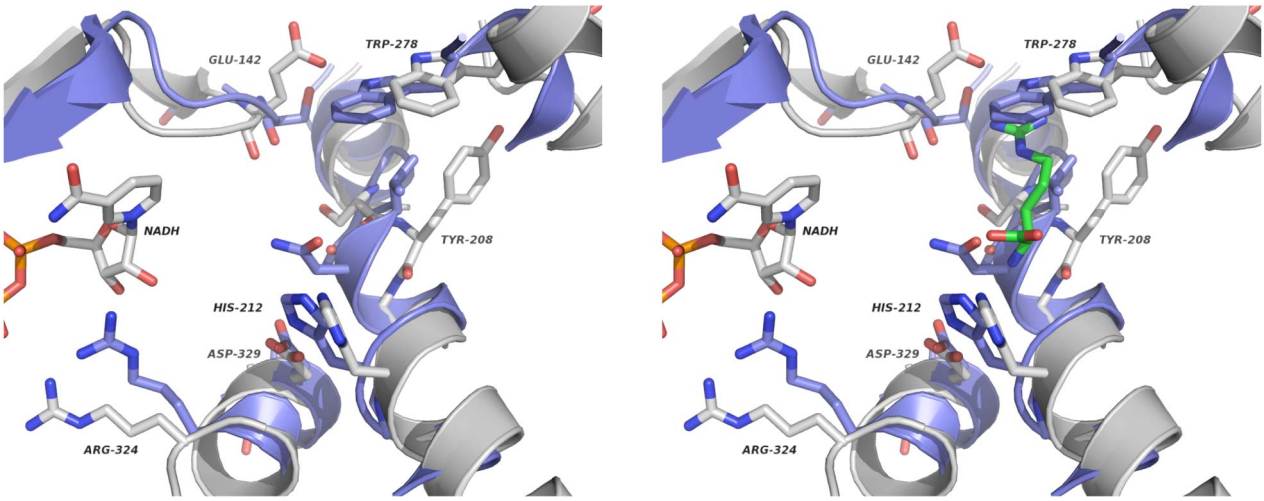

Figure 32: Overlay of the Arginine binding site of OcDH with CENDH. A zoom in picture into the arginine binding site of OcDH (white) overlaid with the CENDH (purple) structure is shown. Left paner) An overlay without arginine and right panel) the substrate arginine is included. For simplicity the amino acid are only labelled for the OcDH residues. The corresponding numbering in CENDH can be found in Table 8.

In the binary OcDH-NADH/pyruvate complex (Figure 28), which was obtained via soaking of pyruvate into preformed OcDH-NADH crystals, pyruvate is coordinated through Gln118 (domain I) and His212 (domain II). The side chain of Gln118 coordinates the carboxyl moiety of pyruvate, whereas His212 imposes orientation restraints and interacts with the carbonyl group via a hydrogen bond. The importance of Gln118 is emphasized by mutational analysis (*103*). Mutation of Gln118 to alanine or aspartate resulted in drastically reduced enzymatic activities, affecting both, k_{cat} and K_M (Appendix Table 10 and (*103*)). Comparison of alanine and aspartate mutants revealed that the introduction of a negative charge (Q118D) had a more pronounced effect on the catalytic efficiency (k_{cat}/K_M) for pyruvate (factor of 10^4) than for L-arginine (factor of 10^3) and NADH (factor of 10^2). In the light of the structure of the binary complex, this mutational data can be rationalized, because the introduction of a negative charge in the binding pocket (Q118D) resulted in a pronounced reduction of activity due to repulsive interactions between aspartate and pyruvate.

The binding site is optimally suited for pyruvate as a substrate since prolongation by a single methylene group reduced activity (Appendix Table 11 and (*103*)) as demonstrated for α-ketobutyrate respectively reducing the catalytic efficiency of OcDH by a factor of 10 and for α-ketovalerate (containing two extra methylene groups) by a factor of 200. Obviously α-acids extended by one or two methylene units are already too long to fit into the binding site, which is built up by voluminous Gln118 and His212. As a corollary, Gln118 is conserved in all invertebrate OpDHs which employ pyruvate as an α-keto acid (Appendix Table 8).

The presence of residues Gln118 and His212, which are conspicuously, placed in domain I and domain II respectively, facilitates pyruvate binding with a concomitant domain closure stabilizing substrate arrangement for the reductive condensation of L-arginine and pyruvate. This joint reaction mode between the two domains can also explain the reduced enzymatic activity in the presence of α-ketobutyrate and α-ketovalerate, since their size prevents complete domain closure required for an efficient hydride transfer and consequently for high enzymatic turnover numbers. Due to the three dimensional orientation of the active center, OcDH can accommodate high anaerobic flux rates of ATP provision necessary during escape swimming in *Pecten maximus*.

In contrast to all invertebrate OpDHs known so far, the bacterial CENDH possesses an alanine (Ala111) at the position of Gln118 (Table 8), which makes CENDH rather promiscuous with respect to the α-keto acids. It employs pyruvate, glyocylate, α-ketobutyrate or oxaloacetate with similar efficiencies (*77*). Since pyruvate is bound to OcDH via interactions with His212 and Gln118, the difference at position 118 suggests that CENDH employs a different binding mode than OcDH or that the carboxylate moiety in CENDH is not specifically recognized.

5.5 Comparison of OcDH with related crystal structures of dehydrogenases

Currently, the structure of CENDH from *Arthrobactersp. strain 1C* (*76*) is the only other known crystal structure of the OpDH superfamily that catalyzes the reductive condensation of a L-amino acid with an α-keto acid. CENDH shows a broader substrate specificity with a putative active site located only in domain II (see below). Structural superposition of OcDH and CENDH (data not shown) did not highlight any gross differences in the overall structure. The NADH/NAD^+ binding site reveals similar interactions of the pyrophosphate moieties with the asparagine and glycine residues located in the Rossmann motif. Whereas the orientation of the nicotinamide hydroxyl group in OcDH is coordinated by the backbone of Cys148 (see above), the density of the nicotinamide ribose group in CENDH was of moderate quality and could not be assigned.

No other dehydrogenase containing the Rossmann fold revealed any structural similarity to OcDH as detected by the DALI server (*115*). Even the saccharopine dehydrogenase from *Saccharomyces cerevisiae* (*116, 117*), which catalyzes the oxidative cleavage of saccharopine to α-ketoglutarate and L-lysine, does not possess a related structure. MDH and LDH, which are members of the α-keto acid dehydrogenase familiy, contain an Asp-X-X-Arg motif at their active sites which binds the carboxylate group of the α-keto acid. It guarantees the correct orientation of the substrate within the active site (*69*). Together with a histidine residue, these amino acids form a His–Asp–Arg triad, which is important for the transfer of the hydrid ion from NAD(P)H to the carbonyl group of the α-keto acid (*69, 72*). Mutational analysis

and sequence motif analysis of OcDH revealed the presence of a similar motif (His212-Asp329-Arg324) in domain II (*78*), suggesting possible mechanistic similarities between OcDH and LDH/MDH. However, as revealed by these current studies, the arginine residue of OcDH (Arg324) does not participate in either L-arginine (Figure 27) or pyruvate binding (Figure 28). The presence of a triad in OcDH does not exist, which implies that this dehydrogenase employs a reaction mechanism different from that of MDH or LDH.

5.6 A catalytic dyad combined with an "L-arginine sensor"

The importance of Arg324 in OcDH has recently been demonstrated by mutational analysis and a canonical His-Asp-Arg triad was proposed (*78*). However, the crystal structure suggests that Arg324 is not involved in substrate binding (neither L-arginine nor pyruvate). Rather, it plays a crucial role due to its close proximity to the pyrophosphate moiety of NADH in domain closure (*17*). A comparison of the OcDH-NADH (colored green in Figure 29A) and the OcDH-NADH/L-arginine complexes (colored blue in Figure 29A) revealed a 42° rotation of domain II towards the NADH binding domain (domain I) in the latter complex as calculated using the DYNDOME server (*106*). This domain closure is triggered by the interaction of Arg324 (domain II) with the pyrophosphate moiety of NADH bound to the Rossman fold in domain I. In the OcDH/NADH complex the distance between Arg324 and the pyrophosphate moiety of NADH is 4.3Å (Figure 29B). In the binary complexes of OcDH-NADH/L-arginine and OcDH-NADH/pyruvate, this distance shortens to 3.6 and 3.2 Å, respectively, increasing the strength of the salt bridge interaction (Figure 29B) and points to a "sensor role" for Arg324. In horse liver alcohol dehydrogenase, a similar Arg-NADH interaction is observed. Here, the strength of the salt bridge is thought to be responsible for domain closure as well as subsequent relaxation post catalysis (*118*). This argues against the general diffusion model proposed for domain closure in proteins (*119*). It rather suggests that OcDH possesses a catalytic dyad and the Arg324 sensor stabilizes a productive conformation of OcDH.

Stable binding of NADH to the Rossman fold of domain I, the first step in the reaction sequence of OcDH, occurs without participation of domain II. A comparison

of the two binary complexes implies that both, pyruvate and L-arginine, are capable of triggering domain closure to a similar extent. However, in the OcDH-NADH/pyruvate complex, pyruvate partially blocks the entrance for L-arginine, while in the OcDH-NADH/L-arginine complex, the accessibility of the pyruvate binding site is not restricted by L-arginine. Thus, it is likely that L-arginine binds to the OcDH-NADH complex in a consecutive step and induces a rotational movement of domain II towards domain I. This semi-closed active center, which is further stabilized using the pyrophosphate moiety of the bound cofactor and by interactions of L-arginine with residues from both domains (Figure 26 and Figure 27), is then poised to accept pyruvate and consequently the hydride transfer can proceed. Thus, we propose that instead of a random binding process, an ordered sequence of substrate binding in the line of NADH, L-arginine and pyruvate will occur. This sequential order of substrate binding might be the key to why pyruvate is not reduced to L-lactate *in vivo* and why opine formation has been preserved as a terminal step of anaerobiosis in some invertebrates during evolution.

5.7 Substrate specificity and stereoselectivity of OcDH

The results presented above provide new insights into the mechanism of OcDH and suggest a sequential binding order of all substrates. Furthermore, the syn-conformation of NADH (Figure 24) leads to a quantitative formation of the D-stereoisomer during the reductive condensation of L-arginine and pyruvate. However, an important question remains, namely how does OcDH ensure this amazingly high specificity for the L-arginine side chain and how is the L-isomer selected?

Surface potential calculation reveals a rather general distribution of charges in OcDH (Figure 33A and B), but inside the cleft between the two domains a highly negatively charged pocket is present, which harbors His212. This conspicuous structure might serve to absorb the positively charged guanidinium group of L-arginine. As other substrates such as canavanine (25%), cysteine (1.2%), L-alanine (<1%), ornithine (<1%), and norvaline (<1%) display reduced or negligible activity (Appendix Table 12 and (*103*)), the presence of this electrostatic sink capturing the highly positively charged guanidinium side chain of L-arginine ensures substrate selectivity. Furthermore, the length of the side chain of the amino acid substrate

imposes restraints on the binding mode of the α-carboxy group of L-arginine. To ensure proper stereo selectivity within the reaction cycle of OcDH, the α-amino- and α-carboxy groups are fixed via electrostatic interactions so that the positively charged α-amino group binds to the negatively charged pocket where as the negatively charged α-carboxy group points away from the pocket towards the solvent (Figure 33C), thereby preventing the binding of D-arginine. The specific interactions of OcDH with L-arginine provide the first level of substrate and stereo selection, but it is conceivable that the negatively charged cavity serves as an electrostatic sink acting as a molecular measuring device, a "charge ruler" that will guarantee that only L-arginine with the proper stereo configuration is recognized and tightly bound to OcDH for the subsequent reaction with pyruvate.

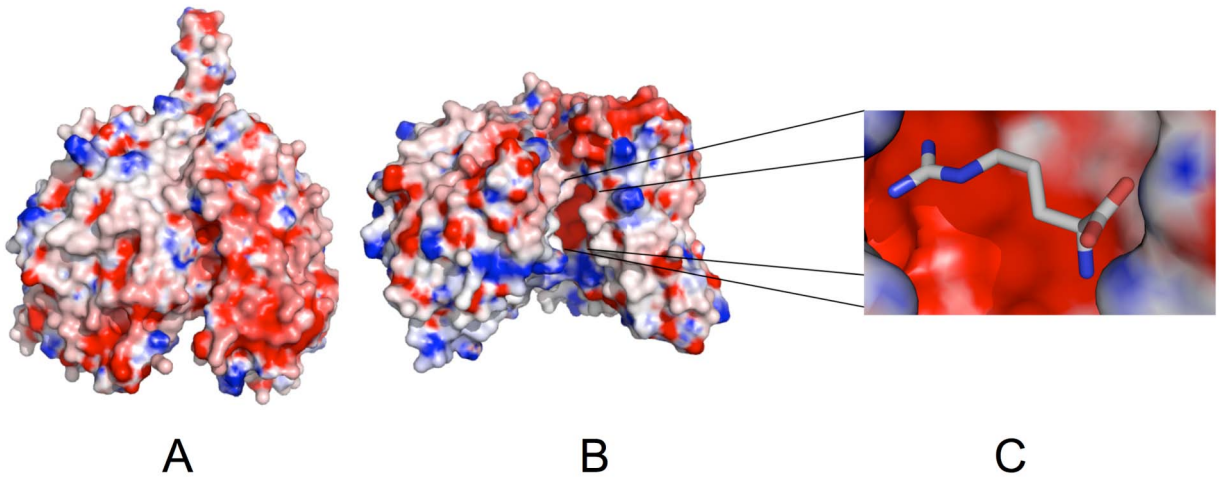

Figure 33: **Charge surface representation of the OcDH-NADH/L-arginine complex. (A)** Front and **(B)** site representation after a 90° rotation perpendicular to the plane of the paper of the surface charges of OcDH. Here a highly negatively charged pocket between the domains becomes visible. **(C)** Charge distribution within the L-arginine binding pocket (shown in stick representation). Red represents negative charge and blue positive charges contoured at 8kT.

The reductive condensation of pyruvate and L-arginine to octopine catalyzed by OcDH is mediated by a reaction mechanism requiring the involvement of both domains of this monomeric dehydrogenase. Biochemical data support the view that the reaction mechanism of all OpDHs proceed via carbinolamine and imino acid intermediates (*120*). However, the proposed catalytic triad composed of His212-Asp329-Arg324 is in structural terms only a dyad, composed of the proton relay system His212-Asp329, while Arg324 represents the important sensor inducing

domain closure via interaction with the pyrophosphate moiety of NADH. Thus, with the determination of principles of how OcDH ensures the reductive condensation of L-arginine with pyruvate and the identification of molecular rulers ensuring substrate and stereo selectivity, it will now be possible to employ OcDH as a framework for a rational design of different OpDHs for a general application of this fascinating enzyme family in biotechnology or enzyme-based chemical synthesis for drug development.

5.8 Order of substrate binding

Since the discovery of OcDH in several organisms the kinetics of this enzyme family have been of great interest. Similar to LDH pyruvate and NADH are needed for activity. In contrast to the LDH where lactate is formed OcDH catalyze the condensation of pyruvate with an amino acid. Due to kinetic analyses two kinetic mechanisms for OcDH-catalyzed reaction have been suggested. Monneuse-Doublet *et al*. (*58*) proposed that substrate binding occurs in a sequential-ordered mechanism. At first, in the presence of NADH the apoenzyme forms a binary complex to which pyruvate is bound. Pyruvate binding causes a conformational change, which enables binding of the second substrate, L-arginine. L-arginine binding is followed by the formation of a Schiff base as a transient intermediate. During the following hydride transfer from NADH, the Schiff base is reduced to D-octopine. Furthermore, the formation of two dead end complexes is described, presumably involved in the regulation of enzyme activity. The dead end complexes are produced by the formation of an ODH·NADH·D-octopine ternary and an ODH·NAD^+·pyruvate·L-arginine quaternary complex.

In contrast, Schrimsher and Taylor (*59*) described a random-ordered mechanism. After the formation of the binary ODH·NADH complex, L-arginine and pyruvate randomly bind to the holoenzyme. Enzyme activity is presumably regulated by the formation of dead end complexes, similar to those described by Monneuse-Doublet *et al*. (58). In addition, pyruvate and L-arginine or D-octopine, respectively, are supposed to bind to the free enzyme.

The structures presented in this thesis allow the proposal of a different binding order of the substrates to OcDH. Stable binding of NADH to the Rossman fold of

domain I, the first step in the reaction sequence of OcDH, occurs without participation of domain II. Already the binding of NADH causes a domain closure of OcDH (see above).

A comparison of the two binary complexes suggests that both, pyruvate and L-arginine, are capable to trigger domain closure to a similar extent. However, in the ODH-NADH/pyruvate complex, pyruvate partially blocks the entrance for L-arginine, while in the ODH-NADH/L-arginine complex, the accessibility of the pyruvate binding site is not restricted by L-arginine. Thus, it is likely that L-arginine binds to the OcDH-NADH complex in a consecutive step and induces a rotational movement of domain II towards domain I. This semi-closed active center, which is further stabilized using the pyrophosphate moiety of the bound cofactor and by interactions of L-arginine with residues from both domains (Figure 27 and Figure 28), is then poised to accept pyruvate and consequently the hydride transfer will proceed. Thus, instead of a random binding process, an ordered sequence of substrate binding in the line of NADH, L-arginine and pyruvate will occur. This sequential order of substrate binding might be the key to why pyruvate is not reduced to L-lactate *in vivo* and why it has been preserved during evolution.

6 Outlook

The structure of OcDH in complex with NADH as well as the substrates L-arginine and pyruvate have been solved, and a binding order were NADH binds first followed by L-arginine and subsequently pyruvate has been proposed. Of course questions concerning OcDH remain still unanswered.

For example the substrate specificity of OcDH, which only uses L-arginine in contrast to other OpDHs which can cope with either one or several different substrates, like glycine, alanine, methionine, strombine, and taurine. By site directed mutagenesis the binding site of OcDH can be changed resembling more the binding site of CENDH. Here the mutation of Tyr208 into valine or threonine would be interesting to determine whether the introduction of a side chain into the L-arginine binding site would alter substrate specificity.

Interestingly the sequences of all OpDHs reveal a clear two domain organisation, where one contains the NADH binding site and the second domain contains the amino acids crucial for substrate binding as well as the condensation reaction. As in the structure of OcDH the two domains are separated by a small loop it would be possible to prolong this loop by an extra amino acid, for example glycine or serine to broaden the pyruvate binding site. Thereby, it is possible to alter the α-keto acid specifity towards α-ketobutyrate or α-ketovalerate, substrates extended by one or two methyl group. Altering the substrate specificity of either the α-keto acid in combination with the α-amino acid would be the foundation of a biotechnological application of OcDH.

7 References

(1) Zebe, E., Grieshaber, M., and Schottler, U. (1980) Biotopbedingte und funktionsbedingte Anaerobiose. *Biologie in unserer Zeit*, 175-182.

(2) Gäde, G., Weeda, E., and Gabbott, P. A. (1978) Changes in the level of octopine during the escape responses of the scallop, *Pecten maximus* (L.). *J Comp Physiol B*, 121-127.

(3) Grieshaber, M. K., Hardewig, I., Kreutzer, U., and Portner, H. O. (1994) Physiological and metabolic responses to hypoxia in invertebrates. *Rev Physiol Biochem Pharmacol 125*, 43-147.

(4) Connett, R. J., Gayeski, T. E., and Honig, C. R. (1984) Lactate accumulation in fully aerobic, working, dog gracilis muscle. *Am J Physiol 246*, H120-128.

(5) Connett, R. J., Gayeski, T. E., and Honig, C. R. (1985) Energy sources in fully aerobic rest-work transitions: a new role for glycolysis. *Am J Physiol 248*, H922-929.

(6) Crabtree, B., and Newsholme, E. A. (1972) The activities of phosphorylase, hexokinase, phosphofructokinase, lactate dehydrogenase and the glycerol 3-phosphate dehydrogenases in muscles from vertebrates and invertebrates. *Biochem J 126*, 49-58.

(7) Grieshaber, M., and Gäde, G. (1977) Energy supply and the formation of octopine in the adductor muscle of the scallop, *Pecten jacobaeus.Comp Biochem Physiol B 58*, 249-252.

(8) Ellington, W. R. (2001) Evolution and physiological roles of phosphagen systems. *Annu Rev Physiol 63*, 289-325.

(9) Ellington, W. R., Roux, K., and Pineda, A. O., Jr. (1998) Origin of octameric creatine kinases. *FEBS Lett 425*, 75-78.

(10) Gäde, G., and Grieshaber, M. K. (1986) Pyruvate reductases catalyze the formation of lactate and opines in anaerobic invertebrates. *Comp Biochem Physiol B 83: 255-272.* , 255-272.

(11) de Zwaan, A., and Wijsman, T. C. (1976) Anaerobic metabolism in *Bivalvia* (Mollusca). Characteristics of anaerobic metabolism. *Comp Biochem Physiol B*

54, 313-324.

(12) De Zwaan, A., Thompson, R. J., and Livingstone, D. R. (1980) Physiological and biochemical aspects of the valve snap and valve closure responses in the giant scallop *Placopecten magellanicus*. *Biochemistry. J Comp Physiol 137: 105-114. 137*.

(13) Thompson, R. J., Livingstone, D. R., and De Zwaan , A. (1980) Physiological and biochemical aspects of the valve snap and valve closure responses in the giant scallop *Placopecten magellanicus*. Physiology. J Comp Physiol 137: 97-104. *Physiology. J Comp Physiol*, 97-104

(14) Portner, H. O., U., K., Siegmund, B., Heisler, N., and Grieshaber, M. K. (1984) Metabolic adaptation of the intertidal worm Sipunculus nudus to functional and environmental hypoxia. *Mar. Biol.*, 237-247.

(15) Stanley, W. C., and Connett, R. J. (1991) Regulation of muscle carbohydrate metabolism during exercise. *Faseb J 5*, 2155-2159.

(16) Ebberink, R. H. M. (1982) Control of adductor muscle phosphofructokinase activity in the Sea mussel *Mytilus edulis* during anaerobiosis. *Mol Physiol*, 345-355.

(17) Storey, K. B., and Dando, P. R. (1982) Substrate specificites of octopine dehydrogenases from marine invertebrates. *Comp Biochem Physiol B*, 521-528.

(18) Clarke, F. M., and Masters, C. J. (1974) On the association of glycolytic components in skeletal muscle extracts. *Biochim Biophys Acta 358*, 193-207.

(19) Zammit, V. A., and Newsholme, E. A. (1976) The maximum activities of hexokinase, phosphorylase, phosphofructokinase, glycerol phosphate dehydrogenases, lactate dehydrogenase, octopine dehydrogenase, phosphoenolpyruvate carboxykinase, nucleoside diphosphatekinase, glutamate-oxaloacetate transaminase and arginine kinase in relation to carbohydrate utilization in muscles from marine invertebrates. *Biochem J 160*, 447-462.

(20) Katz, A., and Sahlin, K. (1988) Regulation of lactic acid production during exercise. *J Appl Physiol 65*, 509-518.

(21) Meyerhof , O. (1924) Die Energieumwandlung im Muskel. *Naturwissenschaften*, 181-186

(22) Livingstone, D. R., De Zwaan, A., Leopold, M., and Marteijn, E. (1983) Studies

on the phylogenetic distribution of pyruvate oxidoreductases. *Biochem SystemEcol* 415-425.

(23) Fletcher, W. M. (1907) Lactic acid in amphibian muscle. *J Physiol 35*, 247-309.

(24) Bennett, A. F. (1978) Activity metabolism of the lower vertebrates. *Annu Rev Physiol 40*, 447-469.

(25) Zebe, E. (1975) Invivo studies on glucose degradation in *Arenicola marina* (Annelida, Polychaeta). *J Comp Physiol 101: 133-145.* , 133-145.

(26) Baldwin, J., and Opie, A. M. (1978) Role of octopine dehydrogenase in adductor muscles of bivalve mollusks. *Comp Biochem Physiol 61*, 85-92. .

(27) Moore, E., and Wilson, D. W. (1937a) Nitrogenous extractives of scallop muscle I. The isolation and a study of the structure of octopine. *J Biol Chem 119*, 573-584.

(28) Moore, E., and Wilson, D. W. (1937b) Nitrogenous extractives of scallop muscle II. Isolation from an quantitative analysis of muscle from feshly killed scallops. *J Biol Chem 119*, 585-588.

(29) Thoai, N. V. R., Y. (1961) Metabolism of guanidyl derivatives. IX. Biosynthesis of octopine: study of the mechanism of the reaction and some properties of octopine synthetase. *Biochim Biophys Acta 52*, 221-233

(30) van Thoai, N., Huc, C., Pho, D. B., and Olomucki, A. (1969) Octopine dehydrogenase. Purification and catalytic properties. *Biochim Biophys Acta 191*, 46-57.

(31) Haas S, Olomucki A,, and Thoai, N. V. (1973) Purification de l'octopine dehydrogenase de Sipunculus nudus. Etude comparative avec l'octopine dehydrogenase de *Pecten maximus*. *CRS Soc Biol 276*, 831-834. .

(32) Gäde, G., and Grieshaber, M. (1975) Partial-purification and properties of octopine dehydrogenase and formation of octopine in *Anodonta cygnea L. J Comp Physiol B 102*, 149-158.

(33) Grieshaber, M. (1978) Breakdown and formation of high-energy phosphates. *J Comp Physiol B 126*, 269-276. .

(34) Gäde, G., and Carlsson, K.-H. (1984) Purification and characterisation of octopine dehydrogenase from the marine nemertean *Cerebratulus lacteus* (Anopla: Heteronemerta): comparison with scallop octopine dehydrogenase.

Mar Biol 79, 39-45. .

(35) Fields, J. H. A., Baldwin, J., and Hochachka, P. W. (1976b) On the role of octopine dehydrogenase in cephalopod mantle muscle metabolism. *Can J Zool 54*, 871-878.

(36) Fields, J. H. A., Guderley, H., Storey, K. B., and Hochachka, P. W. (1976c) The pyruvate branch point in squid brain: competition between octopine dehydrogenase and lactate dehydrogenase. *Can J Zool 54*, 879-885.

(37) Sato, M., and Gäde, G. (1986) Rhodoic acid dehydrogenase - A novel amino acid-linked dehydrogenase from muscle-tissue of Haliotis species. *Naturwissenschaften 73*, 207-209.

(38) Thompson, J., and Donkersloot, J. A. (1992) N-(carboxyalkyl)amino acids: occurrence, synthesis, and functions. *Annu Rev Biochem 61*, 517-557.

(39) Ellington, W. R. (1980) Partial-purification and characterization of a broadly-specific octopine dehydrogenase from the tissues of the sea anemone, *Bunodosoma cavernata* (Bosc). *Comp Biochem Physiol B 67: 625-631. 67*, 625-631.

(40) Storey, K. B. (1977) Tissue specific isozymes of octopine dehydrogenase in cuttlefish, *Sepia officinalis* - roles of octopine dehydrogenase and lactate-dehydrogenase in sepia. *J Comp Physiol 115*, 159-169.

(41) Storey, K. B., and Storey, J. M. (1979) Kinetic characterization of tissue-specific isozymes of octopine dehydrogenase from mantle muscle and brain of *Sepia officinalis.* Functional similarities to the M4 and H4 isozymes of lactate dehydrogenase. *Eur J Biochem 93*, 545-542.

(42) Dando, P. R., Storey, K. B., Hochachka, P. W., and Storey, J. M. (1981) Multiple dehydrogenases in marine mollusks - Electrophoretic analysis of alanopine dehydrogenase, strombine dehydrogenase, octopine dehydrogenase and lactate-dehydrogenase. *Marine Biology Letters 2*, 249-257.

(43) Kanno, N., Sato, M., Nagahisa, E., and Sato, Y. (1996) Tauropine dehydrogenase from the sandworm *Arabella iricolor* (Polychaeta: Errantia): purification and characterization. *Comp Biochem Physiol B Biochem Mol Biol 114*, 409-416.

(44) Perez, J. E., Ramirez, N., Basoa, E., Alfonsi, C., Nusetti, O., and Moreno, J.

(2000) Polymorphisms of octopine dehydrogenase (Odh) in mollusks and implications for the neutralism-selectionism hypothesis. *Rev Biol Trop 48*

(45) Livingstone, D. R. (1990) Cytochrome P-450 and oxidative metabolism in invertebrates. *Biochem Soc Trans 18*, 15-19.

(46) Sato, M., Takeuchi, M., Kanno, N., Nagahisa, E., and Sato, Y. (1993) Purification and properties of tauropine dehydrogenase from a red alga, *Rhodoglossum japonicum*. *Hydrobiologia 26*, 673- 678.

(47) Schell, J., Van Montagu, M., De Beuckeleer, M., De Block, M., Depicker, A., De Wilde, M., Engler, G., Genetello, C., Hernalsteens, J. P., Holsters, M., Seurinck, J., Silva, B., Van Vliet, F., and Villarroel, R. (1979) Interactions and DNA transfer between *Agrobacterium tumefaciens*, the Ti-plasmid and the plant host. *Proc R Soc Lond B Biol Sci 204*, 251-266.

(48) Van Larebeke, N., Zaenen, I., Teuchy, H., and Schell, J. (1973) Circular DNA plasmids in Agrobacterium strains. Investigation of their role in the induction of crown-gall tumors. *Arch Int Physiol Biochim 81*, 986.

(49) Van Larebeke, N., Engler, G., Holsters, M., Van den Elsacker, S., Zaenen, I., Schilperoort, R. A., and Schell, J. (1974) Large plasmid in *Agrobacterium tumefaciens* essential for crown gall-inducing ability. *Nature 252*, 169-170.

(50) Messens, E., Lenaerts, A., Hedges, R. W., and Van Montagu, M. (1985) Agrocinopine A, a phosphorylated opine is secreted from crown gall cells. *Embo J 4*, 571-577.

(51) Asano, Y., Yamaguchi, K., and Kondo, K. (1989) A new NAD^+-dependent opine dehydrogenase from *Arthrobacter sp. strain 1C*. *J Bacteriol 171*, 4466-4471.

(52) Beauchamp, C. J., Chilton, W. S., Dion, P., and Antoun, H. (1990) Fungal Catabolism of Crown Gall Opines. *Appl Environ Microbiol 56*, 150-155.

(53) Gäde, G., and Grieshaber, M. (1986) Pyruvate reductases catalyze the formation of lactate and opines in anaerobic invertebrates. *Comp Biochem Physiol 83*, 255-272.

(54) Carvajal, N., and Kessi, E. (1988) Kinetic mechanism of octopine dehydrogenase from the muscle of the sea mollusc, *Concholepas concholepas*. *Biochim Biophys Acta 953*, 14-19.

(55) Thompson, J., and Miller, S. P. (1991) N5-(1-carboxyethyl)ornithine and related

[N-carboxyalkyl]-amino acids: structure, biosynthesis, and function. *Adv Enzymol Relat Areas Mol Biol 64*, 317-399.

(56) Olomucki, A. (1981) Structure and function of octopine dehydrogenase of *Pecten maximus* (great scallop). *Biochem Soc Trans 9*, 278-279.

(57) Janssen, F. (2000) Klonierung, Struktur und Evolution einiger Octopindehydrogenasen aus marinen Invertebraten. *Dissertation Heinrich-Heine-Universität Düsseldorf.* .

(58) Monneuse-Doublet, M. O., Olomucki, A., and Buc, J. (1978) Investigation on the kinetic mechanism of octopine dehydrogenase. A regulatory behavior. *Eur J Biochem 84*, 441-448.

(59) Schrimsher, J. L., and Taylor, K. B. (1984) Octopine dehydrogenase from *Pecten maximus*: steady-state mechanism. *Biochemistry 23*, 1348-1353.

(60) Zettlmeissl, G., Teschner, W., Rudolph, R., Jaenicke, R., and Gade, G. (1984) Isolation, physicochemical properties, and folding of octopine dehydrogenase from *Pecten jacobaeus*. *Eur J Biochem 143*, 401-407.

(61) Teschner, W., Rudolph, R., and Garel, J. R. (1987) Intermediates on the folding pathway of octopine dehydrogenase from Pecten jacobaeus. *Biochemistry 26*, 2791-2796

(62) Kimura, T., Nakano, T., Yamaguchi, T., Sato, M., Ogawa, T., Muramoto, K., Yokoyama, T., Kan-No, N., Nagahisa, E., Janssen, F., and Grieshaber, M. K. (2004) Complementary DNA cloning and molecular evolution of opine dehydrogenases in some marine invertebrates. *Mar Biotechnol (NY) 6*, 493-502.

(63) Kan-no, N., Endo, N., Moriyama, S., Nagahisa, E., and Sato, M. (2005) The amino acid sequence of tauropine dehydrogenase from the polychaete *Arabella iricolor. Comp Biochem Physiol B Biochem Mol Biol 140*, 475-485.

(64) Branden, C. L., Zeppezauer, E., Boiwe, T., Soderlund, G., Säderberg, B. O., and Nordstrom, B. (1970) X- ray studies of horse liver alcohol dehydrogenase. *Pyridine Nucleotide-Dependent Dehydrogenases. Springer Verlag*, 129-134.

(65) Rossmann, M. G., Moras, D., and Olsen, K. W. (1974) Chemical and biological evolution of nucleotide-binding protein. *Nature 250*, 194-199.

(66) Branden, C. I., and Eklund, H. (1980) Structure and mechanism of liver alcohol

dehydrogenase, lactate dehydrogenase and glyceraldehyde-3-phosphate dehydrogenase. *Experientia Suppl 36*, 40-84.

(67) Wierenga, R. K., De Maeyer, M. C. H., and Hol, W. G. J. (1985) Interaction of pyrophosphate moieties with alpha-helixes in dinucleotide-binding proteins. *Biochemistry 24*, 1346-1357.

(68) Baker, P. J., Britton, K. L., Rice, D. W., Rob, A., and Stillman, T. J. (1992) Structural consequences of sequence patterns in the fingerprint region of the nucleotide binding fold. Implications for nucleotide specificity. *J Mol Biol 228*, 662-671.

(69) Clarke, A. R., Wilks, H. M., Barstow, D. A., Atkinson, T., Chia, W. N., and Holbrook, J. J. (1988) An investigation of the contribution made by the carboxylate group of an active site histidine-aspartate couple to binding and catalysis in lactate dehydrogenase. *Biochemistry 27*, 1617-1622.

(70) Clarke, A. R., Atkinson, T., and Holbrook, J. J. (1989) From analysis to synthesis: new ligand binding sites on the lactate dehydrogenase framework. Part II. *Trends Biochem Sci 14*, 145-148.

(71) Clarke, A. R., Atkinson, T., and Holbrook, J. J. (1989) From analysis to synthesis: new ligand binding sites on the lactate dehydrogenase framework. Part I. *Trends Biochem Sci 14*, 101-105.

(72) Goward, C. R., and Nicholls, D. J. (1994) Malate dehydrogenase: a model for structure, evolution, and catalysis. *Protein Sci 3*, 1883-1888.

(73) Thome-Beau, F., and Olomucki, A. (1973) Presence of a single essential histidyl residue in octopine dehydrogenase as shown by photooxidation. *Eur J Biochem 39*, 557-562.

(74) Kan-No, N., Matsu-Ura, H., Jikihara, S., Yamamoto, T., Endo, N., Moriyama, S., Nagahisa, E., and Sato, M. (2005) Tauropine dehydrogenase from the marine sponge *Halichondria japonica* is a homolog of ornithine cyclodeaminase/mu-crystallin. *Comp Biochem Physiol B Biochem Mol Biol 141*, 331-339.

(75) Sheikh, S., and Katiyar, S. S. (1993) Chemical modification of octopine dehydrogenase by thiolspecific reagents: evidence for the presence of an essential cysteine at the catalytic site. Biochim Biophys Acta 1202: 251-257.

(76) Britton, K. L., Asano, Y., and Rice, D. W. (1998) Crystal structure and active site

location of N-(1-D-carboxylethyl)-L-norvaline dehydrogenase. *Nat Struct Biol 5*, 593-601.

(77) Dairi, T., and Asano, Y. (1995) Cloning, nucleotide sequencing, and expression of an opine dehydrogenase gene from *Arthrobacter sp. strain 1C*. *Appl Environ Microbiol 61*, 3169-3171.

(78) Muller, A., Janssen, F., and Grieshaber, M. K. (2007) Putative reaction mechanism of heterologously expressed octopine dehydrogenase from the great scallop, *Pecten maximus* (L). *Febs J 274*, 6329-6339.

(79) Chayen, N. E. (2005) Methods for separating nucleation and growth in protein crystallisation. *Prog Biophys Mol Biol 88*, 329-337.

(80) Jancarik, J., and Kim, S. H. (1991) Sparse-Matrix Sampling - a Screening Method for Crystallization of Proteins. *J Appl Crystallogr 24*, 409-411.

(81) Drenth, J. (1999) *Principles of Protein X-ray Crystallography*, Springer Verlag, New-York.

(82) Massa, W. (1996) *Kristallstrukturbestimmung*, Teubner, Stuttgart.

(83) Bergfors, T. M. (1999) *Protein Crystallization - Techniques, Strategies, and Tips*, International University Line, La Jolla.

(84) Blow, D. (2004) *Outline of Crystallography for Biologists*, Oxford University Press, Oxford.

(85) Hendrickson, W. A. (1991) Determination of Macromolecular Structures from Anomalous Diffraction of Synchrotron Radiation. *Science 254*, 51-58.

(86) Hendrickson, W. A. (1999) Maturation of MAD phasing for the determination of macromolecular structures. *J Synchrotron Radiat 6*, 845-851.

(87) Hendrickson, W. A., Horton, J. R., and Lemaster, D. M. (1990) Selenomethionyl Proteins Produced for Analysis by Multiwavelength Anomalous Diffraction (Mad) - a Vehicle for Direct Determination of 3-Dimensional Structure. *Embo J 9*, 1665-1672.

(88) Popov, A. N., and Bourenkov, G. P. (2003) Choice of data-collection parameters based on statistic modelling. *Acta Crystallogr D Biol Crystallogr 59*, 1145-1153.

(89) Otwinowski, Z., and Minor, W. (1997) Processing of X-ray diffraction data collected in oscillation mode, in *Meth. Enzymol.* (Carter, C. W., and Sweet, R. M., Eds.), Academic Press, London.

(90) Panjikar, S., Parthasarathy, V., Lamzin, V. S., Weiss, M. S., and Tucker, P. A. (2005) Auto-Rickshaw: an automated crystal structure determination platform as an efficient tool for the validation of an X-ray diffraction experiment. *Acta Crystallogr D Biol Crystallogr 61*, 449-457.

(91) Murshudov, G., Vagin, A. A., and Dodson, E. J. (1997) Refinement of macromolecular structures by the maximum-likelihood method. *Acta Crystallography D 53*, 240-255.

(92) Emsley, P., and Cowtan, K. (2004) Coot: model-building tools for molecular graphics. *Acta Crystallogr. D 60*, 2126-2132.

(93) McCoy, A. J., Grosse-Kunstleve, R. W., Adams, P. D., Winn, M. D., L.C., S., and Read, R. J. (2007) Phaser crystallographic software. *J Appl Cryst 40*, 658-674.

(94) Lamzin, V. S., and Wilson, K. S. (1993) Automated refinement of protein models. *Acta Crystallography D 49*, 129-147.

(95) Kabsch, W. (1988) Evaluation of single-crystal X-ray diffraction data from a position-sensitive decetor. *J. Appl. Cryst. 21*, 916-924.

(96) Terwilliger, T. C., and Berendzen, J. (1999) Automated MAD and MIR structure solution. *Acta Crystallogr. D 55*, 849-861.

(97) Sheldrick, G. M. (2008) A short history of SHELX. *Acta Crystallogr A 64*, 112-122.

(98) Laskowski, R. A., MacArthur, M. W., Moss, D. S., and Thornton, J. M. (1993) PROCHECK: a program to check the stereochemical quality of protein structures. *J. Appl. Crystallogr. 26*, 283-291.

(99) Lee, R. A., Razaz, M., and Hayward, S. (2003) The DynDom database of protein domain motions. *Bioinformatics 19*, 1290-1291.

(100) Frishman, D., and Argos, P. (1995) Knowledge-based protein secondary structure assignment. *Proteins 23*, 566-579.

(101) Emekli, U., Schneidman-Duhovny, D., Wolfson, H. J., Nussinov, R., and Haliloglu, T. (2007) HingeProt: Automated prediction of hinges in protein structures. *Proteins*. 28 532-538

(102) DeLano, W. L. (2002) The PyMol Molecular Graphics System. http://www.pymol.org.

(103) Mueller, A. (2006) Die Octopindehydrogenase der Pilgermuschel *Pecten*

Maximus. Dissertation Heinrich Heine Universität.

(104) Perrakis, A., Morris, R., and Lamzin, V. S. (1999) Automated protein model building combined with iterative structure refinement. *Nat Struct Biol 6*, 458-463.

(105) Bashton, M., and Chothia, C. (2002) The geometry of domain combination in proteins. *J Mol Biol 315*, 927-939.

(106) Hayward, S., and Lee, R. A. (2002) Improvements in the analysis of domain motions in proteins from conformational change: DYNDOME version 1.50. *J Mol Graph Model 21*, 181-183.

(107) Kim, J. H., Yenari, M. A., Giffard, R. G., Cho, S. W., Park, K. A., and Lee, J. E. (2004) Agmatine reduces infarct area in a mouse model of transient focal cerebral ischemia and protects cultured neurons from ischemia-like injury. *Exp Neurol 189*, 122-130.

(108) Yang, M. Z., Mun, C. H., Choi, Y. J., Baik, J. H., Park, K. A., Lee, W. T., and Lee, J. E. (2007) Agmatine inhibits matrix metalloproteinase-9 via endothelial nitric oxide synthase in cerebral endothelial cells. *Neurol Res 29*, 749-754.

(109) Carson, M., Johnson, D. H., McDonald, H., Brouillette, C., and DeLucas, L. J. (2007) His-tag impact on structure. *Acta Crystallographica Section D 63*, 295-301.

(110) McPherson, A. (1985) Crystallization of macromolecules: general principles. *Methods Enzymol 114*, 112-120.

(111) Schulz, G. E. (1992) Binding of nucleotide by proteins. *Cur. Opion. Struc. Biol. 2*, 61-67.

(112) Smith, M. C., Furman, T. C., Ingolia, T. D., and Pidgeon, C. (1988) Chelating peptide-immobilized metal ion affinity chromatography. A new concept in affinity chromatography for recombinant proteins. *J Biol Chem 263*, 7211-7215.

(113) Chant, A., Kraemer-Pecore, C. M., Watkin, R., and Kneale, G. G. (2005) Attachment of a histidine tag to the minimal zinc finger protein of the *Aspergillus nidulans* gene regulatory protein AreA causes a conformational change at the DNA-binding site. *Protein Expr Purif 39*, 152-159.

(114) Tajika, Y., Sakai, N., Tamura, T., Yao, M., Watanabe, N., and Tanaka, I. (2004) Crystal structure of hypothetical protein PH0828 from *Pyrococcus horikoshii*. *Proteins 57*, 862-865.

(115) Holm, L., and Park, J. (2000) DaliLite workbench for protein structure comparison. *Bioinformatics 16*, 566-567.

(116) Andi, B., Xu, H., Cook, P. F., and West, A. H. (2007) Crystal structures of l igand-bound saccharopine dehydrogenase from *Saccharomyces cerevisiae*. *Biochemistry 46*, 12512-12521.

(117) Burk, D. L., Hwang, J., Kwok, E., Marrone, L., Goodfellow, V., Dmitrienko, G. I., and Berghuis, A. M. (2007) Structural studies of the final enzyme in the alpha-aminoadipate pathway-saccharopine dehydrogenase from *Saccharomyces cerevisiae. J Mol Biol 373*, 745-754.

(118) Hayward, S., and Kitao, A. (2006) Molecular dynamics simulations of NAD+-induced domain closure in horse liver alcohol dehydrogenase. *Biophys J 91*, 1823-1831.

(119) Gerstein, M., Lesk, A. M., and Chothia, C. (1994) Structural mechanisms for domain movements in proteins. *Biochemistry 33*, 6739-6749.

(120) Stillman, T. J., Baker, P. J., Britton, K. L., and Rice, D. W. (1993) Conformational flexibility in glutamate dehydrogenase. Role of water in substrate recognition and catalysis. *J Mol Biol 234*, 1131-1139.

8 Appendix

Table 9: **Protein sequence alignment for different opine dehydrogenases**.

Table 10: **Kinetic parameters of the forward reaction (NADH oxidation) catalyzed by recombinant wild-type OcDH and Gln118 mutants.**

Table 11: **Activity of different α-keto acid substrates.**

Table 12: **Substrate specificity of recombinant wild-type OcDH.**

The last three tables were taken from the Dissertation of Andre Mueller from the Zoophysiology Institute Heinrich Heine University Düsseldorf. They allow a detailed discussion on the obtained structures in this thesis.

```
Pecten maximus ODH                ---------MTVKVCVCGGGNGAHTLSGLAASRDGVEVRVLTLFADEAERWTKALGADEL 51
Mizuhopecten yessoensis ODH       ---------MTLKVCVCGGGNGAHTLSGLAASRDGVEVRVLTLFADEAERWTKALGADEL 51
Loligo vulgaris ODH               MAHHQEKPPVLIKLLICGGGNGAHVLTGLASSRHNVKVNVLSLFADEAERWRKTLGDNHF 60
Loligo opalescens ODH             -MTHQEKPPVLVKLLVCGGGNGAHVLTGLASSRHNVKVNVLSLFADEAERWRNTLADNHS 59
Sepia officinalis ODH             MAHHQEKPPVLINLLVCGGGNGAHVLTGLASSRHNVKVNVLSLFADEAERWRNTLGDNHF 60
Pseudocardium sachalinensis ODH   ---MSRSLEKSCNITIFGGGNGAHVLSGLSSDVVNANVTVVDTFQDEAERWTKAMAANGF 57
Haliotis discus hannai TDH        ---MTKK----ITVLVCGGGNGAHVTAGLAASRDDIETRVLTTFADEAERWTNIMKENDL 53
Arabella irriciolor TDH           ----------MVVLTICGGGNAAHTLAGIASNQPNMEVRVLTLYADEAERWIKSMETNDF 50
Fusitriton oregonensis AloDH      ---MADK----LTVCVCGGGNGAHAMAGLAAAHPGTEARVLTLFQDEAPRWANIMKEENF 53
Marphysa sanguinea AloDH          ----------MVVVVVCGGGNGAHTLAGVAASRPNTEVRVLTLFADEAERWTKAMESSDF 50
Marphysa sanguinea StrDH          ----------MVVLVICGGGNGAHVLAGIASSNPNADVRVLTLYADEAERWTKAMEGNDF 50
Arthrobacter spec. CENDH          -------MIESKTYAVLGLGNGGHAFAAYLALKG----QSVLAWDIDAQRIKEIQDRGAI 49
                                             : * **..*. :.  :         :  :  :* *  :

Pecten maximus ODH                TVIVNEKDG---TQTEVKSRPK-VITKDPEIAISGADVVILTVPAFAHEGYFQAMAPYVQ 107
Mizuhopecten yessoensis ODH       TVIVNEKDG---TQTEVKSRPK-VITKDPQVAITGADVVILTVPAFAHEGYFQAMAPYVQ 107
Loligo vulgaris ODH               VVNFREKDG---SSQIITSRPN-MITNDPSKAVPGCNLIIFTVPAFAHEGYFRAIAPYLE 116
Loligo opalescens ODH             VVNFREKDG---SNKIITSRPN-MITNDASKAVPGCNLVIFTVPAFAHEGYFRAIAPYLE 115
Sepia officinalis ODH             VVNFREKDG---TNKIITSRPN-MITNDPSRAVPGCNLVIFTVPAFAHEGYFRAIAPYLE 116
Pseudocardium sachalinensis ODH   TVKYGNGKD----LVQAPGKPKFTVTKEVQKNVEKADVVILCMPAFLHEMVLTSVAPYVP 113
Haliotis discus hannai TDH        RITVDEGDIKSGESVDFKVKLN-CITKDPSKAVPGADVIIFTVPAFAHQSYLEAIEPYIQ 112
Arabella irriciolor TDH           TTIKYATGK---DPVHLKTKPK-LVTKNPEQGATGADIIVITVPAFAHAQYLTALKPHVK 106
Fusitriton oregonensis AloDH      TIQQNKPDK---SVVHIKAKPA-LVTKDASQAVPGANIIIFCVPAFAHAQYFKAIEPYVY 109
Marphysa sanguinea AloDH          VTNIHNHDK---SITKLTNKPR-LVTKDPGKAAIGAEIIILAVPAFVHAQYLEALKPHVT 106
Marphysa sanguinea StrDH          VVTVNNQDK---SQTILKNKPR-LVTKDPALAANKADMIVFTVPAFAHRQYLDALKPHIR 106
Arthrobacter spec. CENDH          IAEGPGLAG--------TAHPD-LLTSDIGLAVKDADVILIVVPAIHHASIAANIASYIS 100
                                             :    :*.:       .:::::: :**: *      : .::

Pecten maximus ODH                DSALIVGLPSQAGFEFQCRDILGDK-AAAVSMMSFETLPWACRIKEFGRKVEVLGTKSVL 166
Mizuhopecten yessoensis ODH       DSALIVGLPSQAGFEFQCRDILGDK-AAAVSMMSFETLPWACRIKEFGRKVEVLGTKSVL 166
Loligo vulgaris ODH               PNTVIVGLPSQPGFQFQCCDLLGIG-GRTSAIVSFESLPWACRIGTFGREVQVLGPKDTL 175
Loligo opalescens ODH             PNTVIVGLPSQPGFQFQACDLLGMG-GRTSAIVSFESLPWACRIGTFGREVQVLGPKDTL 174
Sepia officinalis ODH             PNTVIVGLPSQPGFQFQCCDLLGLG-GRTSAIVSFESLPWACRIGTFGREVQVIGPKDTL 175
Pseudocardium sachalinensis ODH   ETCPIVGLPGQPGFEYQALFHLRQN-GKKGSVMSIETLPWACRIAKYGQEVDVIGTKECI 172
Haliotis discus hannai TDH        PNTTIVGMPGQPGFEFQVFDVLKDK-AKQCVIMSFESLPWACRIAEFGKFVQILMVKVNL 171
Arabella irriciolor TDH           PGTVVVGFPGQPGFDFEIMKIWGDL-AKQCTVMNFVSLPWACRIKEFGKSVEVLATKDMM 165
Fusitriton oregonensis AloDH      PNTAIIGLPGQPGFEFQCFDVLKDK-ARQCAILSYESLPWACRILEFGKLVEILGAKDSL 168
Marphysa sanguinea AloDH          PGTILVGLPGQPGFEFDVYTIWGPL-ASKCSIMAFESLPWACRIAEFGQCVEILGTKESL 165
Marphysa sanguinea StrDH          PGTVLVGLPGQSGFEFEVWTAWGDL-AKQCSIMSFESLPWACRFTEFGRAATVIGTKENL 165
Arthrobacter spec. CENDH          EGQLIILNPGATGGALEFRKILRENGAPEVTIGETSSMLFTCRSERPG-QVTVNAIKGAM 159
                                      ::  *. .*   :          .    :    :: ::**    *  . :   *  :

Pecten maximus ODH                AASLIKG-TAKTVDP--LSTLQMLHGAEPVFRLAKHFLEMLIMSYS-FVHPAILFGRWGS 222
Mizuhopecten yessoensis ODH       AASLIKG-TAETVDP--LSTLQKLHGAEPVFRLAKHFLEMLIMSYS-FVHPAILYGRWGS 222
Loligo vulgaris ODH               ACAIIMRGCRPLFPI--LKTIQYVIGKEPKLTMAANYLSINLLADA-VVHPPMMYGTWKD 232
Loligo opalescens ODH             ACAIIMRGCKPLFPV--LKTIQYVIGKEPKLTMAANYLSINLLADA-VVHPPMMYGTWKD 231
Sepia officinalis ODH             ACAIIMRGCKTLFPI--LPTIQYIIGKEPKLTLAANYLSINLLADS-VVHPPMMYGTWKD 232
Pseudocardium sachalinensis ODH   YFSSVDQQSSGYVGAGLVQLIQTLLGAKPVLKREENIIKYTFLYRP-TVHPPLMYAKWKN 231
Haliotis discus hannai TDH        MGCLIRGQSKPSYDP--MEAVQRVMGKAPILTQANNYIEPILATKS-IIHPPIMYGKWKD 228
Arabella irriciolor TDH           FGSVRNGTVAPKMDP--TAMIQGCLGPLPRLECSGHLLGMSIMAVNGMLHPSIMYNRWHD 223
Fusitriton oregonensis AloDH      MGSEIKGKSQLKPDP--AKTLQAMLGEHPVLKMAHNYLEPYLMTKS-IVHPPLMYGRWKD 225
Marphysa sanguinea AloDH          VGAVHIGSVPSKFDP--TLLLQGCLGPHPSLLTKGHLLGITLMSVNSYIHSSILYGRWHD 223
Marphysa sanguinea StrDH          AGAAWYGSVPPKADP--TLVLQGCLGPHPVLLTRGALLGITLMATNGYIHPSILFGRWHK 223
Arthrobacter spec. CENDH          DFACLPAAKAG-------WALEQIGSVLPQYVAVENVLHTSLTNVNAVMHPLPTLLNAAR 212
                                    .                 ::   .  *        :   :      :*.

Pecten maximus ODH                WDGKPVPEAPLFYQGIDQATADMLTACSNECKDVANAIMAACPGNDLSDVKDIYQWYLEY 282
Mizuhopecten yessoensis ODH       WDGNPVSEAPLFYQGIDQATADMLTACSDECKAVGNAIMAACPGNDLSDVKDIYQWYLEY 282
Loligo vulgaris ODH               WDGKPVAEKPLFYQGLNEFSANLLDKVSSELVQTAQVIHQKYPDMDMKDVIHLFDWYKLN 292
Loligo opalescens ODH             WDGKPVAEKPLFYQGLNEFSADLLDKVSTELVQTAKAIHQKYPDMDMKDVIHLFDWYKLN 291
Sepia officinalis ODH             WDGQPVAEKPLFYQGLNEFSADLLDKVSTELVHTAQAIQQKYPEMDMKDVIHLFDWYKLN 292
Pseudocardium sachalinensis ODH   WDGKPLDAAPLFYQGADEEAVKYLDGATNEMIKIADFLQTKYPDMDFSGISSMQDCFIGE 291
Haliotis discus hannai TDH        WDGKPIEEKPLFYQGLDEEQARYLGGISDELVATAKAIAAQKPEVDLSGVLHLYDWYLRD 288
Arabella irriciolor TDH           WDGKPVDAPPLFYHGLSQAGADLLSDVSNETIAIAKKVMEQRQGVDLSNVIHMHPYYIGA 283
Fusitriton oregonensis AloDH      WDGQPMAEKPLFYQGLDEFGAGSLSTVSDEVLDTARAITKQKPELDLPHVEHLLEWYRQD 285
Marphysa sanguinea AloDH          WNGTPLDEAPLFYQGIDQDTADLMSGMSDEILVIAKEIMKKNPKVDLHNVDHVLQWYLRV 283
Marphysa sanguinea StrDH          WDGNPVNEPPLFYNGLDEFSAQTMSSVSDEILAVASSLMKQRPQVDLTNVAHIWQWYLRV 283
Arthrobacter spec. CENDH          CESG--TPFQYYLEGITPSVGSLAEKVDAERIAIAKAFDLNVP--------SVCEWYKES 262
                                   :.  :     : .*              *    .  .        :  :  :   :
```

```
Pecten maximus ODH                YHEDIQDDHDLYHAITTNKSYKGLVHP-VKAVDGGVAPDFGNRYLTEDIPMGMIVFKGVA 341
Mizuhopecten yessoensis ODH       YHEDIQDDHDLYHAITTNKSYKGLVHP-VKTVDGGVAPDFGNRYLTEDIPMGMIVFKGVA 341
Loligo vulgaris ODH               YKESIKDMSNLRLAMKTCTAYDGLVHPMKETPDKMFVPDFTYRYMTEDIPFGMVVFRGIA 352
Loligo opalescens ODH             YKESIKDMSSLRMAMKTCTAYDGLVHPMKETPDKKFVPDFTYRYMTEDIPFGMVVFRGIS 351
Sepia officinalis ODH             YKESIQDMSNLQMAMKTCSAYDGMVHPMKETPDGKFMPDFNYRYMTEDIPFGMVVFRGIA 352
Pseudocardium sachalinensis ODH   YPEQIKDKSTLLSCLKTNQAYDGLVHPMKKTDDGKFVPDFKYRYLMEDVPYGLLIIKQIA 351
Haliotis discus hannai TDH        HKPYIKDTTSLLTVLQTDTAYDGLVHPMKETEDGKFVPDFRYRYLTEDVPNGLVVTKGLA 348
Arabella irriciolor TDH           YPDDISDKSSLYTCINTNAGFKGLTHPCTKTADGKFVPDFTGRYFGEDIPFGLAVTRGIA 343
Fusitriton oregonensis AloDH      YRETVKDPTSLLTAMRTNTAYNGLVHPMKDAGNGKWVPDFGYRYLAEDIPFGLVVTKGLA 345
Marphysa sanguinea AloDH          YEDDIQDKSNLYTAIRSNEAYIGLTHPMSKTEDGKYLPNFKHRYLSEDIPYGLAVSKGVA 343
Marphysa sanguinea StrDH          YADDIGDKTSLFTTIRTNAAYSGLTHPTTKTDDGKFVPDFKHRYLMEDIPFGLLVSKGIA 343
Arthrobacter spec. CENDH          YGQSP---ATIYEAVQGNPAYRGIAGP----------INLNTRYFFEDVSTGLVPLSELG 309
                                  :         :   :    .: *:. *           ::  **: **:. *:     :.

Pecten maximus ODH                IAAGVAIPSNDKLIMWAQEKIGKEYLVDGALTGKDVATTRCPQRYGFNTLDAILTGKK- 399
Mizuhopecten yessoensis ODH       IAAGVPIPNNDKLITWAQEKIGKVYLVDGALTGKDVATTRCPQRYGFNTLNAILTGKKE 400
Loligo vulgaris ODH               ELAGVPTPAMDETITWGQKILGKEVLVNGKLTGKDMNLTRAPQRFHFHSLFDLVNLR-- 409
Loligo opalescens ODH             ELAGVPTPAMDETIIWGQKILGKEFLVNGKLQGKDMNLTRAPQRFHFNSLFDLVNLR-- 408
Sepia officinalis ODH             QLEGVPTPAMDETLTWGQKILGKEFLVDGELKGKDMNMTRAPQRFHFNSLFDLVNLR-- 409
Pseudocardium sachalinensis ODH   EMAGVATPIIDEIILWAQTKLDAEYLKDGKLCFVDRKHGRIPMAFGIKTLEEFVNYCK- 409
Haliotis discus hannai TDH        QIAGVPTPYHDEVIAWCQKQLGKEIIVGDELKGKDIGSTRCPQRYGINTMDALVNIM-- 405
Arabella irriciolor TDH           EIAGCPTPNIDKIIEWAQKLMGKEYLVGGKFTGKDISATRAPQRYGFNTLDSIL----- 397
Fusitriton oregonensis AloDH      LLAGVPTPETDRVLAWCQDKLGKEFIVGSELKGKDMTSSRAPQAYGFKSLDDLMALM-- 402
Marphysa sanguinea AloDH          EVVGVNTPLIDKVLIWCQEKLGKEYLVDGKMIGKDVTFTRCPQRYSMTTVDAILGK--- 399
Marphysa sanguinea StrDH          EVAGVPTPTIDSVISWAQQKMGKEYIVNGKLAGKDVSSTRCPQRYGLTTVDAILGL--- 399
Arthrobacter spec. CENDH          RAVNVPTPLIDAVLDLISSLIDTDFRKEGRTLEKLGLSG--LTAAGIRSAVE------- 359
                                     .   *  *  :   .  :.      .                : :   ::
```

Table 9: Protein sequence alignment for different opine dehydrogenases. Protein sequences used are octopine dehydrogenases from *Pecten maximus, Mizuhopecten yessoensis, Loligo vulgaris, Loligo opalescens, Sepia officinalis* and *Pseudocardium sachalinensis* , tauropine dehydrogenase from *Arabella irricolor* and *Haliotis discus hannai*, the annotated alanopine dehydrogenase from *Fusitriton oregonensis*, the alanopine dehydrogenase and strombine dehydrogenase from *Marphysa sanguinea* and the carboxyethylnorvalin dehydrogenase (CENDH) from *Arthrobacter spec 1C*. For sequence alignment clustalW was used (www.ebi.ac.uk/CLUSTALW).

		vmax [µmol min^{-1} mg^{-1}]	Km [mmol L^{-1}]	Km_{Mut}/ Km_{Wt}	kcat [s^{-1}]	kcat/Km [$Lmol^{-1}S^{-1}$]
pyruvate	wild-type[#]	1074	0.77	1	775	$1.0 \cdot 10^6$
	Q118A	393	27	35	283	$1 \cdot 10^4$
	Q118D	101	162	208	73	$4.5 \cdot 10^2$
L-arginine	wild-type[#]	886	0.5	1	640	$1.28 \cdot 10^6$
	Q118A	166	5.8	11	120	$2.1 \cdot 10^4$
	Q118D	169	81	153	122	$1.5 \cdot 10^3$
NADH	wild-type[#]	903	$19.8 \cdot 10^{-3}$	1	652	$3.3 \cdot 10^7$
	Q118A	240	$104 \cdot 10^{-3}$	5.3	173	$1.7 \cdot 10^6$
	Q118D	65	$175 \cdot 10^{-3}$	8.9	47	$2.7 \cdot 10^5$

Table 10: Kinetic parameters of the forward reaction (NADH oxidation) catalyzed by recombinant wild-type OcDH and Gln118 mutants. The values for the OcDH wildtype as well as the mutants were taken from Mueller 2006 (*103*). Values for K_m and k_{cat} of the Gln118Ala and Gln118Asp mutants were determined by analyzing the data according to the Michaelis-Menten equation using the enzyme kinetic module 20 of sigma-plot 9.0 (Systat Software, Erkrath, Germany).

	V_{max} [μmol min^{-1} mg^{-1}]	K_M [mmol L^{-1}]	k_{cat} [s^{-1}]	k_{cat}/K_M [L*mmol $^{-1}s^{-1}$]
Pyruvate	1074	0.77	775	1000
Ketobutyrate	728	5.9	526	90
Ketovalerate	377	49.8	272	5

Table 11: Activity of different α-keto acid substrates.The values for the OcDH with pyruvate, ketobutyrate and ketovalerate were taken from Mueller 2006 (*103*). Values for K_m and k_{cat} of the different a-keto acids, ketobutyrate and ketovalerate, were determined by analyzing the data according to the Michaelis-Menten equation using using sigma-plot 9.0 (Systat Software, Erkrath, Germany) and the enzyme kinetic module 2.0.

Substrate	Activity (U/ml)	Specific activity (U/mg)	%
Arginine	12678	634.0	100
Canavanine	3092	155.0	24.7
Cysteine	148	7.4	1.2
L-Alanine	35	1.8	0.3
Orinithine	32	1.6	0.3
Norvaline	3	0.95	0.1

Table 12: Substrate specificity of recombinant wild-type OcDH. The data for OcDH with all different substrates were taken from Mueller 2006 (*103*). Activity and specific activity of the different substrates were determined as described in Materials and Methods.

9 Acknowledgement

The last years had a lot of great stories but also moments were it was good to have people around supporting me. Although I always said that my acknowledgement will be in random order, I changed my mind, at least with the first person.

Lieber Lutz, die letzten Jahre warst Du immer für mich da. Dein Vertrauen in mich und meine Arbeit ist enorm - es wird sich auszahlen. Jeder der poetischen Sätze, die ich formulierte um Dir zu danken ist kläglich gescheitert. Das Einzige was einigermaßen passt ist: DANKE, DANKE, DANKE, DANKE. Jetzt ist es endlich vollbracht und der Spaß kann beginnen. Lass uns die nächsten Jahre “exzellent” machen. Liebe Sabine, dass der Lutz immer wieder so ist wie er ist, liegt auch an Dir. Danke

Lieber Herr Prof. Grieshaber, in sozusagen letzter Sekunde vor Ihrer Emeritierung haben wir uns getroffen. So ein Glück. Es ist schön zu sehen, wie glücklich jemand sein kann mit einer Proteinstruktur und das ist etwas was ich nie vergessen werde und was mir immer im Kopf hängen bleiben wird. Ich hoffe, dass Ihr zweiter Frühling bei uns im Institut noch lange anhält.

Meinem zweiten Gutachter, Prof. Georg Groth: Danke für die Bereitschaft mein Koreferent zu sein.

Stefan, eine positive Eigenschaft, die Du hast, ist Ehrgeiz. Toll wenn ich sehe, wie Du sie einsetzt um die Gruppe zu stärken. Du weisst eine Menge und kannst noch viel mehr. Ich bin sicher, dass Roche einen der besten Leute zu sich gerufen hat. Worauf ich aber am meisten stolz bin, ist, dass du mich nicht zum Klettern bewegen konntest!

Robert, “Sander, Kaffee” schriebst Du in Deiner Danksagung. Ich kann nur zurückgeben: „Wo bist Du? der Kaffee wird kalt“. Danke für die Diskussionen über

alles. Auf der anderen Seite des Teiches wirst Du Dein Ding schon machen. Ehrlich gesagt habe ich viele von Deinen Theorien am Schluss nicht mehr kapiert " Lipid droplets, mit budding sorting und ER" und zwar alles gleichzeitig in einem System. Jedem anderen würde ich an den Kopf werfen er wäre verrückt. Das Problem bei Dir: Du kriegst das hin!

Andre, vor etwas mehr als einem Jahr haben wir uns im Büro von Prof. Weiss kennen gelernt. Mit meinem Bauchgefühl zu den Kristallen lag ich richtig. Die Kristalle waren der erste Schritt und jetzt ist die Struktur da. Danke für Deine Begeisterung über ein tolles Enzym und für Deine "HAMMER!!" und Deine " So und nicht anders habe ich das erwartet". Es war wirklich toll mit Dir zusammen zu arbeiten und Du hast Recht: Was wäre wenn wir uns ein oder sogar zwei Jahre vorher getroffen hätten. Wir können beide nicht wissen, was gewesen wäre. Auf jeden Fall wäre es mit viel Spaß verbunden gewesen.

Petra, eine der richtigen Düsseldorferinnen. Toll, dass Du da bist, wenn auch öfters chaotisch. Bitte denk daran Du kannst das alles ohne Probleme. Auch wenn Du das selbst nicht immer glaubst .

Jan S., Danke für Deinen grenzenlosen Optimismus und auch Deine bildlichen Erklärungen von Klonierungsansätzen bzw. Experimenten. Dein Projekt ist echt nicht ohne und ich zieh meinen Hut davor, dass Du es noch nicht an die Wand geklatscht hast. Das hätte ich wahrscheinlich schon längst gemacht.

Nino, mit mir zusammen auf dem Nisin-Projekt - ich leider viel zu theoretisch aber Du in der Praxis. Lass uns was daraus machen und gucken das jeder endlich dieses System versteht. Ach so, ich hoffe immer noch auf ein Duell Fortuna-KSC. Dann gehen wir hin, oder?

Thorsten, der Ruhige. Obwohl ich manchmal nicht mehr genau weiß, was Du genau machst, ich merke Du machst es einfach ohne große Hoch- bzw. Tiefpunkte. Sozusagen ein ruhende Pol im Institut. Man vergisst den unschätzbaren Wert von so

jemandem ganz schnell. Ich nicht: DANKE.

Die „Complex I Truppe“. Veronika, Martina und am Anfang noch Yasmin, Zwar am Ende des Ganges, aber sorgen immer für die gute Laune und das Lachen. In Zukunft werde ich eure Süßigkeitenschüssel wirklich mal wieder voll machen müssen.

Ulli, Du bist ja länger da als alle anderen. Hast auf alles eine Antwort und eine Idee und kannst sogar noch die jungen “Angeber” schlagen im Klettergarten. Ich freue mich auf die kommende Zeit.

Nils, genau wie ich einer der „Älteren“ im Institut. Ich hoffe, dass wir noch viele Gründe haben werden ein wenig zu feiern. Die letzten Formatierungen habe ich dann doch noch geschafft. Danke.

Herr Prof Weiss, Sie haben die Invasion von uns hautnah mitbekommen. Auch in Zukunft werden Sie maßgeblich dazu beitragen, dass die Studenten das Fach Biochemie von Grund auf lernen. Dass Sie uns und den Studenten erhalten bleiben, ist einfach toll.

Silke, endlich bin ich fertig hinter dem Computer. Jetzt können wir die Nisin-Pläne umsetzen. Danke für die Organisation im Labor, Deine ruhige Art ist ein guter Kontrast zu den auflebenden Charakteren, die da sind.

Britta, Dein „drive“ ist unverkennbar. Behalte den so lange Du kannst. Es wird toll mit Dir mindestens eine der Strukturen zu lösen. Es wird Frustrationen geben, aber die meistern wir mit links.

Dann gibt es noch die Neuen: Nacera, Jan H., Miro, Susanne: Danke, danke, danke, eine gute Atmosphäre im Institut ist mir wichtig und Ihr tragt dazu bei. Wir werden noch eine tolle Zeit erleben.

Frau Simons, die Gummibärchen sind Ihnen sicher!

Die Master- / Diplom-Studenten die mit geholfen haben mit deren jeweiligen Projekten. Thomas, Nino, Justin, Britta, Kim, Margarete. Danke

Frau Blum, danke für die organisatorische Seite des Institutes. Frau Rasid, danke für Ihre an manchen Stellen extrem wichtige Arbeit und Ihre Geschichten aus Mazedonien, die mich an genau der richtigen Stelle zum lachen bringen.

Nicht zu vergessen die Frankfurter: Christine, Tina, Goetz, Rasmus, auch Ihr habt mir geholfen mich nicht entmutigen zu lassen, sondern meinen Weg weiter zu gehen. Danke

Padros en Madros, nou eindelijk het “boekje” is af. Het heeft erg lang geduurd, maar nu is het zover. Bedankt voor alles de afgelopen jaren en nu laten we eindelijk een keertje feest vieren.

Nicki, meine Arbeit ist endlich fertig. Das was Du leistest mit den Jungs ist gigantisch. Danke für Deine Unterstützung. Ich glaube es hat sich gelohnt. Lass uns jetzt mal in Ruhe genießen.

Henri en Benno: Jongens, wat geweldig dat jullie er zijn. Het is zo mooi te zien dat “de glasbak” en “de zandbak” voor jullie het belangrijkste zijn. Papa is blij en geweldig trots op jullie.

Ein letztes Wort an alle,

DANKE, BEDANKT, MERCI, GRACIAS, THANKS, lets have some CHAMPAGNE

Die hier vorgelegte Dissertation habe ich eigenständig und ohne unerlaubte Hilfe angefertigt.
Die Dissertation wurde in der vorgelegten oder in ähnlicher Form noch bei keiner anderen Institution eingereicht.

Düsseldorf, den 10.07.2008